POWDER METALLURGICAL PROCESSING OF TITANIUM AND ITS ALLOYS

by

Hung-Wei Liu

Submitted in partial fulfilment of the requirements
for the degree of Master of Applied Sciences

at

Dalhousie University
Halifax, Nova Scotia
August 2011

DALHOUSIE UNIVERSITY

DEPARTMENT OF PROCESS ENGINEERING & APPLIED SCIENCE

The undersigned hereby certify that they have read and recommend to the Faculty of Graduate Studies for acceptance a thesis entitled "POWDER METALLURGICAL PROCESSING OF TITANIUM AND ITS ALLOYS" by Hung-Wei Liu in partial fulfilment of the requirements for the degree of Master of Applied Science.

Dated: ____August 17, 2011_____

Supervisor: _____

_____

Reader: _____

_____

DALHOUSIE UNIVERSITY

DATE: August 17, 2011

AUTHOR: Hung-Wei Liu

TITLE: POWDER METALLURGICAL PROCESSING OF TITANIUM AND ITS ALLOYS

DEPARTMENT OR SCHOOL: Department of Process Engineering & Applied Science

DEGREE: M.A.Sc CONVOCATION: October YEAR: 2011

_____

Signature of Author

TABLE OF CONTENTS

LIST OF TABLES

LIST OF FIGURES

ABSTRACT

Titanium is well known for its excellent properties, such as high strength-to-weight ratio and outstanding corrosion resistance. However the high cost of this metal has confined its applications to those mostly within the aerospace and military industries. The high purchase price of titanium is primarily driven by the need for intricate metal extraction processes, as well as the sensitivity towards conventional metal working operations. Among the potential solutions, powder metallurgy (P/M) technology provides an economical approach to bring down the price of finished titanium products. However, there are still many problems, such as the residual porosity in the sintered body, that need to be overcome.

In this thesis, a fundamental study was carried out focusing on the P/M press-and-sinter technique, using commercially pure titanium (CP Ti) as well as two binary titanium alloys, namely Ti-Ni and Ti-Sn. The influence of several processing parameters including compaction pressure, lubricant type/concentration, sintering time/temperature were performed on both the CP and binary systems. The principal tools utilized for mechanical characterization were hardness and tensile testing, whereas optical microscopy, x-ray diffraction (XRD), and scanning electron microscopy were employed to identify the microstructural features present.

Press-and-sinter P/M strategies were successfully developed for all of the blends studied. For CP-Ti, a maximum tensile strength >750MPa and near full theoretical density (~99%) were achieved. Transitions in the size and the size distribution of pores and α-Ti grains were also observed and quantified. It was found these transitions, as well as the powder impurities present (i.e. oxygen and carbon), greatly influenced the final mechanical properties. In the case of the binary alloys, it was shown that liquid phase sintering (LPS) significantly improved the sintered density for the Ti-10%Ni composition, when sintered at l100°C. A eutectic microstructure (α-Ti + Ti_2Ni), coupled with grains of α-Ti, were identified as the principal phases present. On the other hand, the Ti-Sn alloys only showed a modest increase in sintered density compared to the CP-Ti, owing to the high solubility of Sn in Ti. In terms of crystal structure, XRD highlighted that the Sn containing samples were fully α-Ti.

LIST OF ABBREVIATIONS AND SYMBOLS USED

ASTM	American Society for Testing and Materials
BCC	Body-centred cubic
BE	Blended elemental
CHM	Cold hearth melting furnace
CIP	Cold isostatic press
CP	Commercially pure
DSC	Differential scanning calorimetry
E	Elastic modulus
EDO	electro-deoxidation process
EDS	Energy-dispersive X-ray spectroscopy
FCC	Face-centred cubic
FFC	Fray, Farthing and Chen
HCP	Hexagonal closed-packed
HDH	Hydride-dehydride
HIP	Hot isostatic press
HRA	Rockwell hardness A scale
ITP	International Titanium Powder company
LC	Licowax

LPS	Liquid phase sintering
MIM	Metal injection moulding
MMC	Metal matrix composite
MPIF	Metal Powder Industries Federation
P/M	Powder metallurgy
PREP	Plasma rotation electrode process
PS	Press and sinter
REP	Rotation electrode process
SEM	Scanning electron microscopy
TRS	Transverse rapture strength
UTS	Ultimate tensile strength
VAR	Vacuum arc remelt furnace
XRD	X-ray diffraction
α	Hexagonal closed-packed phase titanium
β	Body-centred cubic phase titanium

ACKNOWLEDGEMENTS

The author wishes to thank both of his supervisors Dr. Paul Bishop and Dr. Kevin Plucknett for their guidance throughout the whole research. Thanks are also due to Ms. Patricia Scallion for the SEM assistance and Mr. Dean Grijm for the support in sample machining. He would also like to thank Winston Mosher and Steve Buchholz for the help in the lab and friendship for all these days.

Chapter 1. INTRODUCTION

Titanium was discovered independently in the 18th century by William Gregor and Martin Heinrich Klaproth. It then took more than a century for scientists to isolate this metal. Matthew Albert Hunter from Rensselaer Polytechnic Institute in N.Y. was the first able to extract titanium in 1910 (Peters et al., 2003). In nature, titanium exists in the form of an oxide, and can be found in magmatic hard-rock, beach or alluvial placer deposits (Cardarelli, 2008). Titanium is the ninth most abundant element in the earth's crust and the fourth amongst all metals, following iron, aluminum and magnesium (Polmear, 2005).

Titanium and its alloys have many advantages over other materials: high corrosion resistance, good oxidation resistance below 600°C, high specific strength, and excellent bio-compatibility (Lutjering & Williams, 2003). However, the excellent properties of titanium have yet to lead to wide spread applications, indicating that the abundant quantity does not guarantee a broader usage. The core problem is the relatively high costs related to titanium extraction (purification, processing) and metalworking. Consequently, titanium use has been largely restricted to the demanding, high performance aerospace, military and biomedical industries wherein costs are less of a concern.

In order to tackle this problem, extensive investigations have been carried out on titanium. Many technologies have been developed to reduce the cost (Hurless & Froes, 2002; Pickens, 2004). Among the potential solutions, the powder metallurgy (P/M) process has demonstrated several economic advantages, such as low material wastage and energy consumption. In fact, many titanium alloy parts have been successfully fabricated by P/M approaches. For example, P/M Ti-6Al-4V components have been made for aircraft and automobiles (Pickens, 2004; Polmear, 2005). Some titanium P/M products have shown equal or even better mechanical properties over cast or wrought products (Froes et al., 2004; German, 2005). However, some of the properties, such as the fatigue life and ductility (Ivasishin et al., 2004; Petit et al., 1992), still cannot compete with conventionally made products. Considerable effort has been put into titanium P/M

development to improve the inferior properties. Moreover, new technologies have been invented to reduce the costly powder fabrication. Some studies were based on the traditional extraction methods (Crowley, 2003; Deura et al., 1998), while other efforts examined alternate routes (Ward-Close et al., 2005). With the efforts targeted at both performance improvement and process cost cutting of titanium and its alloys, increased application areas and higher usage are anticipated for the future.

The present thesis reports on a fundamental study of titanium produced by the P/M approach in order to better understand the influence of various processing parameters and the related properties. This study has focused mainly on the economical "press-and-sinter" P/M technique. Variables relating to both the compaction and sintering stages were examined and the resultant properties, in terms of densification and mechanical behaviour, were measured.

Pertinent background information relating to titanium and its alloys is addressed in Chapter 2, which includes general titanium properties, the classification of titanium alloys as well as the principles of P/M practice. The experimental study focusing on commercially pure titanium is reported in Chapter 3 in the form of a submitted journal article (submitted to *Powder Metallurgy*, August 2011). In this paper, the experimental procedures are outlined in detail and the P/M processing of commercially pure titanium is investigated and discussed in depth with respect to the sintering response, mechanical properties and microstructural evolution. Two binary titanium systems, Ti-Ni and Ti-Sn, are investigated and reported in Chapter 4. This aspect aims at facilitating the sintering process by means of either persistent or transient liquid phase sintering. Preliminary results are presented and discussed. The overall conclusions relating to the research are then outlined in Chapter 5. This chapter also presents several suggestions and recommendations for future work, based on the prior outlined information from Chapters 3 and 4.

Chapter 2. BACKGROUND

2.1 TITANIUM BASICS

2.1.1 General properties

Titanium has a lustrous gray appearance and it is classified as a light metal. The density of titanium falls between the two major commercial metals: iron and aluminum. Consequently, titanium is typically compared with these two metals (Table 1) (Smith, 1992). Titanium has a much lower density compared to iron (i.e. 57% that of iron) while it and its alloys provide comparable or higher yield strengths (at 0.2% offset), ranging from 470 to 1800MPa (Cardarelli, 2008), than the iron counterparts. As a consequence, titanium possesses an excellent strength-to-weight ratio. On the other hand, although titanium is heavier than its competitor aluminum, it has much higher strength particularly at elevated temperatures. This is because titanium has a high melting temperature of 1668°C, which is an indication of potential for use in high temperate applications. In fact, many titanium alloys have shown adequate strength up to 500°C (Cardarelli, 2008).

Combining the high strength-to-weight ratio with good high temperature strength ensures that titanium is very appealing to the aerospace industry. As a result, more than 50% of titanium metal is used as aerospace parts such as gas turbine engine components and air frames (Polmear, 2005).

Table 1. Comparison of selected properties for Fe, Ti and Al (Smith, 1992).

Properties	Iron	Titanium	Aluminum
Density (g/cc)	7.87	4.51	2.70
Melting point (°C)	1536	1668	660
Crystal structure at room temperature	FCC	HCP	BCC

Titanium also possesses excellent corrosion resistance as it forms a protective oxide layer (TiO_2, 1.2 to 1.6 nm thick) on a clean surface almost immediately when exposed to the atmosphere (Cardarelli, 2008). The TiO_2 layer is highly immune against attack from mineral acids such as HCl, H_2SO_4 or chlorides (Cardarelli, 2008). This impermeable oxide film can regenerate itself with the presence of oxygen or moisture, and continues to grow at a very low rate (25 nm in 4 years) (Cardarelli, 2008). As a result, one of the more favourable applications of titanium is for use in corrosive environments, such as chemical processing and petroleum piping. In addition, the modulus of pure titanium is closer to that of human bones when compared to other metals (e.g. steel), and it is both non-toxic and biocompatible with human tissues and bones. As a consequence, titanium has also proven to be an ideal candidate for many biological applications.

Titanium exists with a hexagonal closed-packed (HCP) crystal structure (α) from room temperature up to the β transus temperature, at 883°C. Above this temperature, titanium experiences an allotropic phase transformation from the HCP (α) to a body-centre cubic (β) structure (Smith, 1992). This crystallographic change enables the possibility of significant microstructural modification (α, β or α/β mixed) for titanium alloys through thermal or thermomechanical processing. Similar to the heat treatment of steel, the high temperature phase can be retained by quenching or with the aid of suitable stabilizers. With sufficient β stabilizer, the high temperature stable phase can be retained to room temperature. Hence the physical or mechanical properties can be adjusted in terms of the HCP and BCC structure combination.

2.1.2 Effects of alloying elements

Interstitial and substitutional solutes can not only strengthen titanium by means of solid solution strengthening but also have the ability to change the crystal structure. These alloying elements can be classified into three groups: α or β stabilizers, and neutral elements, as can be seen in Table 2 (Polmear, 2005). Each alloying element imparts different levels of effect on the titanium crystal structure. The effectiveness and proper operating ranges of these elements are based on empirical knowledge (Polmear, 2005).

Table 2. Classification of solutes for titanium alloys (Polmear, 2005).

Type	α stabilizer	β stabilizer	Neutral
Element	Al, O, N, C, Ga	Mo, W, V, Ta, Cu, Mn, Cr, Fe, Ni, Co, H	Zr, Sn, Si

In terms of functionality, an α stabilizer dissolves favourably in the HCP phase and raises the β transus temperature. Consequently, the α phase domain is expanded with increasing solute content, as shown in Fig. 1 (a) (Polmear, 2005). The dotted phase boundaries refer to an ordered compound, α_2 (e.g. Ti-Al system), which will be discussed later. On the other hand, β stabilizers promote the region of β's existence. There are two types of β stabilized systems, as demonstrated in Fig. 1 (b), (c) (Polmear, 2005). For the first of these, the β stabilizer can dissolve completely in the matrix forming an isomorphous system, as shown in Fig. 1 (b), whereas other β stabilizers may undergo a eutectoid reaction and form a compound. However, the eutectoid reactions are sometimes slow (e.g. Ti-Fe, Ti-Mn system) and those reactions can often not be observed, as indicated through the arrows on Fig. 1 (c). Neutral elements do not strongly promote phase stability, have considerable solid solubilities in *both* α and β phases, and can retard the transformation rate (Polmear, 2005). Among them, tin and zirconium are commonly added to the titanium alloys to promote strengthening by solid solution hardening.

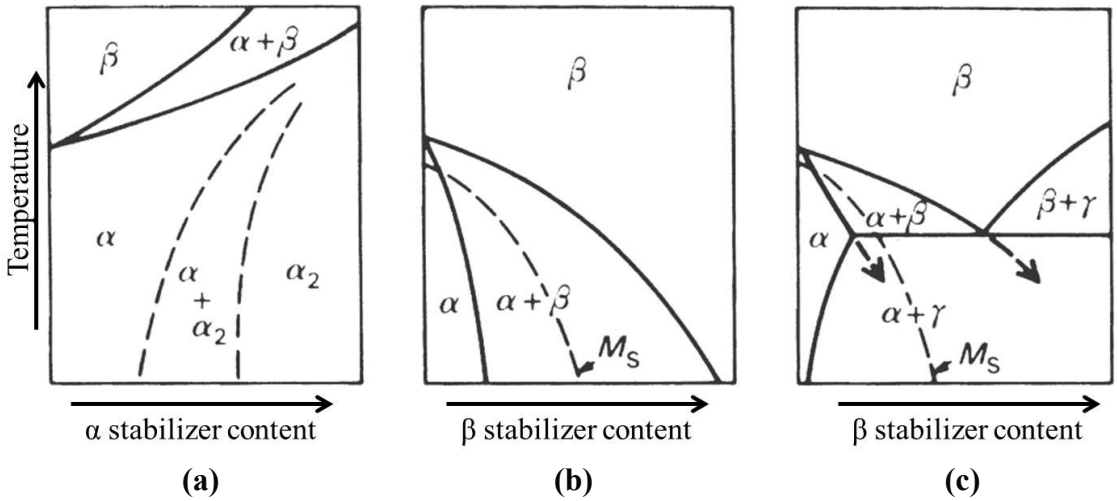

Fig. 1. Basic types of phase diagrams of titanium alloys demonstrating the effects of alloying element additions (a) α stabilizer, (b) β stabilizer forming isomorphous β, and (c) β stabilizer forming eutectoid β phase. It should be noted that M_S is the martensitic α phase (α') starting temperature (Polmear, 2005).

The properties of titanium alloys are primarily determined by the microstructural morphology, namely, the relative volume fraction and properties of the α and β phases. Compared to the β phase, the α phase has a higher resistance to plastic deformation, lower ductility and higher creep resistance (Polmear, 2005). However, it should be noted that *pure titanium* is very ductile; more than a 90% thickness reduction can be achieved through cold rolling (Polmear, 2005). This unusual deformability, compared to other HCP metals (such as Zn, Mg, Co and Zr), is due to the lower c/a axis ratio (1.587) of titanium, which creates more slip systems and twinning planes within the HCP unit cell (Polmear, 2005).

2.1.3 Classification of titanium alloys

Similar to the function of the solute elements, titanium alloys are also separated into three categories (i.e. α, α+β and β alloys) depending on the existing phase(s). Additionally, near-α and near-β are also mentioned on occasion. The classification based on the phase(s) present can be the result of solute stabilization and heat treatment; composition is not the only determinant in this respect.

2.1.3.1 Commercially pure titanium

Titanium which has 99% to 99.5% purity is categorized as commercially pure (CP) titanium. CP titanium is usually discussed distinctly from α alloys, given that it is the second most used form in terms of overall titanium consumption (Polmear, 2005). The ASTM classification stipulates the maximum solute concentrations in the CP titanium as grade 1 to 4 (Table 3) (Cardarelli, 2008). These elements are usually impurities from the environment or extraction processes, but are sometimes added on purpose because those interstitial elements (i.e. oxygen, nitrogen and carbon) greatly increase strength though at the sacrifice of ductility (Fig. 2) (Polmear, 2005). It should be noted that oxygen is the most potent enhancer of tensile properties. Of the remaining elements presented in Table 3, the iron content is mostly present as a contaminant from the reaction vessel in the titanium extraction process; hydrogen should also be avoided because of its detrimental effect (e.g. brittle titanium hydride).

Table 3. Chemical (wt%) and mechanical specifications for ASTM grades of titanium (Cardarelli, 2008).

ASTM grade	N	C	H	Fe	O	Tensile strength,	Yield strength,	Elongation, %
1	0.03	0.08	0.015	0.20	0.18	241	172	24
2	0.03	0.08	0.015	0.30	0.25	345	276	20
3	0.05	0.08	0.015	0.30	0.35	448	379	18
4	0.05	0.08	0.015	0.50	0.40	552	483	15

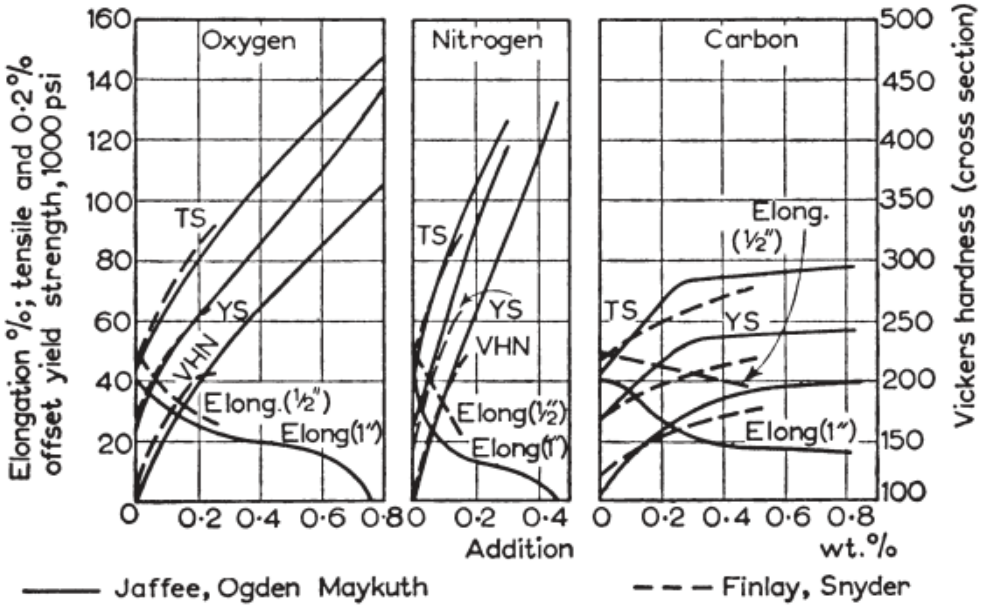

Fig. 2. Effects of the interstitial solutes (oxygen, nitrogen and carbon) on the mechanical properties of CP titanium (Polmear, 2005).

2.1.3.2 α alloys

Among the α stabilizers, oxygen and aluminum are the most important. As mentioned earlier, oxygen enhances the strength greatly. Aluminum on the other hand not only reduces the density but also provides good oxidation resistance. The α alloys are generally used in the annealed or stress-relieved condition where the resulting microstructure is composed of equiaxed grains (Polmear, 2005). This type of structure is ideal for working in a corrosive environment, because the equiaxial microstructure gives no clear attacking spot for corrosion.

In practice, there are limits on the α stabilizer contents, and their relative stabilizing effects usually are expressed in terms of the oxygen and aluminum equivalents (wt%). These empirical equations are:

$$Eq(Al) = W_{Al} + 1/3W_{Sn} + 1/6W_{Zr} + 10W_O \qquad Eq.\ 1$$

$$Eq(O) = W_O + W_{Mo} + (1.2 \text{ to } 2.0)W_N + 0.67W_C \qquad Eq.\ 2$$

These equations indicate that, for example, adding 1 wt% oxygen has the same α stabilizing effect as 10 wt% of aluminum. The aluminum equivalent is normally restricted below 9% in order to avoid the formation of the ordered phase α_2. The α_2 intermetallic, which is in the form of Ti_3X (e.g. Ti_3Al), is a finely dispersed, ordered and coherent brittle phase. The presence of the α_2 phase is detrimental to the mechanical properties (Polmear, 2005). However, the aluminum is invariably further limited to 5~6% owing to unintentional contaminations.

In the α alloy category, many examples (including CP-titanium) contain a small amount of β phase because of the inherent iron impurities. However, a minor amount of β stabilizer is sometimes added (2 wt%) to introduce some amount of this phase (Polmear, 2005). This type of alloy is termed "near-α". The β stabilizer is added to improve the forgeability and to gain some further flexibility to heat treat or change the microstructure of the alloy.

2.1.3.3 α/β alloys

Due to the restricted content of α stabilizer and the difficulties with hot forming of the HCP structure, α alloys have faced certain limitations in their development. Conversely, the β-based alloys have better forgeability and ductility. Hence incorporating β phase into the α alloy structure can overcome many manufacturing obstacles. In fact the dual phase α/β alloys are the most commonly used form of titanium, particularly Ti-6Al-4V, which is the most important alloy in the titanium industry. The major application of Ti-6Al-4V is in the production of forged components, for instance the fan blades of jet engines. The two-phase microstructure usually exhibits the characteristic "basket weave" Widmanstatten pattern, as shown in Fig. 3 (Polmear, 2005), which can provide relatively high tensile strengths.

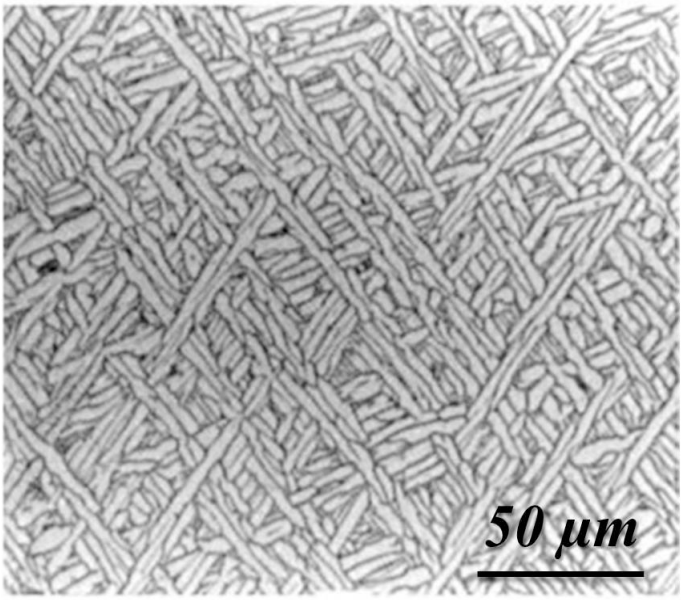

Fig. 3. Widmanstatten pattern of Ti-6Al-4V slowed cooled from β phase (Polmear, 2005).

2.1.3.4 β alloys

The β alloys are invariably referred to as metastable, because there is no commercially available stable β alloy. The heavily-alloyed stable β titanium is high in density and low in ductility. However, to retain metastable β phase a sufficient amount of β stabilizer is necessary. The β phase, due to its BCC structure, is the most easily forged and machined structure when compared to the α phase. From the literature, there is an equivalence equation (Polmear, 2005)expressed by molybdenum content, for the β alloys:

$$Eq(Mo) = W_{Mo} + 1/5W_{Ta} + 1/3.6W_{N} + 1/2.5W_{W} + 1/1.5W_{V} + 1.25W_{Cr} + 1.25W_{Ni} + 1.7W_{Mn} + 2.5W_{Fe} \qquad Eq.\ 3$$

The molybdenum equivalent, together with the aluminum and oxygen equivalents outlined previously, are useful when designing a titanium-based alloy.

2.1.4 Titanium production (ore extraction)

Today the production of titanium is mainly performed using the Kroll process, which was developed in the late 1930s (Sibum, 2003). The production route begins with either rutile or ilmenite ore. Rutile, which is titanium dioxide (TiO_2), is often mined from alluvial deposits. It has been used as the primary raw material for the extraction of titanium due to its higher purity. Ilmenite ($FeTiO_3$), on the other hand, contains more iron and other impurities which will affect the properties of the subsequent product. Hence, prior refining treatments are required for ilmenite (Lutjering & Williams, 2003). Once the rutile is mined, it is then combined with petroleum coke and chlorine in a fluid bed reactor at 1000°C. The reactions in this environment are as follows (Lutjering & Williams, 2003):

$$TiO_{2\,(s)} + 2Cl_{2\,(l)} + C_{(s)} \rightarrow TiCl_{4\,(g)} + CO_{2\,(g)} \qquad \textit{Eq. 4}$$

$$TiO_{2\,(s)} + 2Cl_{2\,(l)} + 2C_{(s)} \rightarrow TiCl_{4\,(g)} + 2CO_{(g)} \qquad \textit{Eq. 5}$$

The titanium dioxide is chlorinated and turns into gaseous titanium tetrachloride ($TiCl_4$). The gaseous products are sent to a fractional distillation unit to filter out the unwanted CO and CO_2. The purified liquid $TiCl_4$ is then slowly fed into a retort and reacts with molten magnesium at 900°C in an argon atmosphere. In the sealed retort, $TiCl_4$ is reduced back to metallic titanium by the magnesium. The reduction reaction is:

$$TiCl_{4\,(l)} + 2Mg_{(l)} \rightarrow Ti_{(s)} + 2MgCl_{2\,(s)} \qquad \textit{Eq. 6}$$

After a few days, the reducing reaction reaches the equilibrium state. The reaction forms a sintered, porous mass of a combination of titanium, salt, and unreacted chemicals. The bulk mass is called “sponge cake”. The next step is to remove the unreacted chemicals and the reaction by-product, $MgCl_2$. Conventionally, the sponge cake is

cleaned by acid leaching, followed by washing with water and then drying. However, any residual acid will contaminate the sponge cake and have a detrimental effect on subsequent properties. This purifying can also be done by an inert gas sweep or vacuum distillation, which typically results in a cleaner product. Fig. 4 illustrates the semi-continuous Kroll reactor and vacuum distillation chamber (Lutjering & Williams, 2003).

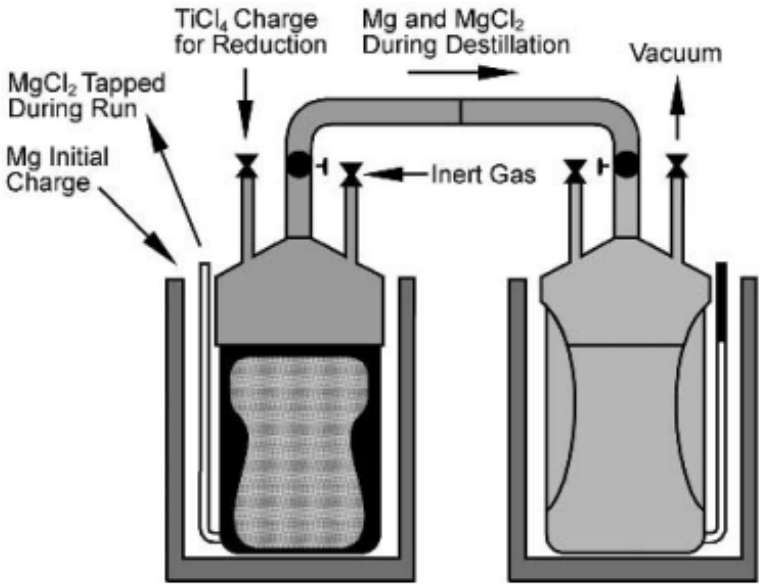

Fig. 4. Schematic of the Kroll reactor and vacuum distillation chamber (Lutjering & Williams, 2003).

The cleaned sponge cake is then crushed and ground into smaller granules, typically to less than 3-5 cm, on average. Later the sponge powder can be used for implementation in either a P/M or melting procedure. The whole titanium sponge manufacturing process is shown schematically in the flowchart in Fig. 5.

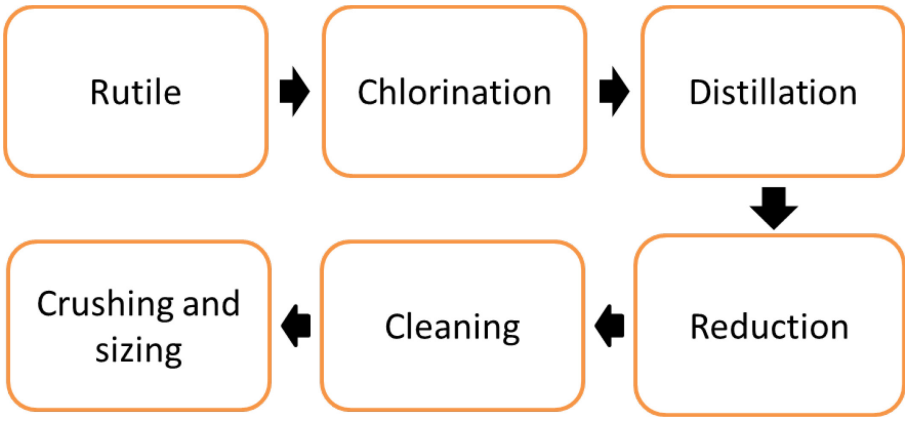

Fig. 5. The Kroll process stages.

Instead of crushing into finer particles, the bulk sponge can also be compressed into an electrode form to produce ingots for mill products and the remelt stock for casting. The titanium is melted in a vacuum arc remelt (VAR) furnace or in a cold hearth melting (CHM) furnace (Lutjering & Williams, 2003). Alloying elements or titanium scrap can be added at this time. The electrode is usually remelted two or three times for further purification.

Developed earlier than the Kroll method, the Hunter process was invented in 1910 (Lutjering & Williams, 2003), and was the first industrial titanium extraction procedure. The Hunter and Kroll processes are generally similar in that both extraction methods convert TiO_2 to $TiCl_4$. The major difference is the reductant being used. In the Hunter process, $TiCl_4$ is reacted with molten sodium. Table 4 shows the reactions involved in each of the methods (Lutjering & Williams, 2003).

Table 4. The Kroll and Hunter reactions for titanium production (Lutjering & Williams, 2003).

Method	Reaction	Temperature
Kroll	$TiCl_4 + 2Mg \rightarrow Ti + 2MgCl_2$	900°C
Hunter	$TiCl_4 + 4Na \rightarrow Ti + 4NaCl$	700–800°C

During the period between 1960 and 1990 there was a significant amount of titanium sponge manufactured using the Hunter process (Lutjering & Williams, 2003). However, due to the higher operational cost in comparison with the Kroll process, there is only small scale Hunter production today, and the last Hunter-based processing plant was closed in 1993 (Deura et al., 1998). Other metallic titanium extraction processes, such as electrowinning and electrolytic refining, have also faced the same economic difficulties and are only operated on a small scale nowadays (Lutjering & Williams, 2003).

2.2 POWDER METALLURGY

2.2.1 Powder fabrication

Though elemental titanium powder can be acquired directly after the Kroll process, different applications mandate varying powder requirements. For instance, some applications require very high purity, for demanding performance, or ultra-fine particles, for superplasticity (Hopkins, 2010). Besides producing titanium powders from sponge, they can also be made from ingots in order to obtain both higher quality (i.e. purity) and alloyed powders. Fig. 6 indicates the relationship between various types of powder production. Powder fabrication methods such as the hydride-dehydride (HDH) process, rotation electrode process (REP) and gas atomization method will be introduced in this section.

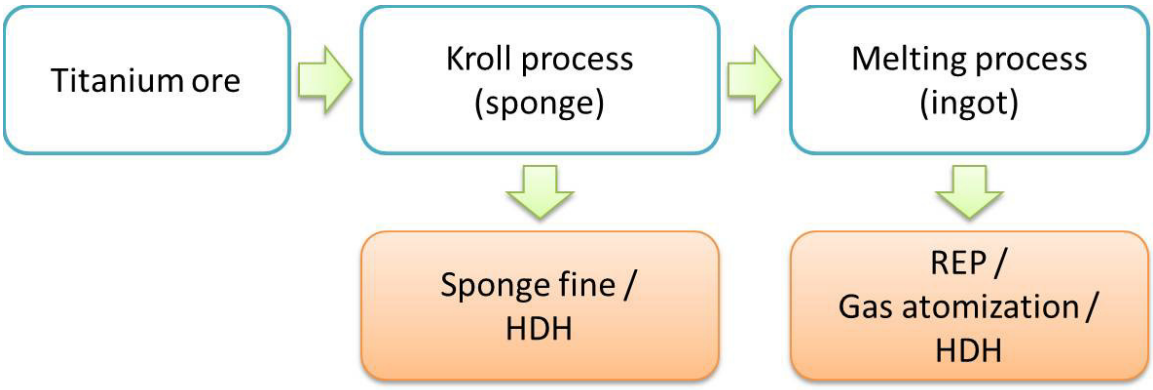

Fig. 6. Titanium powder development chart.

2.2.1.1 Sponge powder

When the sponge titanium mass is acquired from the reduction reaction it is removed for the production of titanium sponge powder. The small particles formed directly from the reduction retort are called the "sponge fines". These fine powders range down to 80 mesh in size (approximately 200 μm) (Lutjering & Williams, 2003). The coarser granules and large chunks of the sponge mass are crushed into smaller particles.

Fig. 7 shows a scanning electron microscope (SEM) image of titanium sponge powder. The porous morphology makes the removal of impurities very difficult. Even extensive attempts to clean the residual chlorine impurities show little success because the deep recesses of the porous morphology are not able to be flushed thoroughly or gas purged. Hence, the residual chlorine level is generally around 1,000-2,000 ppm in the leached titanium sponge (Hanson et al., 1990). As a consequence, residual chlorine has been a serious concern for the sponge powders. The remaining chlorine could hinder the attainment of high sintered density and chloride inclusions dispersed in the microstructure can create a network of potential fatigue failure nucleation sites (Hanson et al., 1990).

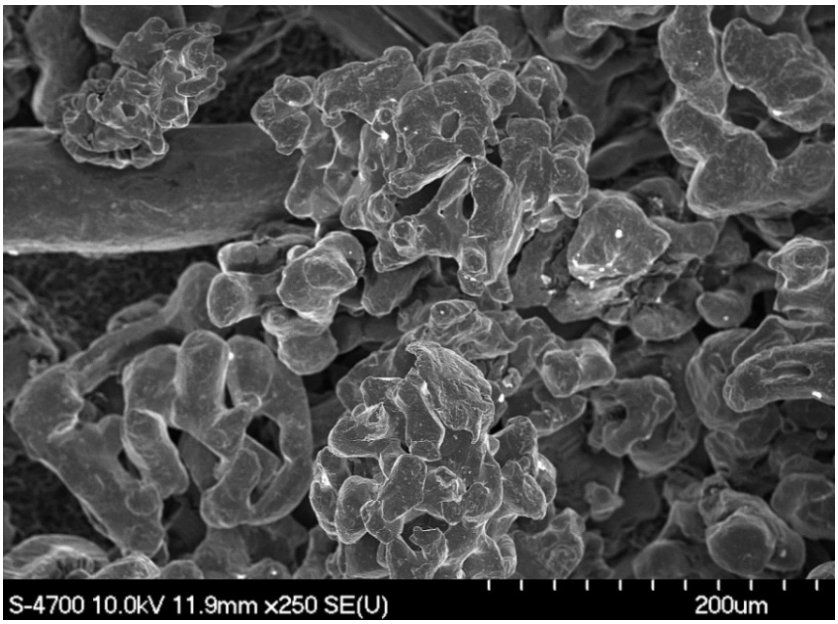

Fig. 7. SEM micrograph of sponge titanium.

2.2.1.2 Hydride-dehydride process

The hydride-dehydride process helps the breakdown of titanium powders. It can be applied to either unalloyed or alloyed titanium, and is able to deal with many forms of titanium such as the Kroll sponge mass, ingots or chips.

In this process, titanium feedstock is initially heated to 350-700°C under a hydrogen atmosphere (Lutjering & Williams, 2003). This prompts the formation of titanium hydride (TiH_2) without difficulty, owing to the great affinity of titanium to hydrogen at high temperature. The TiH_2 is highly brittle and can be easily crushed and milled into small particles until the desired size is achieved. Subsequently, the ground product is heated at 700-800°C under vacuum to reverse the hydrogenation reaction and thereby form metallic titanium once again. The reactions associated with this process are (Lutjering & Williams, 2003):

$$Ti_{(s)} + H_{2(g)} \rightarrow TiH_{2(s)} \qquad \textit{Eq. 7}$$

$$TiH_{2(s)} \rightarrow Ti_{(s)} + H_{2(g)} \qquad \textit{Eq. 8}$$

If the titanium feedstock is refined through vacuum arc melting, the resulting HDH powder has a lower level of residual chlorine compared to the sponge source. Although the HDH powder could contain very low residual chlorine, the oxygen content may increase during the process (i.e. hydrogenation, grinding), depending on the quality of hydrogen and the degree of vacuum used (Lutjering & Williams, 2003). The increase in oxygen enhances strength, due to interstitial strengthening. However, the oxygen also lowers ductility and fatigue strength (Donachie, 2000c). Fig. 8 shows an SEM micrograph of a typical HDH powder. The angular but irregular powder shape provides a better packing density but less particle interlocking compared to sponge fines.

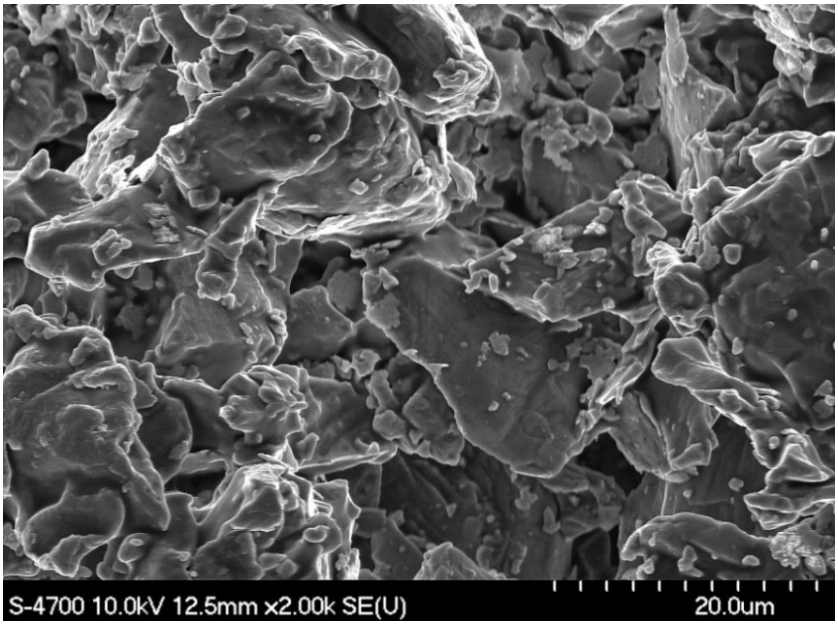

Fig. 8. SEM micrograph of a typical HDH titanium powder.

2.2.1.3 Rotating electrode process

The other titanium powder fabrication category is the molten metal fragmentation approach, also known as atomization process. These methods produce powder using molten metal to form small droplets. The droplets can be produced by two primary techniques, namely the rotating electrode process (REP) and the gas atomization method.

For the REP approach an arc is generated by a tungsten electrode in an atmosphere controlled chamber, and then focused onto the surface of a rotating bar of titanium. The arc generates a considerable amount of heat and melts the titanium locally. The melt is then spun out from the end of the rotating bar by centrifugal force. This forms droplets that then solidify rapidly during their free falling route, with surface tension making the droplets spherical in shape. Fig. 9 illustrates a schematic of the process chamber (Lutjering & Williams, 2003). During the process, the tungsten electrode may be eroded, which is a source of contamination in the finished product. In some scenarios, the heating source can be replaced with a plasma torch. Here, the technique is referred to as the plasma rotating electrode process (PREP). Although PREP eliminates tungsten contamination, it creates a huge amount of fumes in the form of fine particulate matter. Those very fine particles then have to be removed before the powder is consolidated.

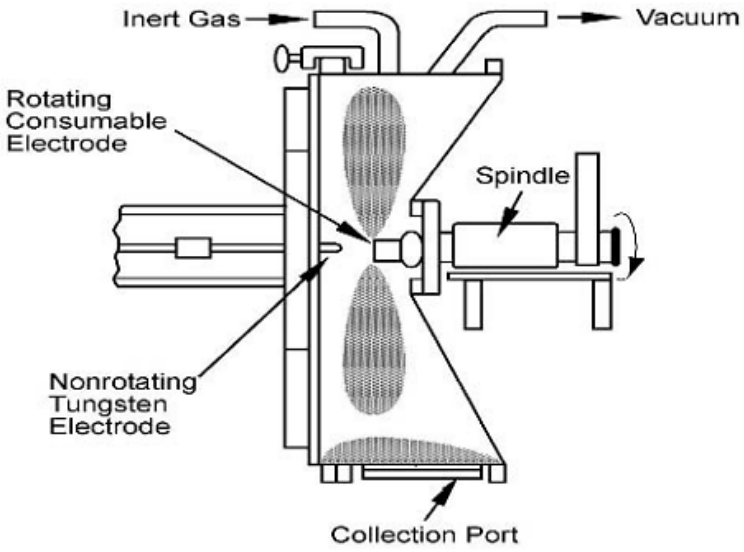

Fig. 9. A schematic representation of the REP for titanium powder synthesis (Lutjering & Williams, 2003).

Fig. 10 shows an SEM image of a typical spherical powder fabricated using the REP process (Lutjering & Williams, 2003). Powder made by this method has a uniform spherical particle size with little variation. The actual particle size depends on the rotational velocity of the electrode. Usually the REP derived powder has a larger average size when compared to a gas atomized powder (described later). The spherical shape promises a higher packing and tap density, which can be as high as 70% by volume (Lutjering & Williams, 2003). However, the spherical powder cannot be cold compacted well, owing to the lack of an interlocking geometry.

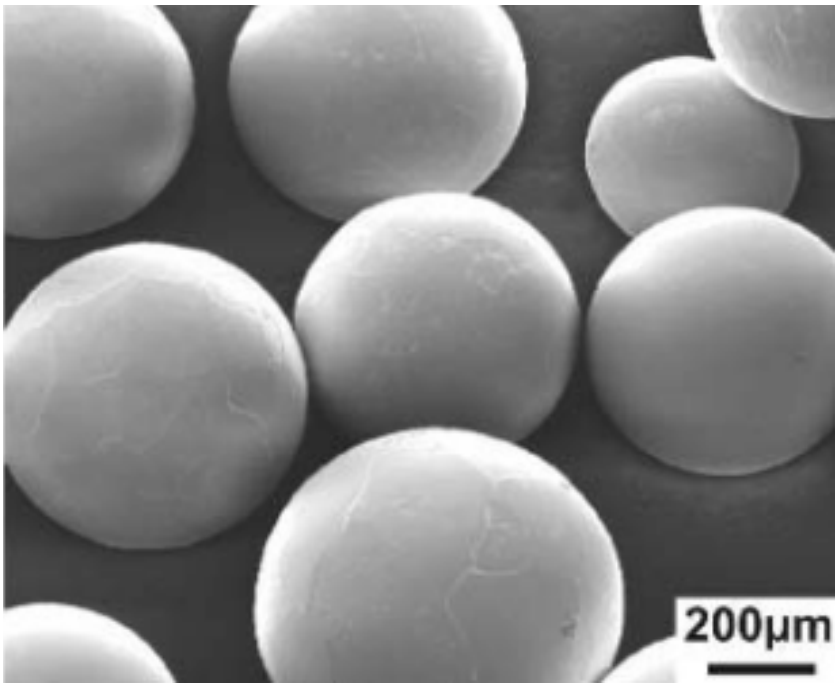

Fig. 10. A SEM micrograph of titanium powder produced using the REP (Lutjering & Williams, 2003).

2.2.1.4 Gas atomization process

In a gas atomization process, the raw material is melted in a crucible and then flows through a small nozzle into a vacuum chamber. The metal stream exiting the nozzle is struck by a rapidly expanding high pressure gas, as depicted schematically in Fig. 11 (Lutjering & Williams, 2003). The metal stream is broken up by the gas, and falls freely down to the chamber bottom. The broken stream first forms a hollow cone, and then into the shape of a sheet, ligament, ellipsoid, and finally a sphere provided that the rate of solidification is slow enough.

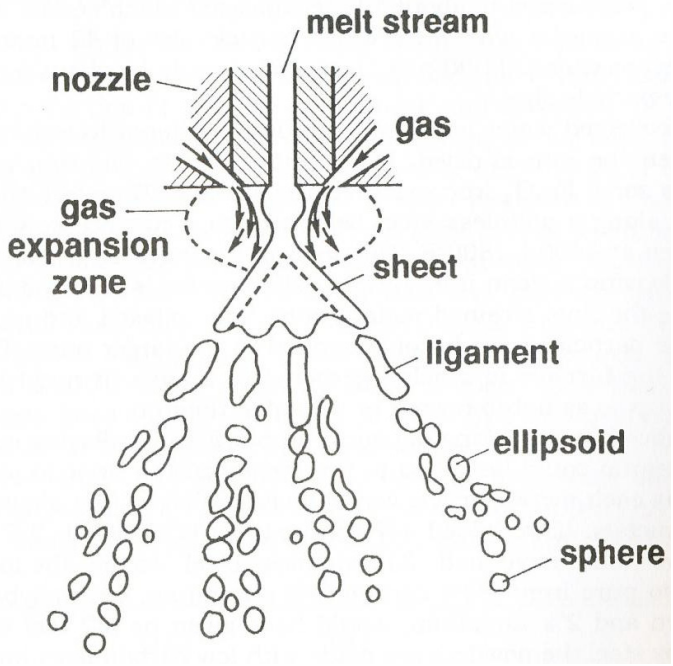

Fig. 11. Formation of metal powder by gas atomization near the gas nozzle (Lutjering & Williams, 2003).

The gas atomization process has been successfully used for producing iron, steel, copper and other metallic powders. However, the conventional gas atomization process does not work well for titanium. Titanium melt can easily be contaminated by the crucible because of its high reactivity at elevated temperature. Hence, a modified atomisation process is needed. The Crucible Materials Corporation has developed the

vacuum-induction skull-melting gas atomization process for titanium powder production (Fig. 12) (Moll, 2000). The main feature of this system is a cold hearth skull melter. The water-cooled copper crucible keeps the outer layer of the melt remaining solid. The titanium is melted from the core of the feedstock by a heat induction device. As a result, the melt is only in contact with solid titanium ensuring that no reaction or impurity diffusion will occur. In addition, the high pressure jet should only be an inert gas to further minimize contamination.

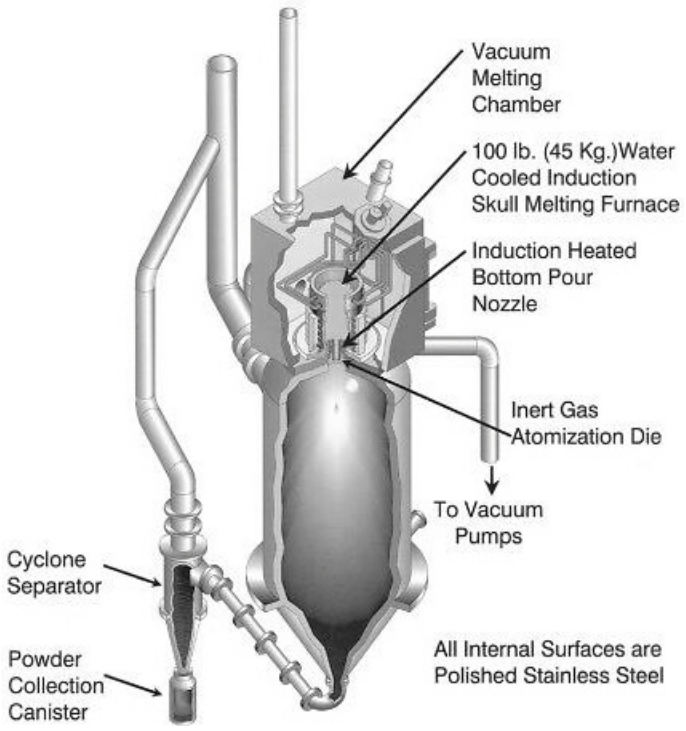

Fig. 12. Crucible Materials' gas atomization process (Moll, 2000).

The structure of gas atomized titanium powder is shown in Fig. 13. As can be seen the particle size is relatively small, and usually smaller than can be achieved with REP powders. It should be noted that with the gas atomised powder there are typically "satellites", which are fine particles attached to the larger primary powder. This can occur if the cyclone separator fails to completely filter the fine particles thereby enabling them to be re-introduced into the atomization zone (German, 2005).

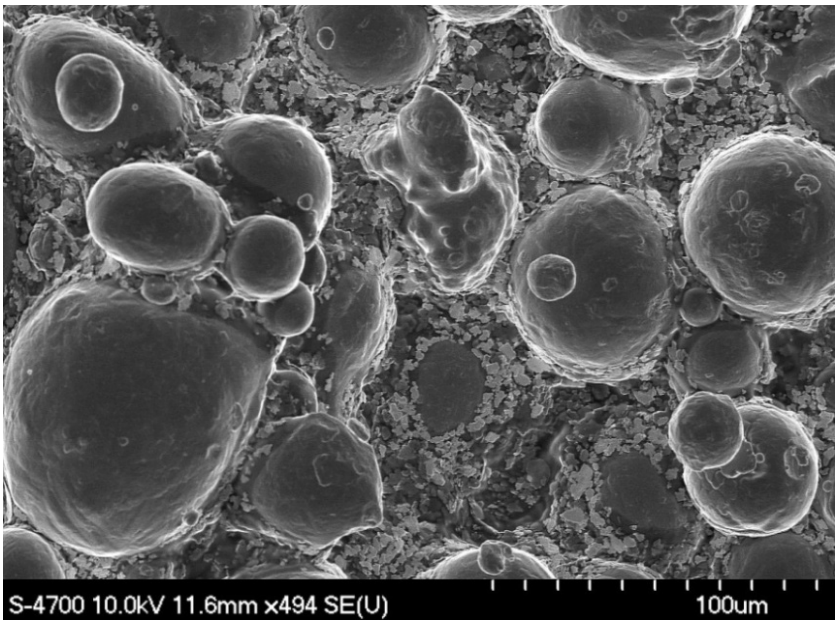

Fig. 13. SEM micrograph of gas atomized titanium powder.

2.2.1.5 Current state-of-the-art in titanium powder manufacturing

The extraction methods used for metallic titanium have remained essentially unchanged for decades, since the Hunter and Kroll processes were invented in the 1910s and 1940s, respectively. After the Hunter process was no longer in commercial operation, the supply of titanium powder and ingot has largely relied on the Kroll process. The slow development of titanium synthesis routes is due to technical difficulties and the lack of market demand owing to the high production costs (Crowley, 2003).

However, in recent years, several new powder fabrication processes have been developed to lower the cost. Some processes such as the Armstrong process from International Titanium Powder (ITP) (Crowley, 2003) and the $TiCl_4$ gas injection method from Japan (Deura et al., 1998) modify the Kroll and Hunter methods. Those processes aim to improve productivity and demonstrate potential cost reduction. Furthermore, a whole new titanium extraction method, named the electro-deoxidation process (EDO), has been invented in recent years (Ward-Close et al., 2005). It has great potential to decrease the cost of titanium production from direct extraction of titanium oxides. Fig. 14

illustrates the recent developments in titanium powder production. In this section the EDO and Armstrong process will be discussed.

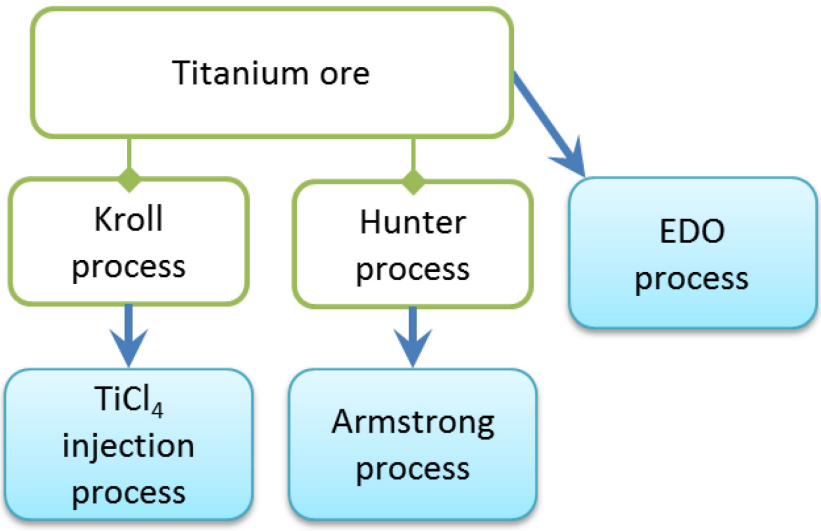

Fig. 14. Recent titanium powder development approaches.

The EDO process, also known as the FFC (Fray, Farthing and Chen) Cambridge process, was invented at Cambridge University in 1997 (Ward-Close et al., 2005). Since early 2000, QinetiQ in the UK has scaled up the process (later adopted by Metalysis), successfully producing commercial grade CP titanium powders and some that are alloyed (Mohandas, 2004; Ward-Close et al., 2005). This process is divergent from the conventional Kroll and Hunter processes in that it does not require the expensive chlorination stage. Therefore, the $TiCl_4$ in the Kroll process, as presented in Fig. 15 (Lutjering & Williams, 2003), can be completely eliminated.

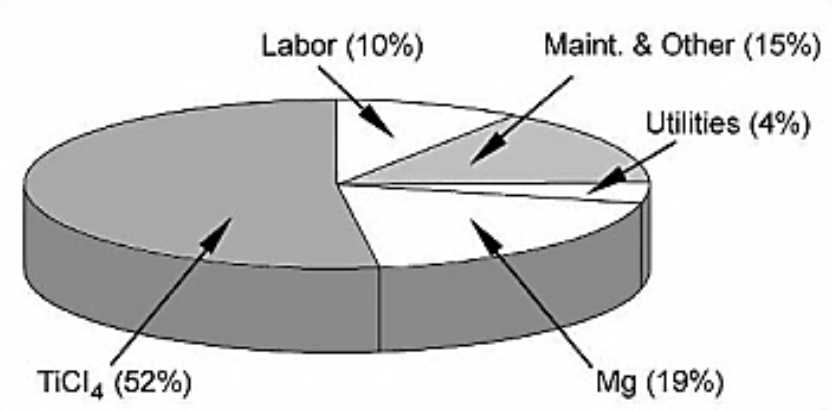

Fig. 15. Cost breakdown of conventional titanium sponge production (Lutjering & Williams, 2003).

The EDO process uses molten salt electrolysis to directly convert titanium dioxide into pure metallic titanium. Fig. 16 schematically illustrates the reactions occurring in this method (Ward-Close et al., 2005). Unlike aluminum and magnesium production, the EDO process is different from conventional electrolytic powder production. Here, the titanium dioxide does not dissolve in the electrolyte. Instead, the oxygen diffuses from the metal oxide and leaves pure titanium. The oxygen ions are attracted to the graphite anode and form oxygen and carbon monoxide or carbon dioxide bubbles. As a consequence, the cathode becomes oxygen-free, pure titanium. The microstructure of the residual titanium cathode is shown in Fig. 17 (Ward-Close et al., 2005). The particle morphology can be classified as “spongy”, but not like the titanium sponge which possesses a lot of internal porosity.

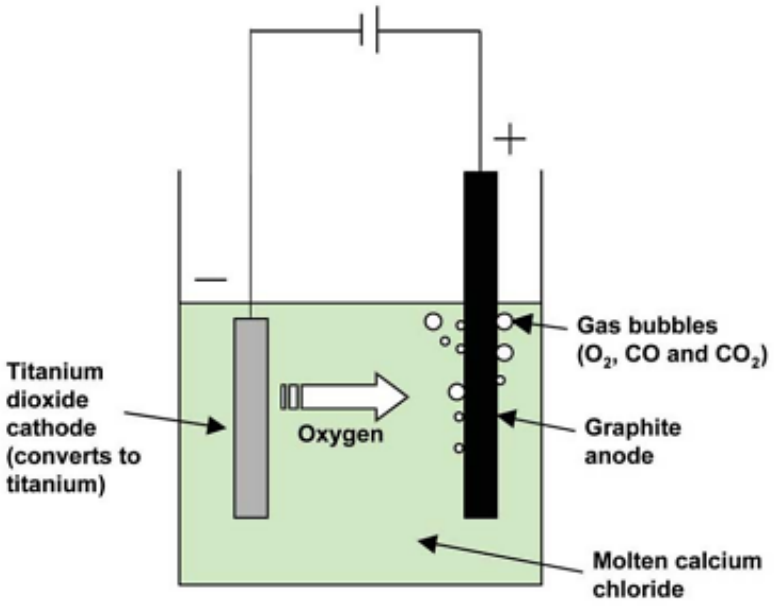

Fig. 16. Schematic representation of the EDO process (Ward-Close et al., 2005).

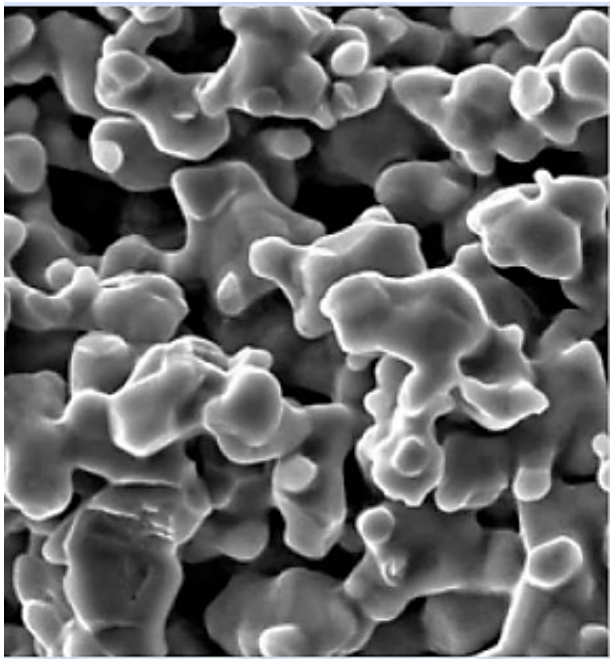

Fig. 17. SEM micrograph of EDO derived titanium powder (Ward-Close et al., 2005).

In the EDO process reaction, only the oxygen is extracted from the compacted cathode. Therefore, the residual impurities within the titanium dioxide are the major consideration for the EDO process. Furthermore, prealloyed powder can be acquired using an appropriate elemental oxide mixture. For instance, the Ti-6Al-4V powder can be directly produced from a titanium, aluminum and vanadium oxide mix sintered block from the cathode (Ward-Close et al., 2005).

The Armstrong process is based on the Hunter extraction technique, with both methods using sodium as the reductant. The major difference relates to the reaction zone design, as illustrated in Fig. 18 (Crowley, 2003). Here, a flowing sodium liquid loop is applied, enabling sodium to be recycled, filtered, and re-injected back into the reactor. The conventional Hunter batch process is consequently turned into one that is continuous.

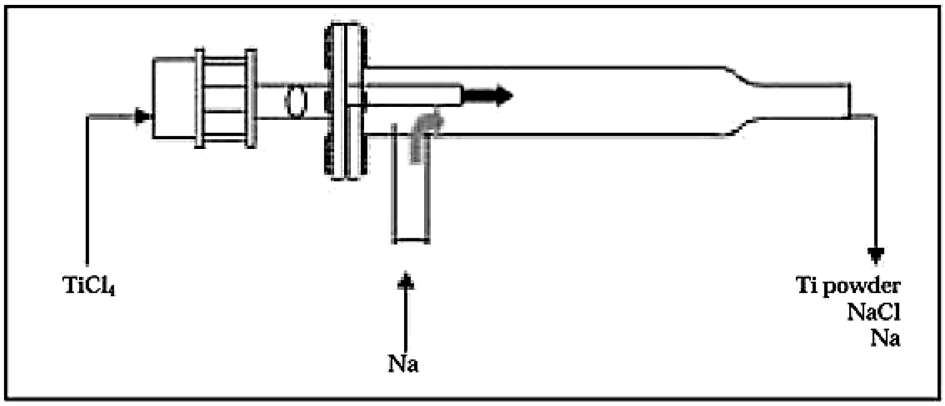

Fig. 18. Schematic diagram of the Armstrong process reactor (Crowley, 2003).

During operation, a controlled and continuous injection of $TiCl_4$ vapour reacts with the constant flow of molten sodium. The flow of sodium prevents the growth of the product, which could trap unreacted raw materials or co-products (Crowley, 2003). Hence, the result is purer and finer titanium powders. Fig. 19 shows the typical powder morphology that can be achieved using the Armstrong process (Crowley, 2003). The powder shape and size distribution can be controlled by the relative flow rate and the geometry of the reaction zone. The solid titanium is then collected and subsequently

washed. The final washed titanium metal powder is claimed to directly meet the specifications for commercially pure titanium (Crowley, 2003).

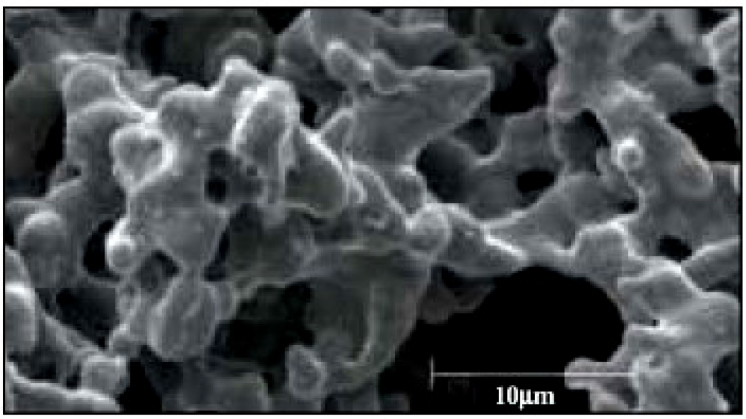

Fig. 19. SEM micrograph of titanium powders made by the Armstrong process (Crowley, 2003).

Another advantage declared by ITP is that titanium alloy powders can be made directly by the Armstrong process technology (Yamamoto, 2010). Multiple metal chloride reactants can be fed into the reactor simultaneously to form the designated composition. Fig. 20 illustrates the multi-reactant process used for alloy powder production (Crowley, 2003). This single step process greatly simplifies the procedure for producing titanium alloy powders. Reportedly, the product from a pilot scale plant shows a consistent blend of all metals in every particle. To date, ITP has made over 100 runs using their Armstrong process. The titanium powder typically has an oxygen content of 0.2%, which lies in the range for ASTM grade 2. Up to 2001, it has not been possible to reduce the oxygen level below 0.2% (Crowley, 2003).

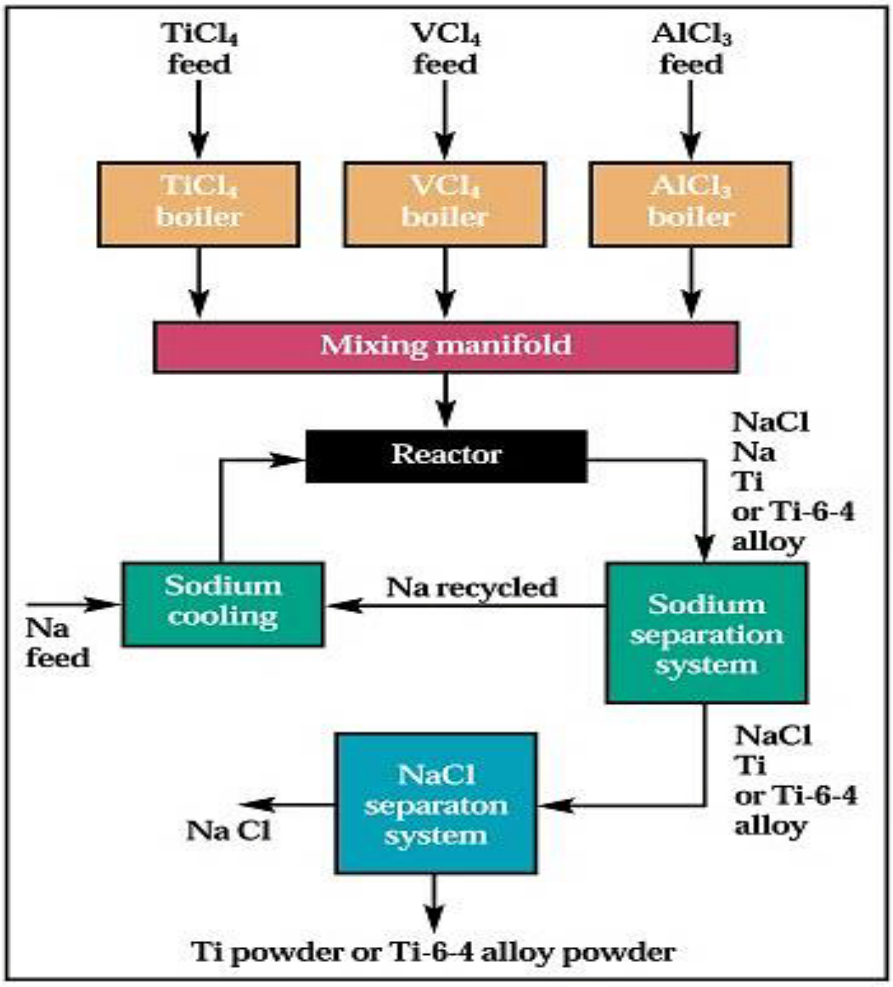

Fig. 20. Schematic representation of the Armstrong process for direct Ti-6Al-4V powder production (Crowley, 2003).

2.2.2 Powder characterization

Powder is the primary ingredient of the powder metallurgy process. The characteristics of the powder affect the P/M operations and the final product properties. Among those powder properties, powder size and shape are the most obvious and direct attributes. Therefore, an understanding of the powder characteristics is necessary. The following sections briefly outline the approaches that are typically used for powder characterisation.

2.2.2.1 Powder size

Powder size is not always easy to determine because there can be significant differences between particles. Even in the same lot, it is not possible for the particles to all have equal size and shape. However, different fabrication methods tend to produce distinct powder shapes and size distributions. Another source of deviations can arise from the measurement techniques and the specific parameters (German, 2005). Most particle size measurement instruments measure a single geometric parameter and make the assumption that the particle shapes are all spherical.

The screening method is a common and easy-to-use technique. It is also known as the sieve analysis. In this method mesh screens, with a controlled "mesh size", are used to separate different size particles. A mesh is a square grid of wires with evenly sized openings, as shown in Fig. 21 (German, 2005). The opening size is determined by the number of wires per inch; the higher the wire numbers, the smaller the openings are. Mesh designation is widely used in industry for powder characterisation. The mesh number and the corresponding size are listed in Table 5 (Pease & West, 2002).

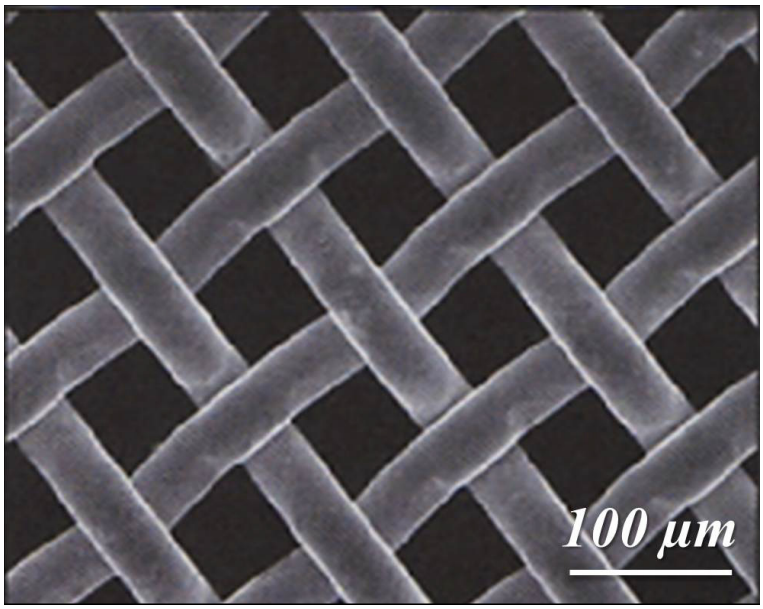

Fig. 21. SEM photo of a 200 mesh sieve screen (German, 2005).

Table 5. Mesh number and corresponding maximum particle size (Pease & West, 2002).

Mesh No.	Size (µm)
80	177
100	149
120	125
140	105
170	88
200	74
230	63
270	53
325	44
400	37

The general procedure for sieve analysis is illustrated in Fig. 22 (German, 2005). This approach uses a stack of screens with decreasing mesh openings. Powder is loaded on the top screen and then the stacks are agitated for a set period of time. Particles larger than the mesh opening will be retained above the screen, while smaller particles will pass through to the lower stack. The powder passing through a mesh is designated by a "-"

sign, and that retained on a mesh is designated by a "+" sign (German, 2005). Thus for powders retained on each sieve screen, there is a mesh number range for them.

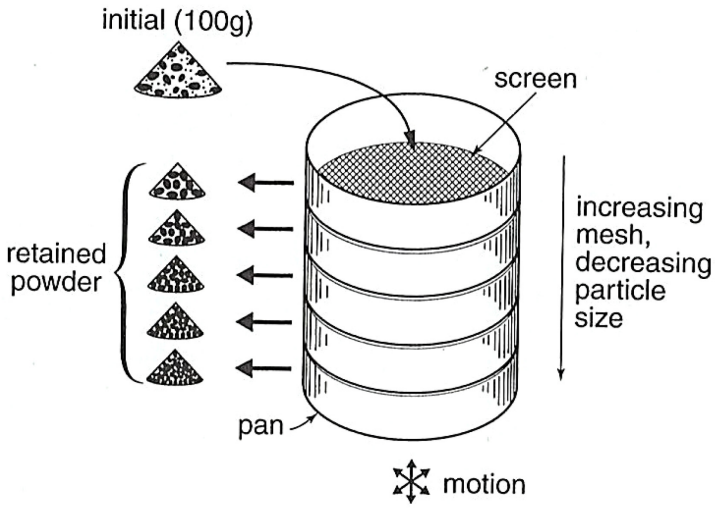

Fig. 22. Schematic of the sequence of screening sieves in order to determine particle size distribution (German, 2005).

An alternative approach for particle sizing uses the laser scattering analyzer, which measures the particle size by detecting diffracted laser light. Fig. 23 illustrates this analysis method schematically (Pease & West, 2002). Here, the powder is suspended into a solution, stirred to obtain a homogeneous suspension and finally pumped into the chamber. When the incident beam strikes the floating powder particles, it is diffracted and then detected by an array of photodiodes. Different size particles produce different extents of diffraction, as shown in Fig. 24 (Pease & West, 2002). Hence, through analyzing the diffracted beam, a particle size distribution can be acquired.

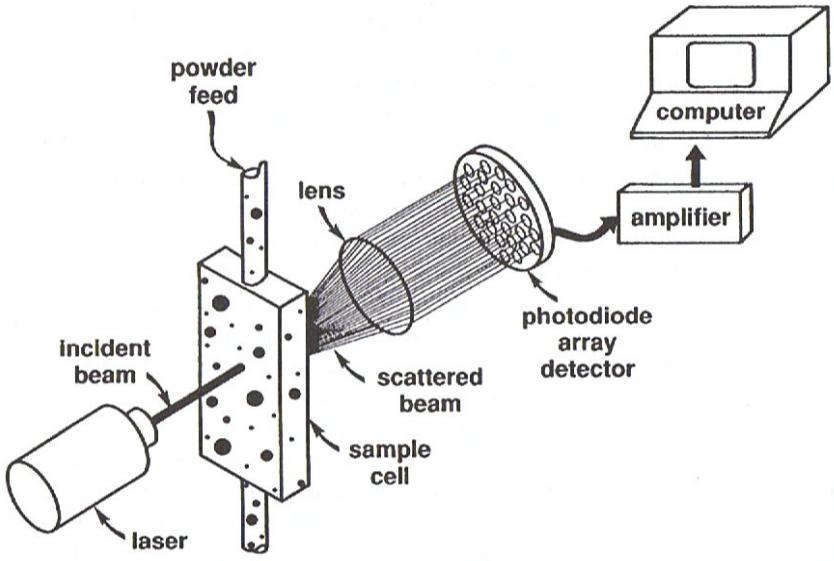

Fig. 23. Schematic representation of the laser scattering particle size analyzer (Pease & West, 2002).

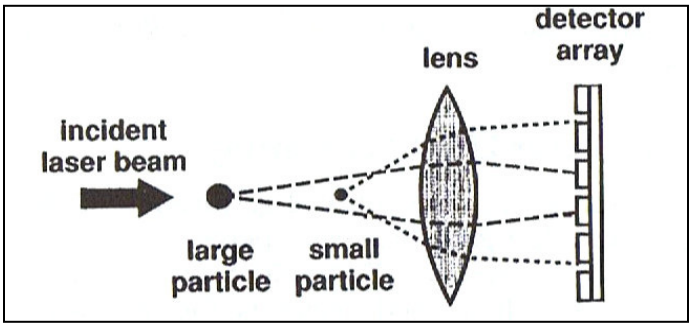

Fig. 24. Schematic representation of the different laser light scattering response caused by particles of varying size (Pease & West, 2002).

2.2.2.2 Particle shape

There are many types of powder morphologies, with the powder shapes invariably being the consequence of their production methods. Fig. 25 demonstrates SEM micrographs of some common particle shapes (German, 2005). Describing the powder morphology with a few parameters is not an easy task. Simple shapes, like sphere or flake particles, are easy to describe. However, complex shaped particles need more than one

variable to provide quantitative descriptions. Fig. 26 shows some basic shapes and the parameters needed to define them (German, 2005).

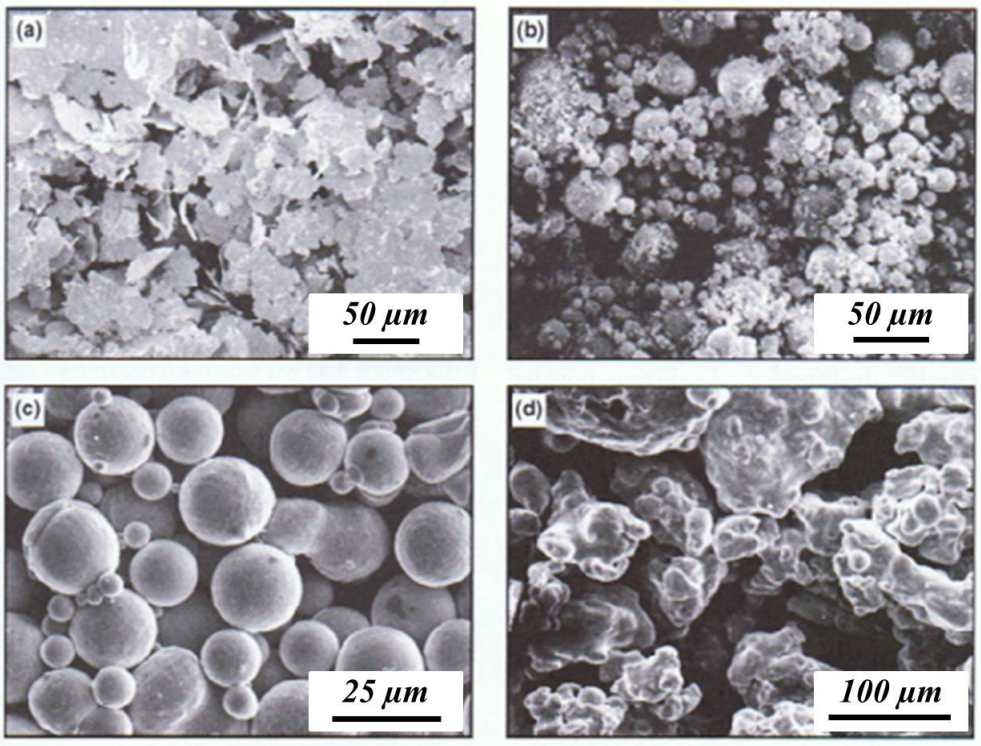

Fig. 25. Examples of the variety of powder morphologies (German, 2005).

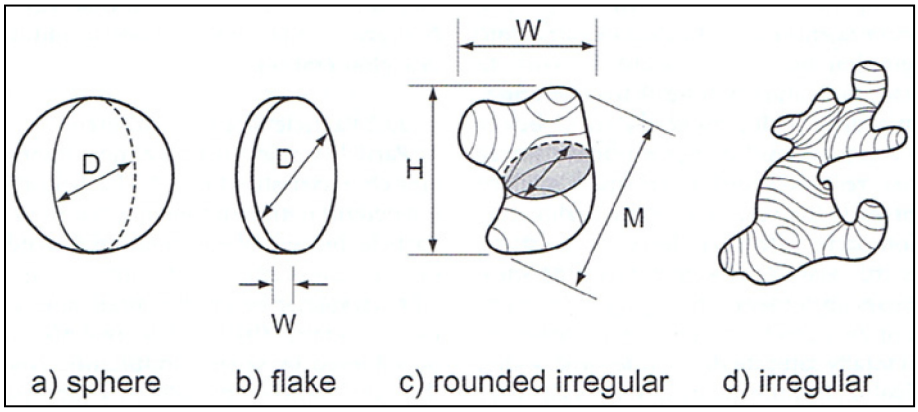

Fig. 26. Common particle shape classification and shape parameters (German, 2005).

2.2.2.3 Packing density and flow rate

Microscopic analysis provides detailed particle information. However, this approach sometimes does not sufficiently represent the whole powder lot when dealing

with industrial scale practices. An obvious question is how does a type of powder, which has a particular size distribution and shape variation, behave through the various P/M processes? To understand and answer this question, methods of quantitatively defining powder behaviour are needed. The apparent density and flow rate are the two most important indicators of powder attributes in the P/M industry. They represent how the powder packs within the mould and the time needed for a specific amount of powder to flow through a nozzle.

Apparent density is the density of a powder in a loose state, and it reflects the friction between particles. Interparticle or particle-tooling friction can affect many P/M operations, such as powder loading, pressing and compact ejection. The friction is the result of powder geometry, surface roughness and surface chemistry. Among these various factors, the particle geometry affects apparent density the most (German, 2005).

An Arnold meter is the instrument used to measure the apparent density, as shown in Fig. 27 (Pease & West, 2002). This device mimics the real die compaction practice in the P/M industry, using a hollow metal cylinder to imitate the feed shoe. This hollow cylinder is loaded with an amount of powder and moves back and forth on a metal brick which has a cylindical hole of 20 cm^3 at the center. The powder falls and fills into the cavity in a loose condition. After it is filled with powder, the Arnold meter is then removed. The powder retained within the volume is then weighed and used for the apparent density calculation.

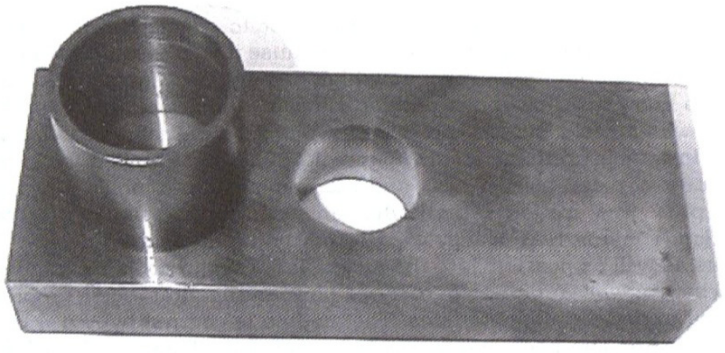

Fig. 27. The Arnold meter used for apparent density determination (Pease & West, 2002).

Flow rate is the indicator of powder "flowability". Like the apparent density, flow rate is also affected the most by particle shape. The smoother morphology of a powder with a spherical shape improves the flowability. The Hall meter is the device used to determine the flow rate, as shown in Fig. 28 (Pease & West, 2002). It is expressed as the time for 50 g of powder to flow through the Hall meter. The powder is placed into a cone with a 2.54mm diameter orifice, which is initially blanked off. After the orifice is opened, the time needed for the 50 g of powder to fully flow through the opening is measured. If the powder does not flow well, the Carney funnel, with a larger orifice (5.08mm) is used (Pease & West, 2002).

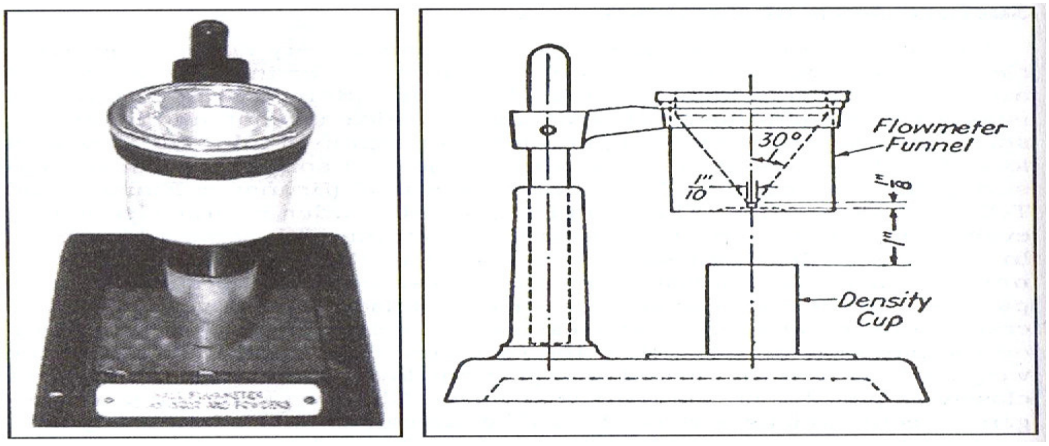

Fig. 28. Hall meter for powder flow rate determination (Pease & West, 2002).

2.2.3 Die compaction

2.2.3.1 Mixing and blending

Powders can be categorized into three types: elemental, master or pre-alloyed (German, 2005). An elemental powder is one comprised only of the pure element and is usually the most readily available powder on the market. A master powder is the semi-finished product. It contains the base metal, with a relatively high amount of one or more alloying elements. A pre-alloyed powder is prepared with some specific composition and ready to be used. Mixing one or more of these types of powder to achieve the final required composition is the first step prior to compaction. Fig. 29 shows a simple

example of how a titanium alloy, in this case Ti-6Al-4V, can be obtained using different powder combinations.

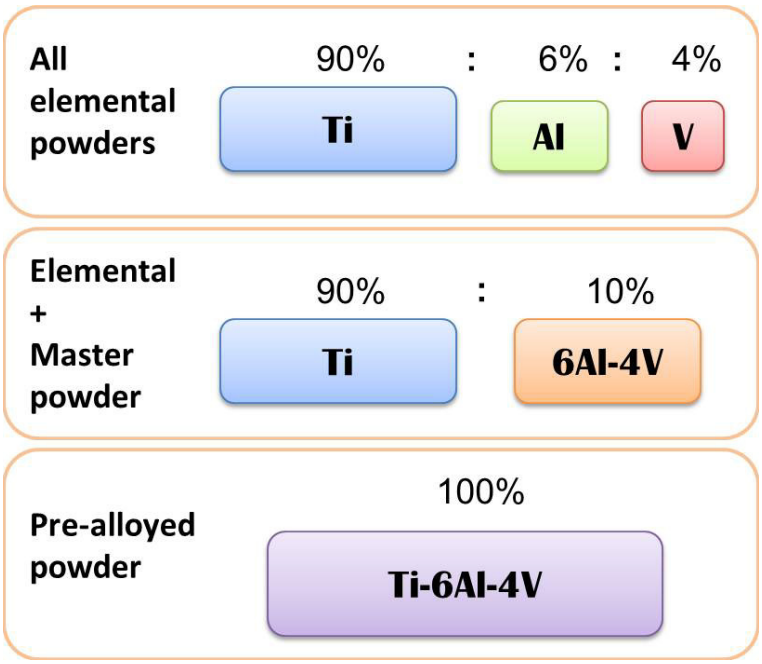

Fig. 29. Examples of differing powder combinations to produce Ti-6Al-4V.

Achieving the targeted composition with elemental powders alone is economical, simple, and readily adjustable. The mixture is invariably softer compared to the same composition of pre-alloyed powder and thus beneficial to the compaction operation. The chemical homogeneity, however, is an important concern when the elemental powders do not distribute evenly. In contrast, there is no such problem for pre-alloyed powders. Table 6 provides a summary of the characteristics of the three types of powders (German, 2005).

Table 6. Characteristics of three types of starting powders used for P/M processing, adopted from (German, 2005).

Powder type	Elemental	Master	Pre-alloyed
Cost	economical	In between	expensive
Composition adjustment	easy	In between	difficult
Hardness	soft	In between	hard
Chemical gradient	more	In between	less

Beside the powders themselves, processing aids in the form of lubricants are usually added to the mix. The lubricant eases the friction between particles and die walls, so as to facilitate compact ejection and minimize tool wear. Many kinds of lubricants can serve this purpose, such as stearates, stearic acid, polytetrafluoroethylene, polyvinyl fluoride, and wax (German, 2005). However, a proper lubricant that only alleviates the friction but does not introduce contamination is a fundamental requirement in titanium P/M. Additionally, the amount of lubricant has to be sufficient to fulfill its purpose without deteriorating the product properties.

Once the powders and lubricant are prepared, the mixture is loaded to a blender (Fig. 30) for a pre-determined time period (Pease & West, 2002). The tumbling action promotes mixture blending and increases the overall homogenisation of the various components.

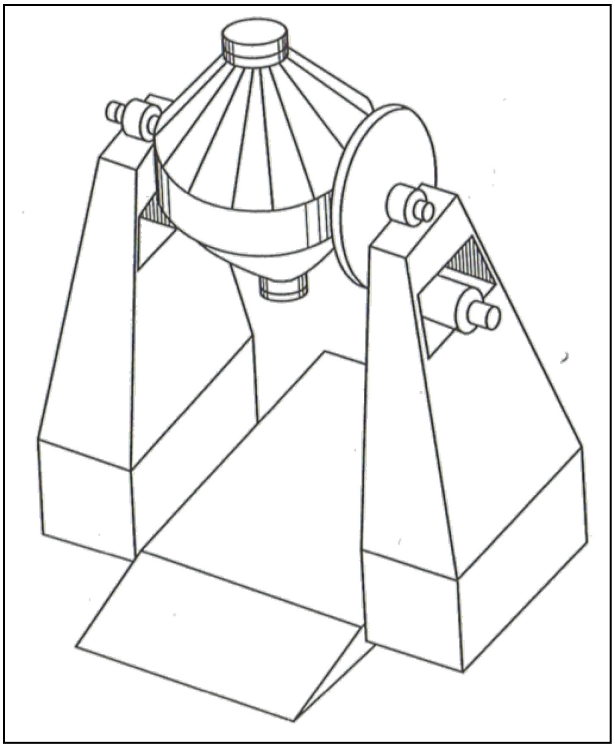

Fig. 30. A typical blender for mixing powders and lubricants (Pease & West, 2002).

2.2.3.2 Compaction cycle

The purpose of compaction is to acquire the designed product shape and to provide the component with sufficient strength for handling for the subsequent processes. First, the powder is placed in a die in a loose state. As the pressure is applied, the particles rearrange to a tighter packing density and then are deformed with the increasing pressure. The number of contacting points between particles increases and so does the contacting area. In the end these particles are cold welded and interlocked, as illustrated in Fig. 31 (German, 2005). This process gives the compact strength.

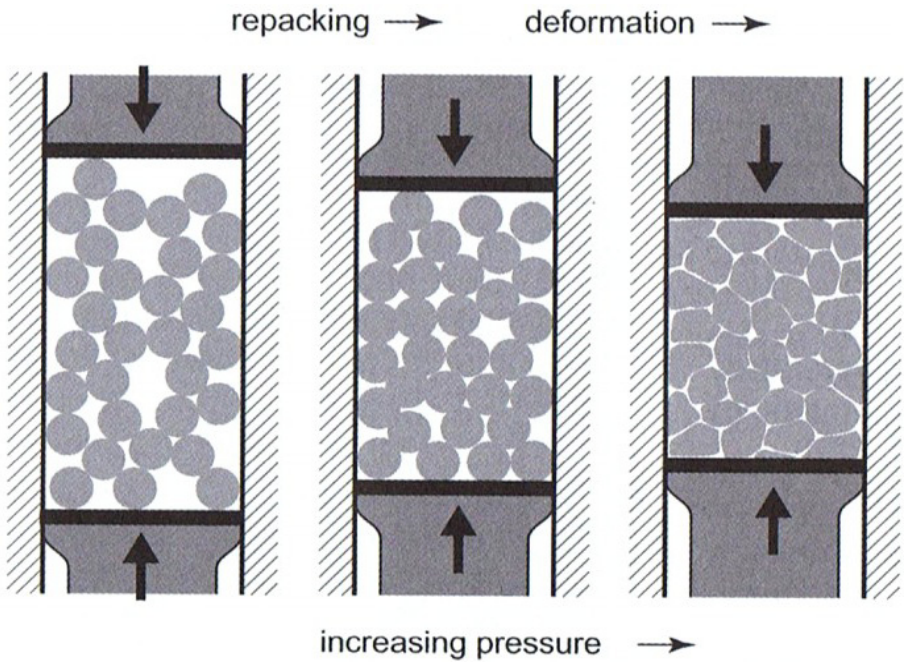

Fig. 31. Particle deformation with increasing pressure during uniaxial compaction (German, 2005).

Fig. 32 illustrates the various stages of powder consolidation for a uniaxial die compaction process (German, 2005). Before the powder is loaded, the upper punch is retracted and the lower punch is maintained at the fill position. The next step is to load the powder into the cavity of the die. The feed shoe moves back and forth to inject the powder evenly. During filling, the lower punch may move down to help obtain uniform powder distribution and loading. The pressing process is then accomplished by punch movement, and the powder is formed into a compact with the designed geometry.

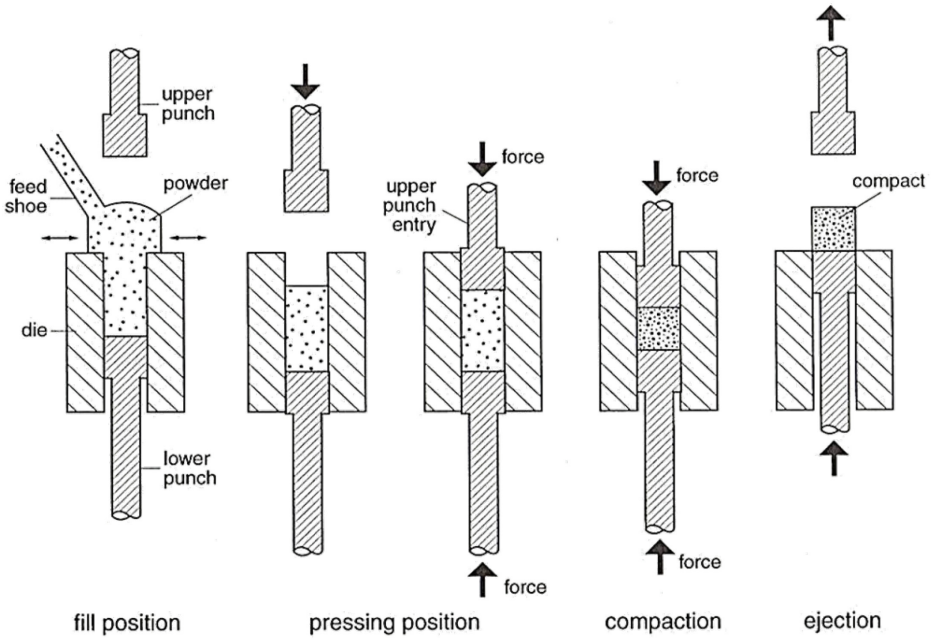

Fig. 32. Typical uniaxial pressing cycle (German, 2005).

As a compact is ejected, it undergoes an expansion called “springback” (German, 2005). The expansion is the elastic relaxation of a compact after it has been ejected. This phenomenon may be visually apparent, as the compact will often no longer fit back into the die cavity. This expansion should be carefully controlled, since it may result in size variation and even component cracking. After the compact is ejected by the lower punch, the compaction step is finished and the component is then ready for the subsequent processing steps.

2.2.4 Sintering process

2.2.4.1 Mechanisms

The process of sintering is the heating step of P/M, whereby the individual particles are fused together through diffusional processes. At this stage the compact acquires most of its strength and properties. Compacts are heated at an elevated temperature, usually of the order of 75% of the melting point of the material being sintered. When the heat provides adequate activation energy atoms begin to diffuse within the compacted powder. Particles then start to bond together and form interconnecting necks. A micrograph of typical neck formation is shown in Fig. 33 (German, 2005).

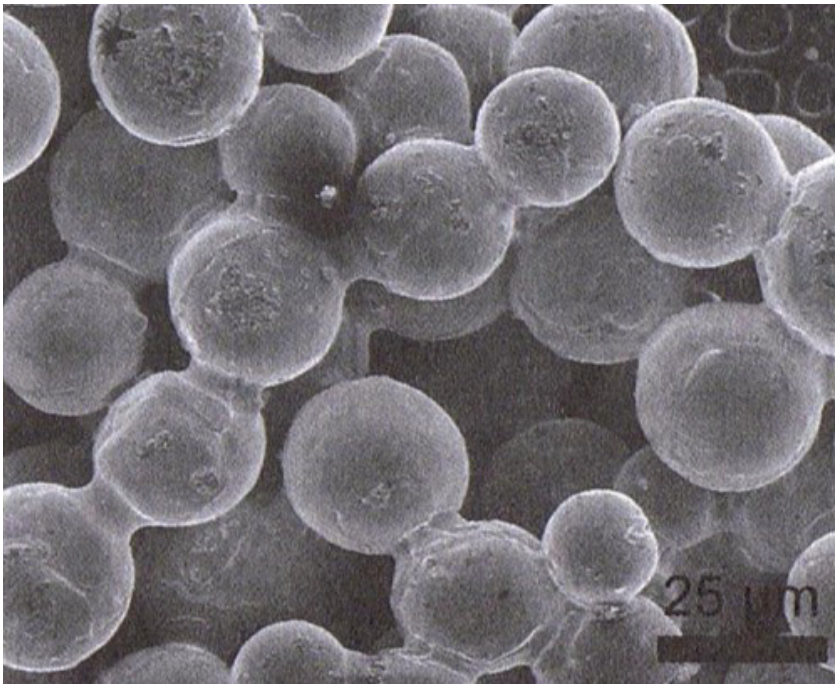

Fig. 33. SEM micrograph of neck formation (German, 2005).

When a neck forms, the total surface area of the powder compact decreases. As a consequence, the surface energy is also reduced. This energy difference (i.e. reduction) is the driving force that promotes the sintering process. From the atomic viewpoint, the

vapour pressure associated with a surface prompts the onset of mass transport. At a concave surface, which is near the particle-particle contact point, the vapour pressure is lower than that of the convex surface region. This pressure difference drives the atoms to fill the contact point, increasing the radius of curvature at that point, as shown schematically in Fig. 34 (German, 2005).

Interparticle necks grow from the flow of atoms, either by diffusion or vapour transport. Depending on the source of the diffusing atoms, there are two classifications of mass flow, namely the surface transport and bulk transport mechanisms. Fig. 34 depicts the atomic diffusion routes (German, 2005). They are differentiated by the starting site of the atoms. For the surface transportation mechanism, atoms move from the area adjacent to the contacting point. The surface transport mechanism includes two flowing paths, one based on surface-diffusion and the other on evaporation-condensation (i.e. vapour phase). Surface mass flow dominates most of the diffusion occurring at low sintering temperatures, although it does not promote shrinkage or densification, instead resulting in coarsening.

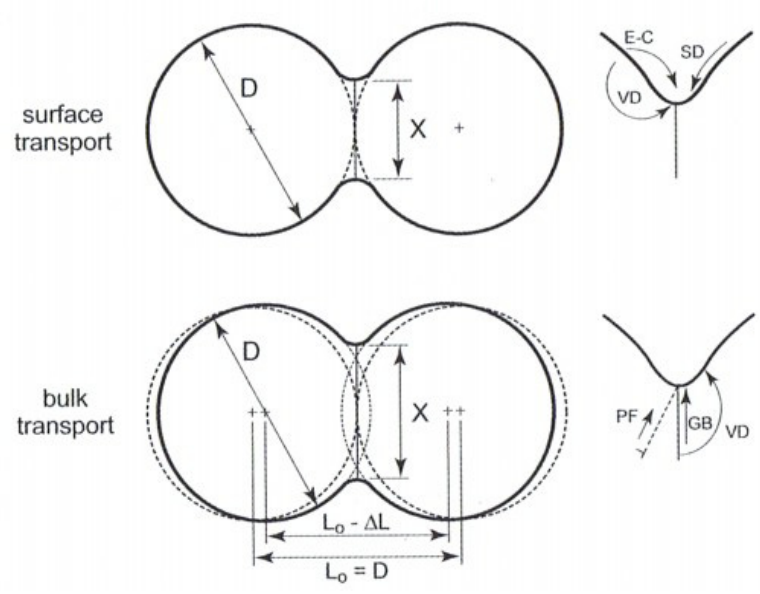

Fig. 34. Mass transport mechanisms (German, 2005).

As for the bulk transport mechanism, atoms are transported from inside the particle, and mostly from the grain boundary region. Here the mass flow is driven by the vacancy concentration gradient for solid state sintering. Atoms can diffuse following several processes, including, volume or grain-boundary diffusion, and plastic flow routes. The bulk transport mechanism, unlike the surface transport mechanism, can cause shrinkage and lead to densification. Generally, bulk transport processes dominate at higher temperatures.

2.2.4.2 Liquid phase sintering

Sintering is an atomic diffusion process. This ensures that the net amount of densification is highly dependent on the diffusion rates of the different species present. In general, such rates are significantly faster within a liquid metal as opposed to its solid counterpart. To capitalize on this concept, many different materials are processed through liquid phase sintering (LPS) techniques. In this approach the raw powder mixture is designed in such a way that heating to a prescribed temperature will invoke the formation of a small but controlled amount of liquid within the sintering compact. The liquid phase provides a route for rapid diffusion that consequently improves sintering kinetics and the final density achieved.

Fig. 35 (German, 2005) illustrates the densification steps of classical LPS involving a non-reactive liquid. When the additive powder melts, the associated liquid spreads and wets the base particles. The liquid then rapidly fills the pores as a result of capillary action, causing the solid particles to undergo a grain rearrangement process whereby a tighter particle packing (higher density) is achieved. After this initial period of rapid densification, the solubility and diffusivity effects become dominant. Here, the so-called “solution-reprecipitation” process takes place, wherein atoms initially diffuse from the smaller solid particles and dissolve into the liquid phase. This prompts the formation of a compositional gradient within the liquid that then invokes the reprecipitation of atoms on the surfaces of the larger solid grains. This process is similar to Ostwald ripening and reshapes the starting particle morphology considerably so as to reduce the overall surface energy (grain shape accommodation) (German, 2005).

In LPS practice, the liquid component can evolve in several ways. In one instance, it is a stable phase that is present throughout the complete isothermal hold at the required sintering temperature. This is referred to as persistent LPS. In another scenario, the liquid phase may form early in the heating cycle, but is then absorbed by the solid base phase owing to solubility considerations; an approach termed transient LPS. Both concepts are common throughout the P/M industry and are employed in many material systems.

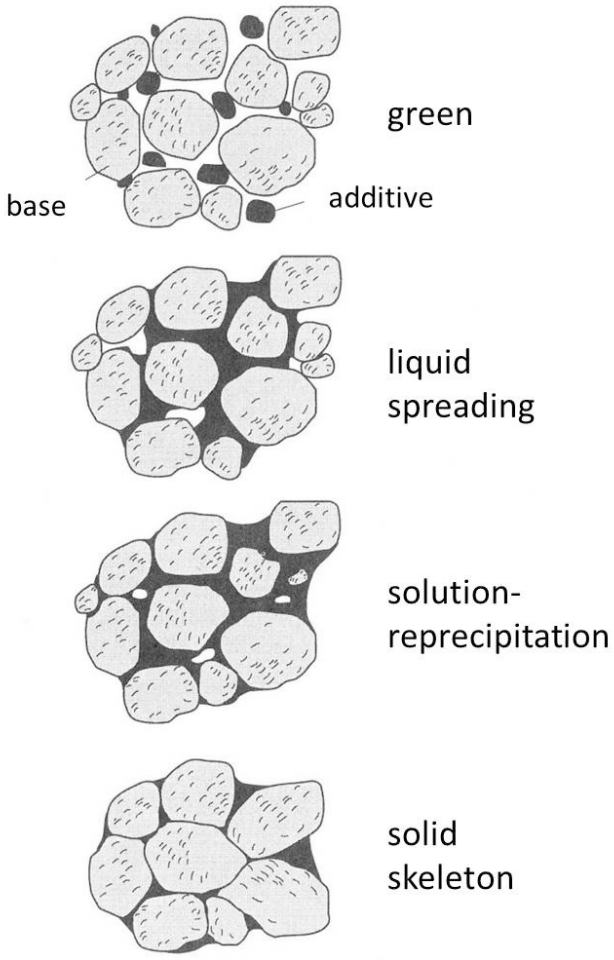

Fig. 35. Illustration of a liquid phase sintering process using two powders where the base powder remains solid while the additive melts and contributes to the liquid phase sintering (German, 2005).

2.2.4.3 Microstructure evolution

The sintering process can be described as occurring in three stages (Fig. 36) (German, 2005). Each has distinct characteristics with respect to the particle and pore configurations. During the initial stage, necks form and begin to grow, and the pores are irregular in shape. The necks grow independently and do not interact with the pores. In the intermediate stage, the necks grow larger and each particle merges further with the adjacent particles. The concave regions gradually diminish and become flat. Moreover, the pores become more rounded and smoother. Most of the densification happens in this stage. In the final stage, the pores are closed and become spherical. The grains begin to grow, as there are fewer pores impeding the grain boundary motion (typically termed "pore-drag"). Fig. 37 illustrates the pore and grain boundary interaction (German, 2005).

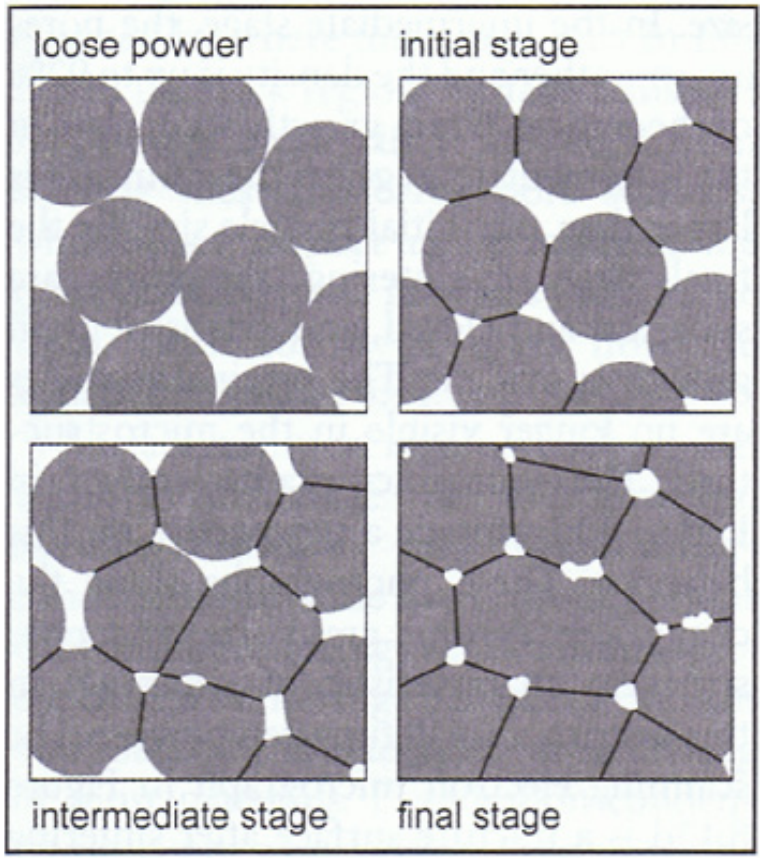

Fig. 36. Stages during the solid state sintering process (German, 2005).

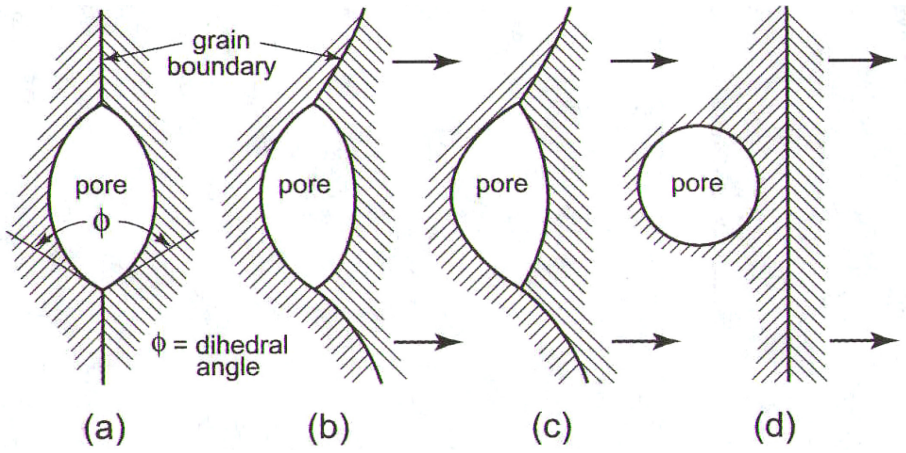

Fig. 37. Sequence of pore isolation during final stage sintering (German, 2005).

2.2.4.4 Sintering practice

A typical continuous sintering furnace (as shown schematically in Fig. 38 (German, 2005)) comprises three stages: preheat zone, hot zone and cooling zone. In the preheat zone, the lubricant is removed using a controlled burn out step; this stage is also called "delubrication." The compacts undergo the delubrication step before they are sintered. The process is designed to efficiently remove the lubricant that was added in the powder blend to assist the compaction practice. The residual lubricants may react with the compacts at elevated temperature, potentially forming gases that are detrimental to the final sintered properties.

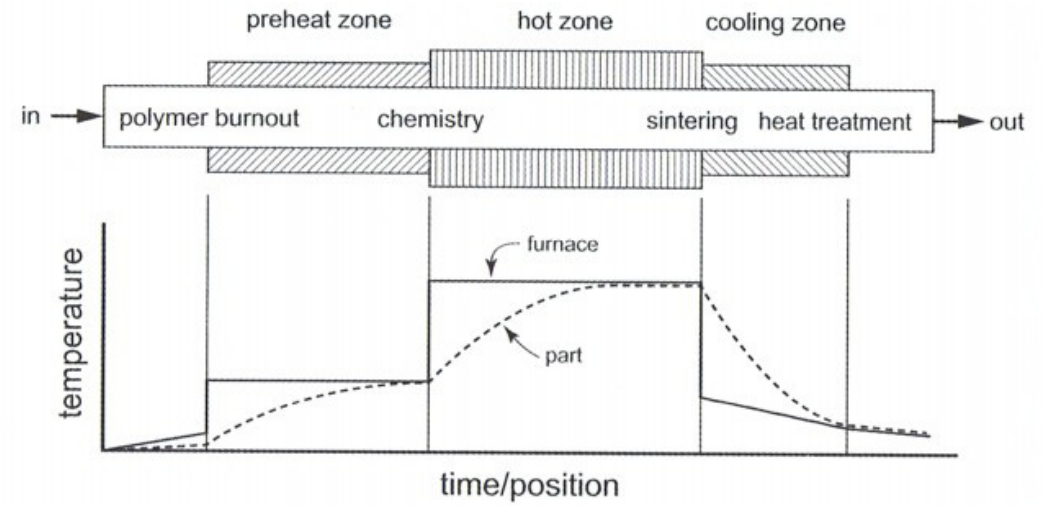

Fig. 38. Operational sequences of a continuous sintering furnace (German, 2005).

Most lubricants are polymers that have the same basic carbon, hydrogen, and oxygen constituents. Therefore lubricants usually burn out within generally similar temperature ranges. Lubricants that are commonly used in the P/M process start melting below 150°C, and evaporate between 300 and 500°C (German, 2005). The atmosphere for this step is carefully controlled, invariably being an inert gas such as argon or nitrogen, and selected to prevent reaction with the component.

As the compacts move into the hot zone, the process enters the sintering stage. The peak temperature is reached in this section of the furnace, and is usually maintained at a constant level until the final stage. The temperature ramping rate is carefully controlled; too fast and the compacts may crack, and the densification could also be affected. If the grain boundary moves too fast, pores may be left behind and become isolated within grains, making them extremely difficult to remove (German, 2005). As long as the pores migrate with the grain boundaries, the compact can still achieve further densification. The last stage involves the samples entering into the cooling zone. Like the heating rate, the cooling rate is also carefully controlled.

2.2.5 Titanium P/M

The currently high cost of titanium is always going to be an obstacle in essentially all applications. Fig. 39 shows the cost breakdown for forming a 25 mm thickness titanium alloy plate (Ward-Close et al., 2005). As can be seen, more than 60% of the cost is associated with the manufacturing stage. Although production is usually identical to that of large-scale specialty steels, the considerable waste of expensive titanium material during machining makes up a sizeable portion of the overall cost. On average, every 1.3 kg titanium sponge that is used only results in 0.4 kg product. Consequently, almost 70% of the material is actually wasted (Lutjering & Williams, 2003). In some aircraft components more than 90% of the material is actually machined away (Lutjering & Williams, 2003).

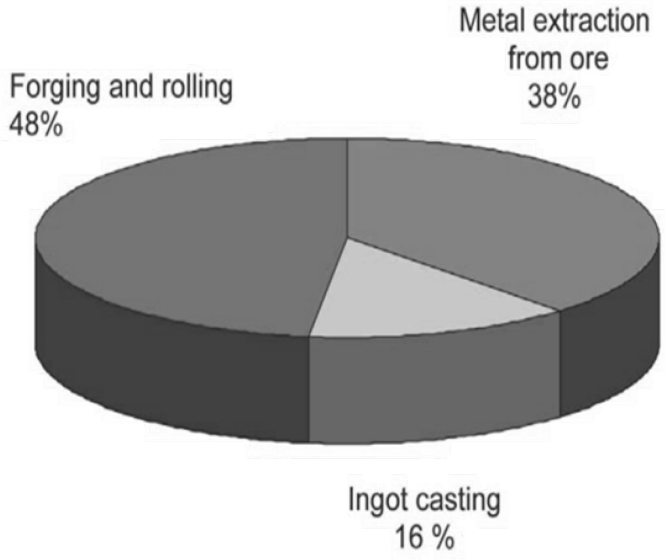

Fig. 39. Cost breakdown for production of a 25 mm titanium alloy plate (Ward-Close et al., 2005).

To tackle the problem of material wastage, near-net-shape technologies such as P/M have been developed. P/M technologies can significantly minimize the material loss due to machining. This is especially important for expensive titanium powders. P/M

technology has already shown considerable success in the commercial production of steel and aluminum alloys. As a consequence, this economical fabrication route also gives the titanium industry an opportunity to significantly decrease manufacturing costs.

Among the many powder metallurgy techniques, the blended elemental (BE) press-and-sinter and metal powder injection moulding (MIM) processes provide the most promising economical approaches for titanium P/M manufacture (Froes, 2005). They are suitable for medium to high volume production and can produce parts with moderate complexity. These fabrication technologies complement the billet machining and casting processes. Fig. 40 shows the suitability of P/M and MIM fabrication processes (Froes, 2005).

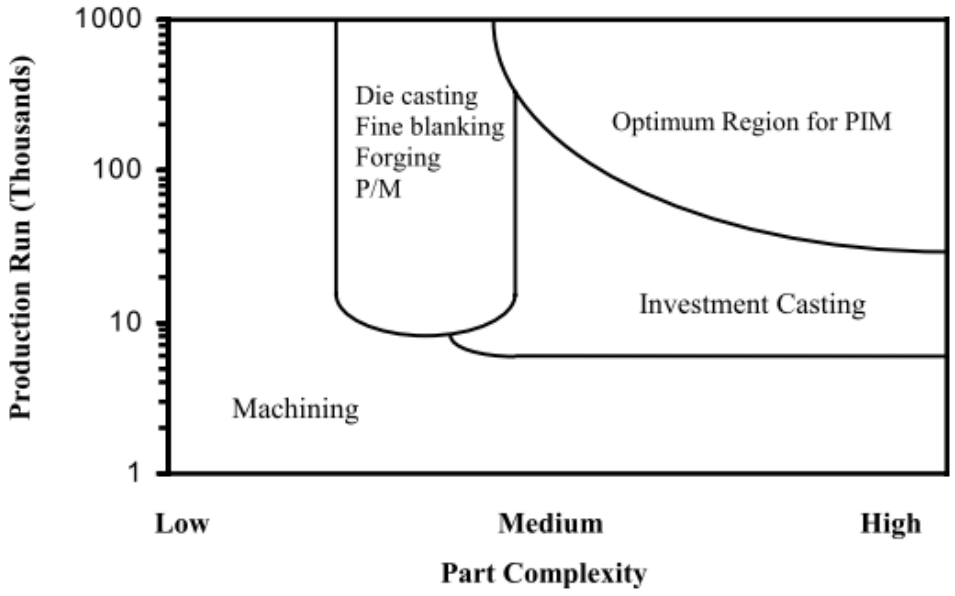

Fig. 40. Fabrication map showing where P/M and MIM fit in comparison to competing technologies (Froes, 2005).

MIM is based on the plastic injection moulding process. It is designed for small and complex part fabrication in long production runs. A substantial cost reduction can be predicted owing to the high volume production (Froes, 2005). In the MIM process, metal

powder is combined with a significant amount of thermoplastic binder. The binder helps the mixture stay together before being injected into a mould. However, the binders used could also create contamination, for example adding carbon, hydrogen, oxygen to the parts; resulting interstitial impurities can significantly degrade the ductility of sintered titanium MIM parts (Froes, 2005; Lutjering & Williams, 2003). Therefore, a carefully selected binder is the key to a successful MIM process.

On the other hand, the BE press-and-sinter process is also anticipated to undergo a significant commercial growth (Hanson et al., 1990; Ivasishin et al., 2000; Kim et al., 1985). The relatively inexpensive BE powders are one of the keys to produce low price products. The press-and-sinter process could also produce goods for far less cost. Nevertheless, the purity of powders affects the quality of products; components that are not fully dense may need to be strengthened by a secondary hot isostatic pressing (HIP) stage (Ivasishin et al., 2004). Such post-sinter techniques will increase the cost and offset the economic advantage of the press-and-sinter process itself.

As for the P/M titanium alloy design, it basically follows that used for the wrought products. Consequently, there are almost no P/M exclusive compositions. Some common titanium alloys are listed in Table 7 (Cardarelli, 2008). Titanium alloys are invariably designed for three main purposes: for high corrosion resistance, high strength and good strength at high temperature. Although many alloys have been developed, to date most of the efforts in titanium P/M are placed on the Ti-6Al-4V composition (Badini et al., 2000; Delo & Piehler, 1999; Ivasishin et al., 2002; Neto et al., 2003). The conservative development approach is due to the critical-operational environments in which the parts are typically used. For example, no risk can be taken when the structural components are used in an airplane.

Table 7. Common titanium alloys (Cardarelli, 2008).

Corrosion resistant	High strength	High temperature
Commercially pure grade 1~4	Ti-6Al-4V grade 5	Ti-6Al-2Sn-4Zr-2Mo
Ti-Pd grades 7 and 16	Ti-5Al-2.5Sn grade 6	Ti-6Al-2Sn-4Zr-6Mo
Ti-Ru grades 26 and 28	Ti-2.5Cu	Ti-11Sn-5Zr-2.5Al-1Mo
Ti-3Al-2.5V grades 9 and 18	Ti-6Al-7Nb	Ti-5.5Al-3.5Sn-3Zr-1Nb
Ti-Pd grades 11 and 17	Ti-4Al-4Mo-2Sn	Ti-5.8Al-4Sn-3.5Zr-0.7Nb
Ti-0.3Mo-0.8Ni grade 12	Ti-6Al-6V-2Sn	
Ti-3Al-8V-6Cr-4Zr-4Mo (Beta C)	Ti-10V-2Fe-3Al	
Ti-15Mo-3Nb-3Al-0.2Si	Ti-15V-3Cr-3Sn-3Al	
Ti-45Nb grade 36	Ti-5.5Al-3Sn-3Zr-0.5Nb	
	Ti-5Al-2Sn-4Mo-2Zr-4Cr (Ti 17)	
	Ti-8Al-1Mo-1V	
	Ti-6Al-5Zr-0.5Mo-0.25Si	

Besides the conventional alloys, titanium metal matrix composites (MMC) have also gained attention (Even et al., 2008; Furuta & Saito, 1995; Kainer, 2006; T. Saito et al., 1995), especially from the automotive industry. Titanium-based MMC have been developed for over two decades (T. Saito et al., 1995). Base alloys could attain high wear resistance, high temperature strength, or change the thermal or electric conductivity by combining the titanium-based metal matrix with secondary ceramic or intermetallic components. However, the reinforcement segregation arising from the conventional processing methods, such as casting, can cause anisotropy problem. The P/M approach can help to alleviate or even eliminate the segregation problems, and the reinforcements can be well dispersed in the matrix. Titanium MMC, such as TiB whisker reinforced

titanium alloy (Furuta & Saito, 1995; T. Saito, 2004), have been manufactured commercially. Fig. 41 shows examples of the valve parts used in a family car (T. Saito, 2004).

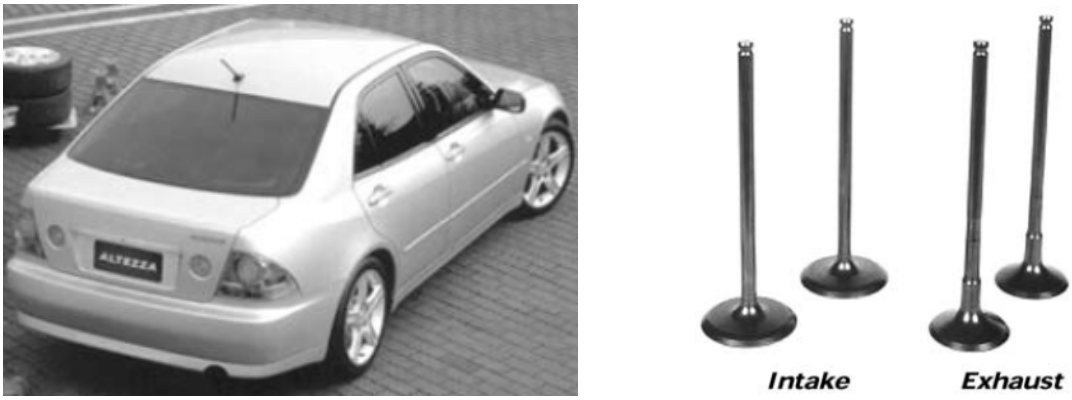

(a) **(b)**

Fig. 41. (a) Toyota Altezza (1998), the first family car adapted titanium valves (b) Ti-6Al-4V intake valve and TiB reinforced MMC exhaust valve (T. Saito, 2004).

In addition, the biomedical industry has utilised the excellent corrosion resistance and biocompatibility of titanium. Metallic titanium implants, especially for orthopaedic, dentistry and cardiovascular surgery (Mohandas, 2004), have been used for many years (De Oliveira, 2001; He, 2006; Henriques, 2001; Schaeffer, 2008; Taddei et al., 2004). For example, artificial hip joints made from Ti-6Al-4V and Ti-3Al-5V are used to help patients walk and relieve the pain from bone-to-bone contact friction (Barreiro, 2010; De Oliveira, 2001). Conversely, the conventional 316L stainless steel implant suffers from pitting and fretting corrosion (Norgate & Wellwood, 2006). The occurrence of this corrosion is critical, because it can lead to many detrimental effects, including inflammation or toxicity in the human body; the corrosion also means the implants degrade and their mechanical integrity is then at the risk of failure.

However, the conventional casting suffers from composition segregation which leads to networks of brittle intermetallics and has high Young's modulus compared to

human bones, as shown in Table 8 (De Oliveira, 2001). The mismatch of elastic modulus can lead to shear stress in the interface of implant and bone, resulting loosening and fracture of the implant. The P/M approach not only can alleviate the segregation but modify the elastic modulus by controlling the powder size or sintering process (Barreiro, 2010). Furthermore, the P/M implant provides a porous structure which can enhance the ingrowth for bone tissue, giving a better intergradation (De Oliveira, 2001).

Table 8. Young's modulus of metallic biomaterials and bone (De Oliveira, 2001).

Material	Young's Modulus (GPa)
Titanium	110-124
Stainless steel	210
Cobalt alloys	240
Bone	17

Chapter 3. THE INFLUENCE OF PROCESSING VARIABLES ON THE PRODUCTION OF POWDER METALLURGICAL TITANIUM

Hung-Wei Liu, D. Paul Bishop and Kevin P. Plucknett

Materials Engineering, Department of Process Engineering and Applied Science, Dalhousie University, 1360 Barrington St., Halifax, Nova Scotia, Canada

Keywords: Hydride-dehydride titanium powder, Uniaxial die compaction, Delubrication, Sintering, Microstructure development, Mechanical behaviour

Status: Submitted to Powder Metallurgy, August 2011

Abstract

Hydride/de-hydride titanium powder has been processed using a conventional die compaction powder metallurgical approach. The effects of various processing parameters have been assessed in terms of the microstructural development and mechanical behaviour, including lubricant type and amount, compaction pressure, delubrication atmosphere, and sintering conditions. While lower lubricant content results in higher sintered densities, a minimum is required to maintain die life. It was also demonstrated that a compaction pressure of 300 MPa is sufficient to provide high sintered densities, while again minimising potential for die damage. Densities of ~99 % of theoretical could be achieved when sintering at 1450°C for 4 h. Tensile strengths in excess of 750 MPa were obtained when sintering at 1300 or 1400°C. The resulting mechanical behaviour was strongly influenced by a combination of intrinsic powder impurities (i.e. oxygen), residual carbon contamination from the lubricant, grain growth and retained porosity.

3.1 INTRODUCTION

Titanium is well known for its high strength-to-weight ratio and excellent corrosion resistance making it a competitive candidate material in the demanding aerospace and military industries (Cardarelli, 2008). For example, the titanium alloy Ti-6Al-4V is used as a structural material in fighter aircraft (German, 2005), while commercially pure (CP) titanium has been used in heat exchanger applications in naval vessels (Pickens, 2004). Although titanium is the fourth most abundant metal in the earth's crust (Sibum, 2003), this has not lead to widespread usage of this lightweight and high performance metal, largely due to the expense of both refining the metal and processing titanium based components. Consequently, there is a considerable drive to reduce costs in all aspects of titanium production and component fabrication.

Titanium is mainly found in nature in the form of rutile (TiO_2) or ilmenite ($FeTiO_3$), particularly in alluvial deposits and beach sands (Cardarelli, 2008; Sibum, 2003). However, strong oxide bonding makes extraction of the pure metal very difficult. In the conventional Kroll process, TiO_2 is reacted with chlorine to replace the oxygen, and then reduced back to metallic titanium by molten magnesium (Lutjering & Williams, 2003). These reactions are complicated and expensive. The high affinity of titanium for oxygen, nitrogen and hydrogen at elevated temperature also greatly hinders the attainment of high purity. In addition, the high stiffness and hardness of metallic titanium make deformation processing and machining very challenging. As a result, from the initial material acquisition to manufacturing, the costs are high, which impedes development of the titanium industry and expansion into the consumer market.

Several methods are presently being examined to lower the cost of titanium production (Crowley, 2003; Deura et al., 1998; Gerdemann, 2001; Ward-Close et al., 2005). The Armstrong process is based on the same chemistry as the Hunter procedure (a forerunner of the Kroll method), although the approach changes the metallic reduction from a time consuming batch operation to one of continuous production (Crowley, 2003). The Fray, Farthing and Chen (or FFC) method of titanium refinement has opened a new window to titanium reduction processing (Ward-Close et al., 2005). The direct extraction

of pure titanium from titanium oxide eliminates the costly $TiCl_4$ purification and reduction, such that a high-purity powder can be produced directly in a single reactor.

In terms of component fabrication, powder metallurgy (P/M) is a highly promising and inexpensive technology for the production of both aluminum and iron (i.e. steel) based components (Donachie, 2000b). In particular, P/M based fabrication techniques help to minimise materials wastage during shaping, while also avoiding potential casting flaws such as localized void formation. Consequently, adopting P/M technology for titanium component manufacturing could potentially reduce the cost, and hence this approach has received significant recent interest (Froes et al., 2004; Hurless & Froes, 2002; Norgate & Wellwood, 2006). Using P/M-based approaches, the traditionally high processing cost of titanium can be significantly reduced in several aspects. Sintering reduces the cost by removing the melting step and lowering the potential for contamination at high temperature. The near-net-shape aspect of P/M further minimises or eliminates the need for final machining. P/M also allows alloys to be used that cannot easily be cast, or do not readily lend themselves to subtle microstructural control processes. These recent efforts on titanium P/M manufacturing have made the production of titanium based products more economically feasible and consequently broadened the potential scope of applications.

In the present work, a fundamental investigation of P/M titanium processing has been conducted using the conventional press-and-sinter (PS) process. Aspects relating to the initial forming method were evaluated, notably the compaction pressure and lubricant type/amount. The densification response was also studied for a range of sintering temperatures and atmospheres. Finally, the influence of the various processing conditions upon the sintered microstructure, hardness and tensile strength was assessed.

3.2 MATERIALS

The titanium powder studied in this paper was -325 mesh, 99.5% commercially pure (CP) grade (Alfa Aesar, Ward Hill, MA, USA; lots #G05L35 and #I90T027); the manufacturer's quoted compositions for the two powder batches are provided in Table 9.

The powder was fabricated by the hydride-de-hydride (HDH) process. The particle morphology was examined using a scanning electron microscope (SEM; Model S-4700, Hitachi High Technologies, Tokyo, Japan), as shown in Fig. 42. X-ray diffraction (XRD; Model D8 Advance, Bruker AXS Inc., Madison, WI, USA) confirmed the powder to be hexagonal close-packed α-titanium (ICCD Ti-00-001-1147). Table 10 highlights the chemical composition of the starting powder, in terms of carbon, hydrogen, nitrogen and oxygen content, as determined using chemical analysis (CS 2000 and ONH 2000, Eltra GmbH, Neuss, Germany); samples were tested in accordance with ASTM E1019-08, ASTM E1409-08 and ASTM E1447-09. The powder size was analysed using a Malvern Particle Sizer (Model# 20600, Worcestershire, UK), as outlined in Table 11.

Two types of commercial lubricant were used to aid the compaction process, namely Licowax® C (Clariant, Muttenz, Switzerland), subsequently referred to as LC, and a proprietary lubricant supplied by GKN Sinter Metals LLC, denoted as HD.

Table 9. Chemical analysis provided by the powder supplier (wt%).

Lot #	C	N	H	O	Fe	Cl	P	Others*
G05L35	0.010	0.011	0.026	0.224	0.03	0.02	<0.02	≤0.01
I09T027	0.009	0.018	0.024	0.235	0.03	0.01	<0.02	≤0.01

*= Al, S, Si, Mn, Mg, Na individual concentration

Table 10. Analysed carbon, hydrogen, nitrogen and oxygen contents of the as-received HDH powder (wt%).

	C	N	H	O
HDH Ti powder	0.030	<0.005	0.077	0.70

Table 11. Particle size analysis of the HDH titanium powder.

Particle size (μm)	HDH Ti
D_{90}	48.2
D_{50}	27.4
D_{10}	13.6

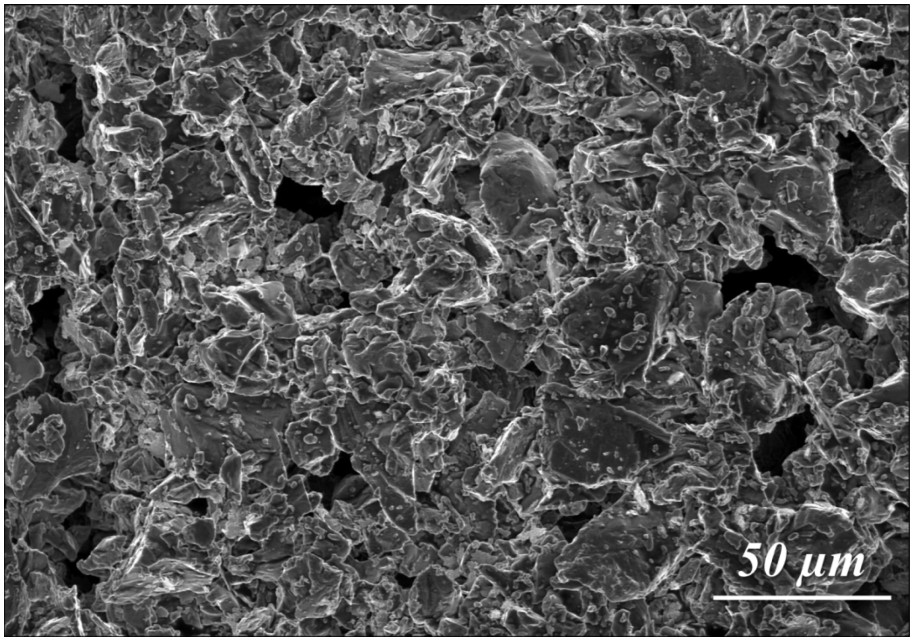

Fig. 42. SEM image of the as-received HDH titanium powder.

3.3 EXPERIMENTAL METHODS

Titanium powder was prepared for uniaxial pressing by mixing with either the LC or HD lubricant, added in amounts ranging from 0.75 to 1.5 wt%, in a Turbula® T2F mixer (Glen Mills Inc., Clifton, NJ, USA) for 30 minutes.

The powder blends were compacted in tungsten carbide/cobalt (WC/Co) floating dies, with peak pressures ranging from 100 MPa to 500 MPa, using a servo-hydraulic press (Model 5594-200HVL, SATEC Industries, Grove City, PA, USA). Disc-shaped samples (15 mm dia. x various mm height) were pressed for green and sintered density

measurements. Rectangular transverse rupture strength (TRS) bars (31.7 x 12.7 x 5 mm) were produced for green strength measurements, while cylindrical tensile testing samples were machined from rectangular Charpy bars (75 x 12.5 x 12.5mm). Green density was determined following a simple water displacement technique (conducted in accordance with Metal Powder Industries Federation (MPIF) standard 42) (MPIF, 2002a). Green strength determination of TRS bars was performed in three-point-bending, according to MPIF standard 15 (MPIF, 2002b).

Delubrication treatments were conducted in a tube furnace (Model Blue M-1100, Thermal Product Solutions, White Deer, PA, USA). The chamber was initially evacuated to 4×10^{-2} torr using a mechanical pump and then purged with high purity nitrogen (99.999%). After two cycles of evacuation and backfilling, the third nitrogen backfill maintained flowing gas through the chamber during the whole delubrication process. Nitrogen was replaced by argon (99.999%) in selected experiments to assess the effects of atmosphere on delubrication behaviour. For delubrication the furnace was heated to 400°C at 10°C per minute, held at temperature for 20 minutes, then furnace cooled to room temperature.

To compare CP titanium prepared with and without lubricant, additional samples were compacted using cold-isostatic pressing (CIP). In this instance the titanium powder was loaded into a rectangular latex rubber mould, without any added lubricant, sealed and then compacted at a pressure of 220 MPa in a wet-bag CIP system (Loomis, Levittown, PA, USA). As lubricant was not used with CIP compaction, there was no need for a subsequent delubrication cycle.

Samples were sintered in zirconia crucibles, with alumina lids, in a tungsten element vacuum furnace (Materials Research Furnaces, Suncook, NH, USA). The furnace was initially evacuated to 10^{-5} torr, and the samples were then heated at the rate of 10°C per minute to the designated sintering temperature, which was held for a period of 2 hours. The effects of an argon sintering atmosphere were also assessed. In this instance a heating rate of 10°C per minute was maintained under flowing argon held with a nominal pressure of 800 torr. The sintered samples were cooled at the rate of 15°C per minute in the furnace, with either the vacuum or argon atmosphere condition retained.

Sintered density was then measured using an oil impregnation technique, following the MPIF standard 42 (MPIF, 2002a).

The microstructure of sintered samples was assessed using a combination of optical microscopy (Model BX-51; Olympus Corp., Tokyo, Japan), SEM and XRD. Sectioned sintered samples were vacuum cold mounted in epoxy, ground using 100, 400 and finally 800 grit SiC paper, and then polished using 0.005 μm alumina powder to a mirror-like surface. Modified Kroll's etchant (96 ml distilled water, 3 ml HNO_3, 1 ml HF) was used to reveal the microstructure for optical microscopy.

Hardness was measured with a Rockwell hardness tester (Leco, St. Joseph, MI, USA), using the HRA scale (diamond indenter, 60 Kg force); an average of six indents was taken for each sample. Tensile tests were performed using the SATEC™ hydraulic system outlined earlier, using an extensometer (Model 3542; Epsilon Technology Corp., Jackson, WY, USA) to measure axial strain. Tension tests were performed at a loading rate of 2 MPa/sec, with the ultimate tensile strength (UTS) and elongation to failure then calculated using Partner software (Instron Corp., Norwood, MA, USA). All data presented in the property plots were acquired from the average of two readings and standard deviations were also calculated.

3.4 RESULTS AND DISCUSSION

3.4.1 Green body formation

To understand the basic compaction responses of the HDH titanium powder, initially prepared with 1.5% LC lubricant, discs were compacted at pressures ranging from 100 MPa to 500 MPa. It is apparent that green density increases steadily with the compaction pressure, as shown in Fig. 43. However, the increase gradually reduces as the compaction pressure reaches 500 MPa. At the highest compaction pressure, the achieved density was approximately 80 % of theoretical.

The green strength was measured using TRS bars compacted at 100, 300, 500 MPa (Fig. 43). Samples pressed at 100 MPa exhibited minimum strength and were easily

damaged even during basic handling. The green strength was significantly increased when the compaction pressure was increased to 500 MPa, with a measured strength of over 10 MPa, which was double that achieved for compaction at 300 MPa. However, compacting samples at the highest pressure raises the risk of tooling wear and punch jamming. For that reason, it can be generally recommended that the compaction pressure is limited to 300 MPa, which provides adequate strength for handling and minimizes the risk of die damage. However, for the purpose of the present study, further examination of compaction pressures in the range outlined earlier was continued.

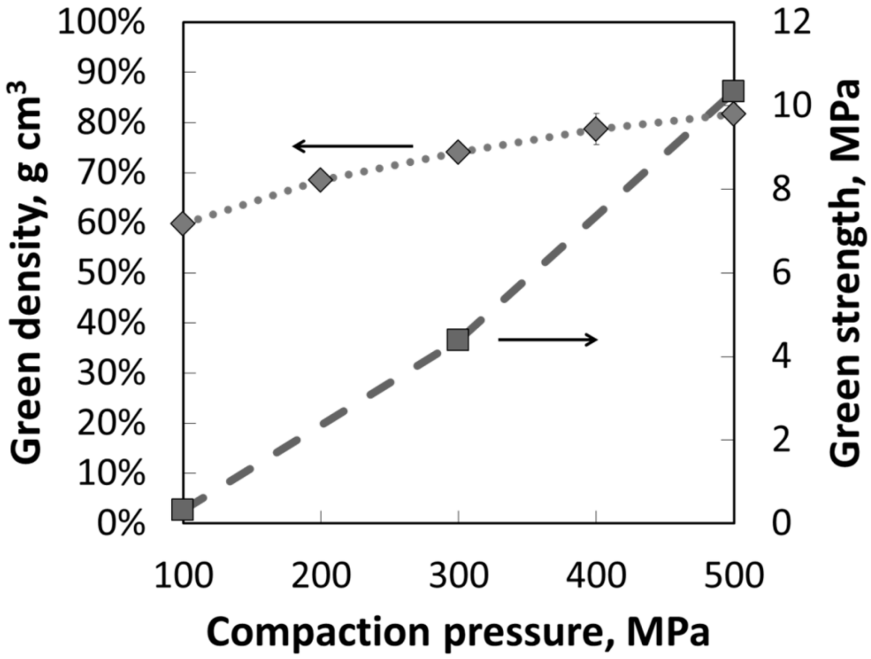

Fig. 43. The green density and strength of HDH titanium powder (with 1.5% LC) processed at various compaction pressures.

In PS P/M practice, lubricants are invariably added to minimise the friction between powder particles themselves, the die walls, and the punch faces. However, incorporation of a lubricant raises the concern of potential contamination, and any excess amount should be avoided. It is therefore important to determine the minimum amount necessary for successful die compaction. In the present study two lubricants, LC or HD, were blended in the amounts of 0.75% to 1.5% with the titanium powder to examine the effects of lubricant type and concentration. The results of these compaction trials are

presented in Fig. 44. For trials of 0.75% LC and HD lubricants (data not presented), the die regularly jammed. Consequently, the lubricant content was restricted at 1% and 1.5%. From Fig. 44, it can be seen that the green density increases with applied pressure for both lubricants, and the compaction response was generally comparable between the lubricants at any given pressure.

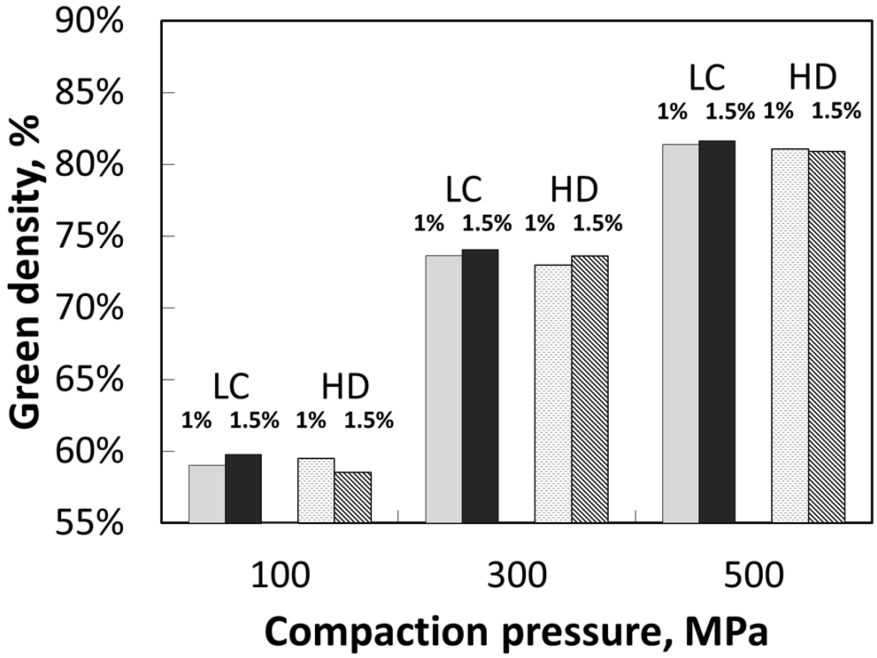

Fig. 44. The effects of lubricant type and amount on the green density of HDH titanium at various compaction pressures.

3.4.2 Sintering response

3.4.2.1 Effects of lubricants

Although the influence of lubricant type/amount was not significant in terms of the compaction response, a clear difference was revealed after the compacts were sintered (1300°C/2h), as shown in Fig. 45. Here it was apparent that the lower lubricant contents gave higher sintered densities, especially for the LC variant which provided better sintered densities than the HD lubricant for all pressures examined, especially at 500MPa. However, concerns regarding potential tool damage still need to be considered in spite of

the higher sintered density that can be achieved when using 1% lubricant. Based on these findings future tests were limited to the use of admixed LC for lubrication purposes.

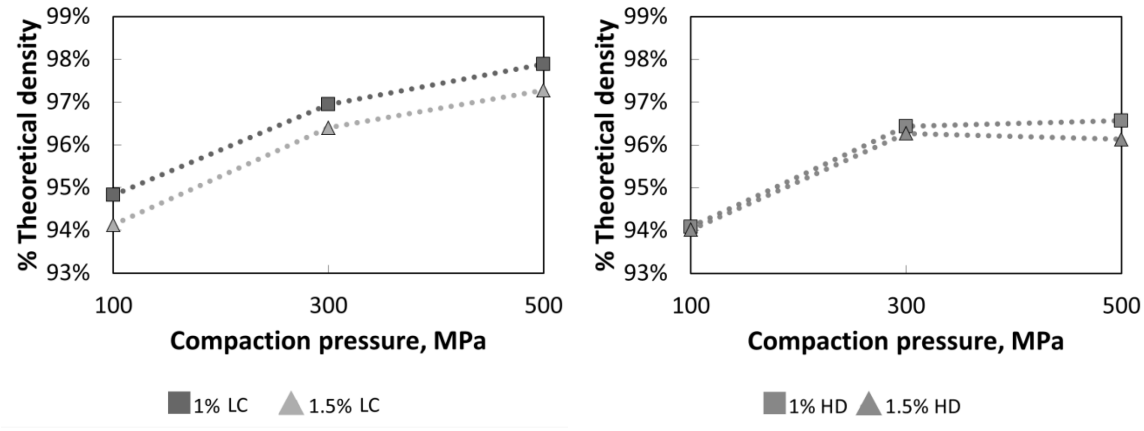

(a) **(b)**

Fig. 45. The effects of lubricant content (1% and 1.5%) on the sintered density (1300°C/2h/vacuum) for (a) LC and (b) HD lubricant.

The delubrication step could not be performed under vacuum due to equipment limitations. Consequently, a protective (inert) atmosphere had to be employed to avoid the detrimental oxidation of titanium, with both argon and nitrogen examined. Argon is inert to titanium and hence prevents titanium from potential oxidation during delubrication. Conversely, nitrogen is widely used to prevent oxidation in many P/M applications, such as sintering aluminium alloys (German, 2005). In the present case, delubrication was performed in a separate furnace, prior to vacuum sintering, while for commercial purposes it is desirable to conduct both steps in the same furnace.

The general extent of lubricant removal was assessed by measuring the net mass change, as shown in Fig. 46. The compaction pressure did not significantly affect the delubrication process (Fig. 46(a)). Subtle gains were realized with the argon atmosphere, but complete lubricant removal was still not achieved (Fig. 46 (b)). For both LC contents, the lubricant was only reduced by approximately 80 to 85 % of the initial content (by weight). This could be due to the relatively short delubrication time (20 minutes). While

nitrogen is inert for many materials, it can be reactive to metallic titanium at elevated temperature. The lower mass loss observed for delubrication under nitrogen may indicate mass gain from reaction with the titanium surface. However in some titanium forgings and heat treatments, nitrogen has been used successfully as the low-cost protective atmosphere (Donachie, 2000a). In this study, nitrogen was still considered owing to its cost and availability.

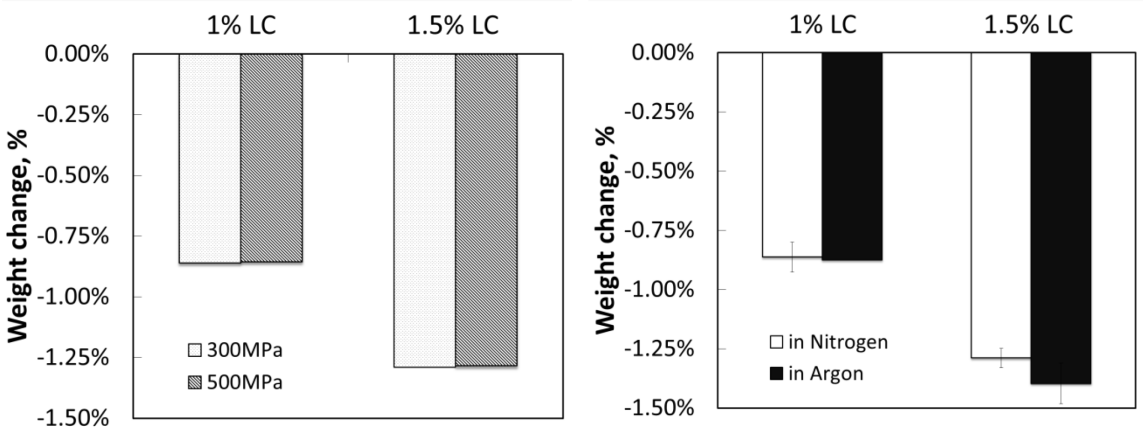

(a) **(b)**

Fig. 46. The mass loss of 1% and 1.5% LC lubricant blended compacts under different delubrication conditions: (a) 300MPa vs. 500MPa compaction pressure (nitrogen atmosphere), and (b) nitrogen vs. argon delubrication atmosphere (300MPa).

3.4.2.2 Effects of sintering time, temperature and compaction pressure

The influence of sintering time upon the final density was examined for hold times between 10 and 240 minutes (1.5% LC/300MPa/1450°C/vacuum), as shown in Fig. 47. While the sintered density reached 95% of theoretical after only 10 minutes, this residual 5% internal porosity is invariably unacceptable in most applications. Conversely, the samples sintered for 240 minutes reached near full density (~99% of theoretical). Nevertheless, 240 minutes was viewed as being too long in terms of a commercial P/M sintering process, and the resulting benefit of increasing sintering time from 120 to 240 minutes was not that significant. Consequently, a 120 minute hold time was considered more economical and therefore selected for subsequent experiments.

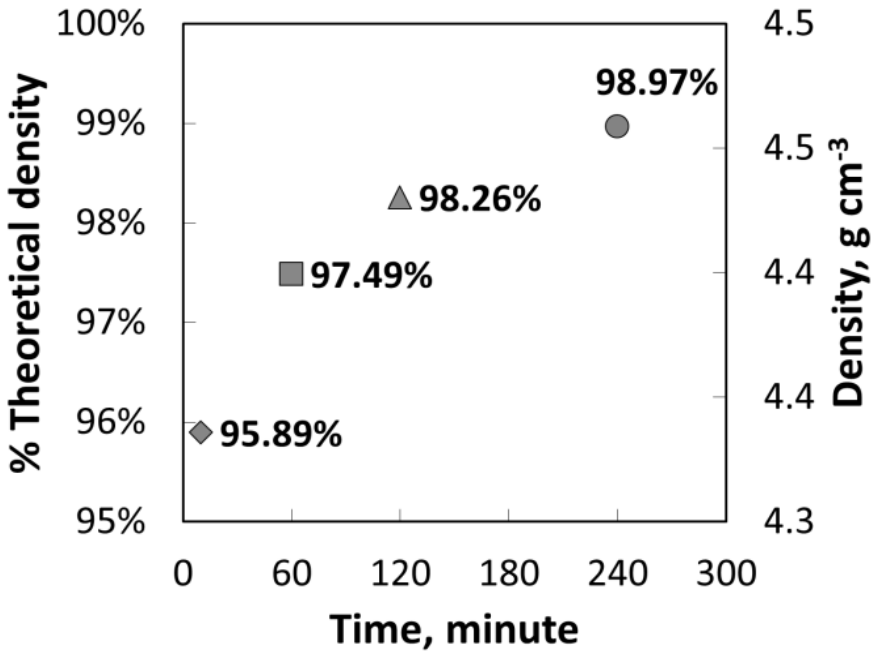

Fig. 47. The effect of vacuum sintering time on the density of P/M processed HDH titanium samples (1.5% LC/300MPa/1450°C).

To study the effects of sintering temperature and compaction pressure, samples with 1% or 1.5% LC were compacted at either 300 or 500 MPa, and vacuum sintered at temperatures between 1000°C and 1500°C for 120 minutes. Similar sintered density trends were found for samples compacted at either pressure, as shown in Fig. 48. In general, the sintered density increased more rapidly as a function of temperature at the lower sintering temperatures (i.e. below 1400°C). It was also apparent that the higher compaction pressure gave higher sintered densities for both sets of samples, with both 1% and 1.5% LC, as the higher compaction pressure enhances the contact and interlocking of particles, thus promoting inter-diffusion. At the higher sintering temperatures the density difference achieved for samples prepared at the two compaction pressures was reduced, indicating that the differing levels of cold welding achieved during compaction was ultimately compensated for by the increased thermal energy.

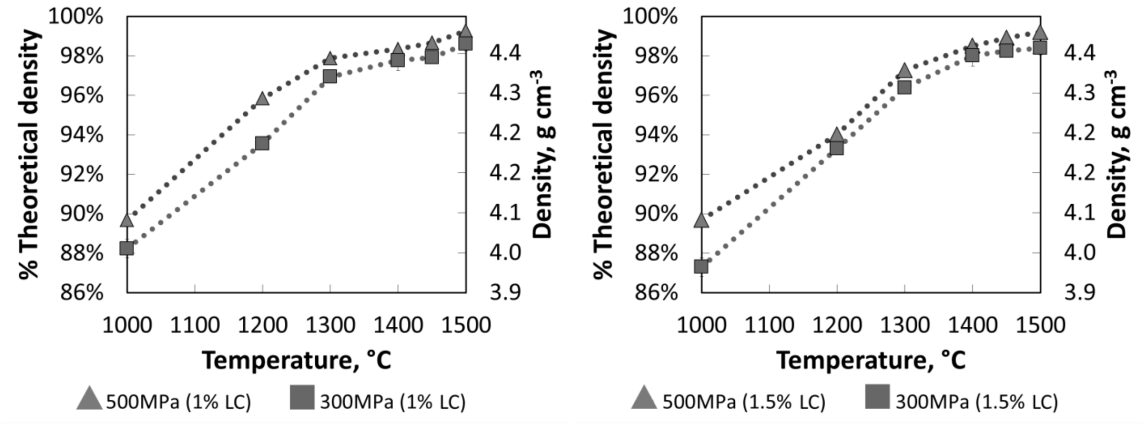

(a) **(b)**

Fig. 48. Sintered density of samples compacted at 300MPa and 500MPa with (a) 1% LC (b) 1.5% LC lubricant.

The effects of sintering temperature on microstructural evolution of samples pressed at 300 MPa and 500MPa (1.5%LC) sintered at 1200°C and 1500°C are highlighted in Fig. 49. It is clear that there is both a continuing elimination of porosity and an increase in the titanium grain size with increasing sintering temperature. These observations are confirmed through quantitative measurements of grain and pore size (Fig. 50 and Fig. 51), using the lineal intercept method for at least 150 grains/pores (Mendelson, 1969). It is also notable that there is little difference in terms of the influence of compaction pressure (i.e. 300 vs. 500 MPa) on the final grain size whereas the sintering temperature has a considerable effect.

There is a similar response in terms of the effects of sintering temperature upon the final pore size distribution (Fig. 51). Here it can be seen that the *mean* pore size increases with sintering temperature, although it is also important to note that the pore concentration (i.e. the number of pores per unit volume) decreases significantly at the higher sintering temperatures. Furthermore, Fig. 52 reveals a gradual change in the pore morphology with increasing processing temperature, from somewhat rounded pores at the lower sintering temperatures (i.e. 1200°C), to faceted, hexagonal-shaped pores when sintering at 1500°C.

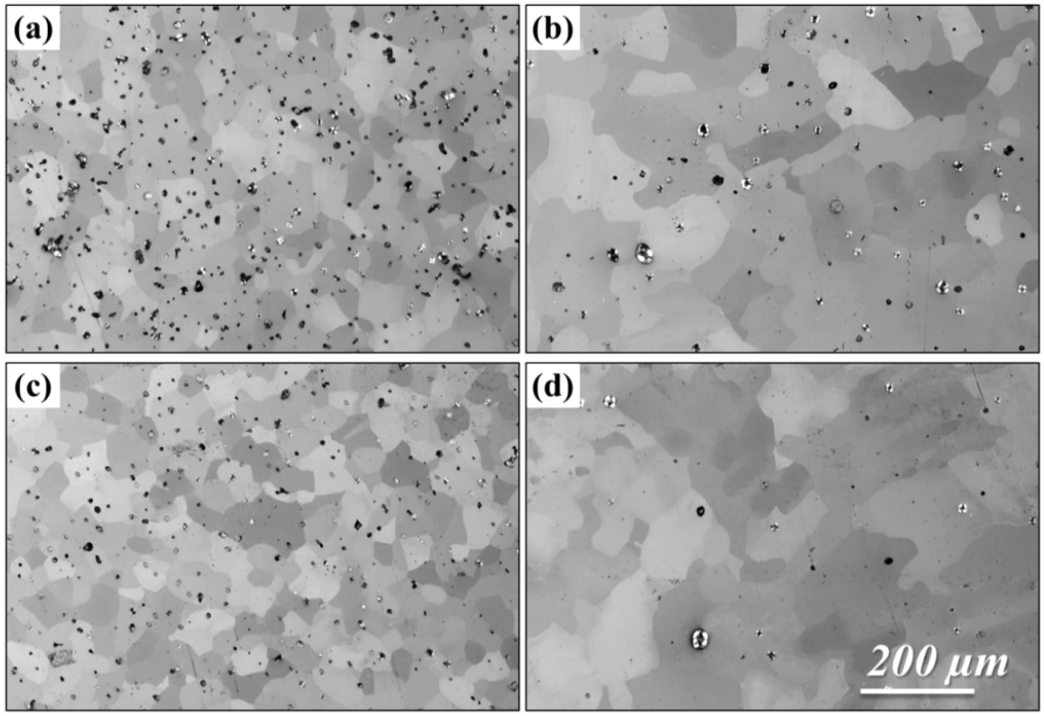

Fig. 49. Polarised light optical micrographs of polished sample cross-sections (a) 300MPa, 1200°C (b) 300MPa, 1500°C (c) 500MPa, 1200°C (d) 500MPa, 1500°C.

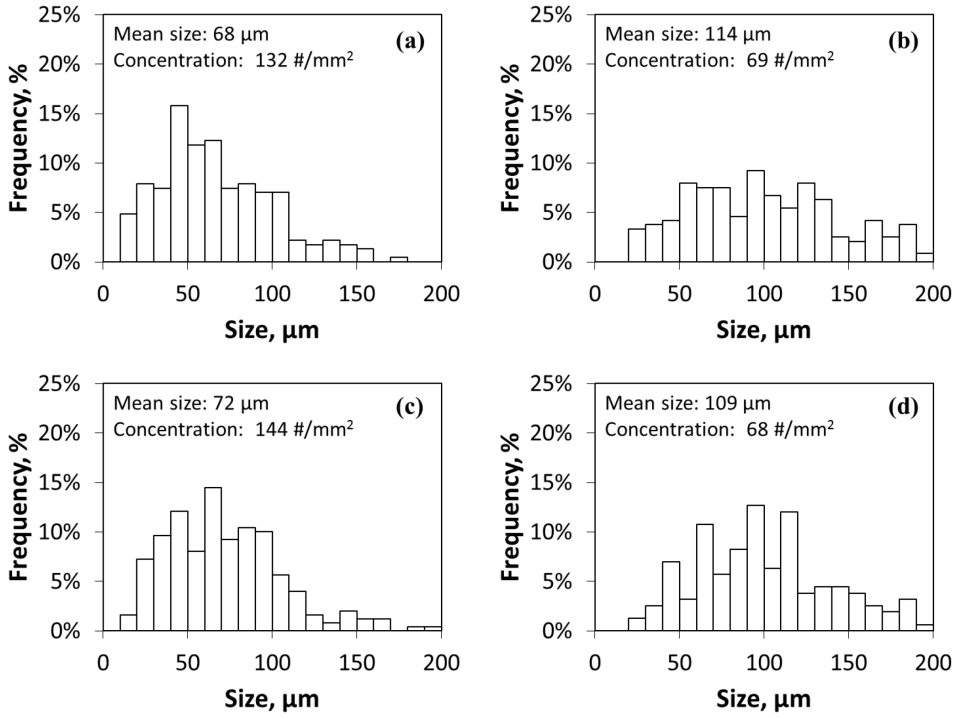

Fig. 50. Grain size distributions of HDH titanium processed under a variety of compaction pressures and sintering temperatures: (a) 300MPa, 1200°C (b) 300MPa, 1500°C (c) 500MPa, 1200°C (d) 500MPa, 1500°C.

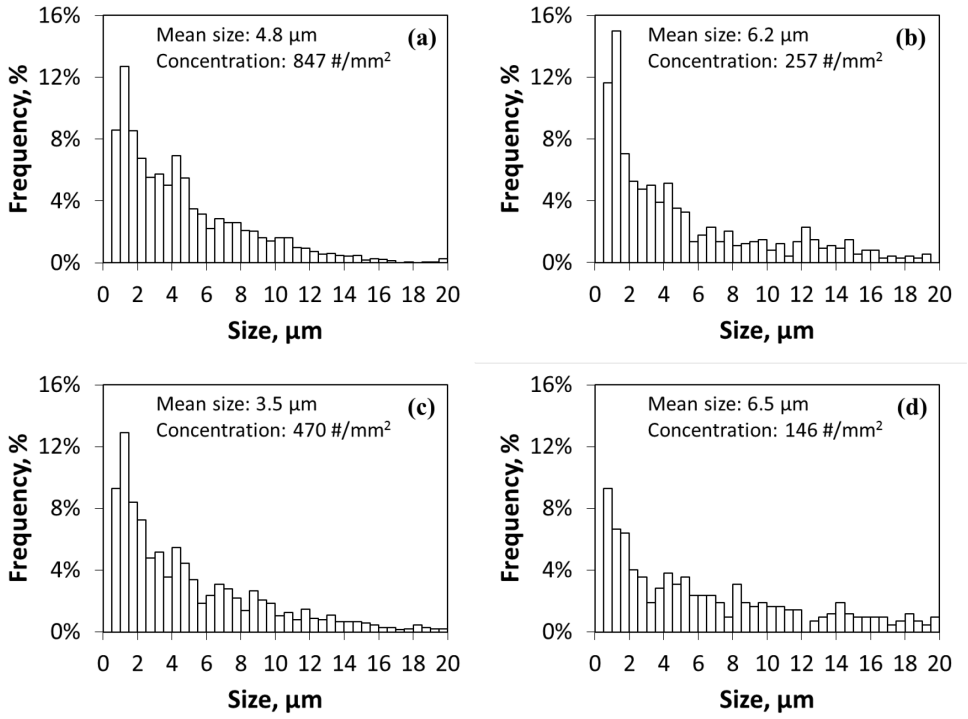

Fig. 51. Pore size distributions of HDH titanium processed under a variety of compaction pressures and sintering temperatures: (a) 300MPa, 1200°C (b) 300MPa, 1500°C (c) 500MPa, 1200°C (d) 500MPa, 1500°C. Figures show both the mean pore size and the concentration.

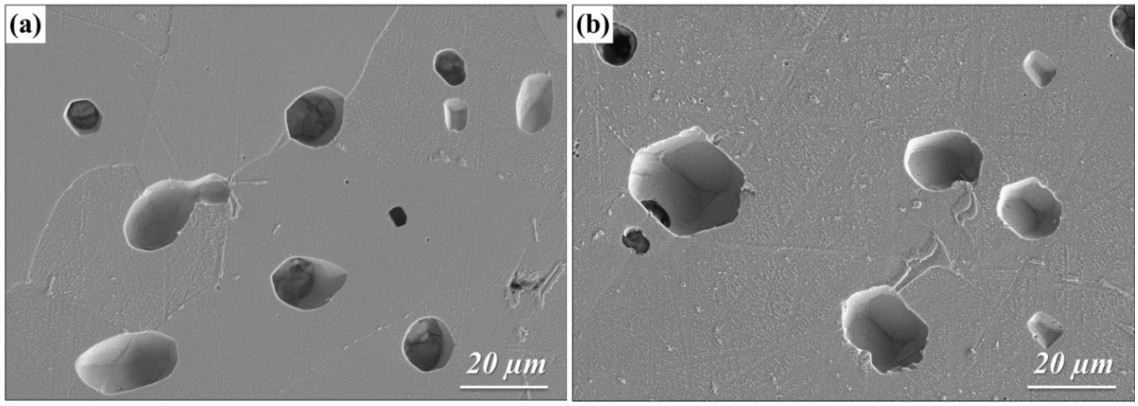

Fig. 52. SEM images of the pore morphology observed for HDH titanium samples pressed at 300MPa and sintered at (a) 1200°C and (b) 1500°C.

The chemical analyses of selected sintered samples, in terms of their carbon, nitrogen, hydrogen and oxygen contents, are shown in Table 12. The sintered samples

show an increase in both carbon and nitrogen content relative to the HDH starting powder (Table 10). The higher carbon content likely indicates that the samples retained residual carbon from the pressing lubricant, which was not fully removed during the delubrication cycle. The increased nitrogen content after sintering can be anticipated to arise from the delubrication step, where a nitrogen atmosphere is used. However, it is interesting to note that the higher compaction pressure results in a greater retained nitrogen impurity.

Conversely, both the hydrogen and oxygen concentrations are decreased after sintering in vacuum. In particular, hydrogen content decreases dramatically from that present in the as-received HDH powder, and is well below the maximum level stipulated in the ASTM standard for CP titanium Grades 1-4. However, it is notable that the oxygen content for *both* the as-received HDH powder and the sintered materials is slightly higher than the acceptable level for CP titanium. The measured levels for both oxygen and hydrogen are approximately 3 times greater than the manufacturer specifications listed in Table 9, indicating a possible issue with physically or chemically adsorbed water on the powder surface, although powders were stored in tightly sealed bottles within a desiccator cabinet upon receipt from the manufacturer. However, the high retained oxygen content *after* vacuum sintering indicates the oxygen content is more likely interstitial at that stage.

Table 12. Chemical analysis of the sintered samples and the ASTM maximum specifications for CP grade titanium (wt%).

Sample		C	N	H	O
300MPa	**1300°C**	0.07	0.088	<0.001	0.50
	1500°C	0.06	0.087	<0.001	0.54
500MPa	**1300°C**	0.06	0.096	<0.001	0.46
	1500°C	0.06	0.096	<0.001	0.52
ASTM CP-Ti grade 1-4		0.08	0.03-0.05	0.015	0.18-0.40

3.4.3 Mechanical properties

3.4.3.1 Hardness

The Rockwell hardness (HRA scale) of the titanium P/M samples increased steadily with sintering temperature, as shown in Fig. 53. This nominally monotonic increase relates directly to sample densification and a consequent decrease in the amount of residual porosity in the sintered samples, in accordance with the sintered density data in Fig. 48. The hardness values in the current study compare favourably with the highest values for non-alloyed titanium (HRA 62.4, ASTM Grade-4). It is apparent that the hardness relates directly to both the initial compaction pressure and the resulting sintered density.

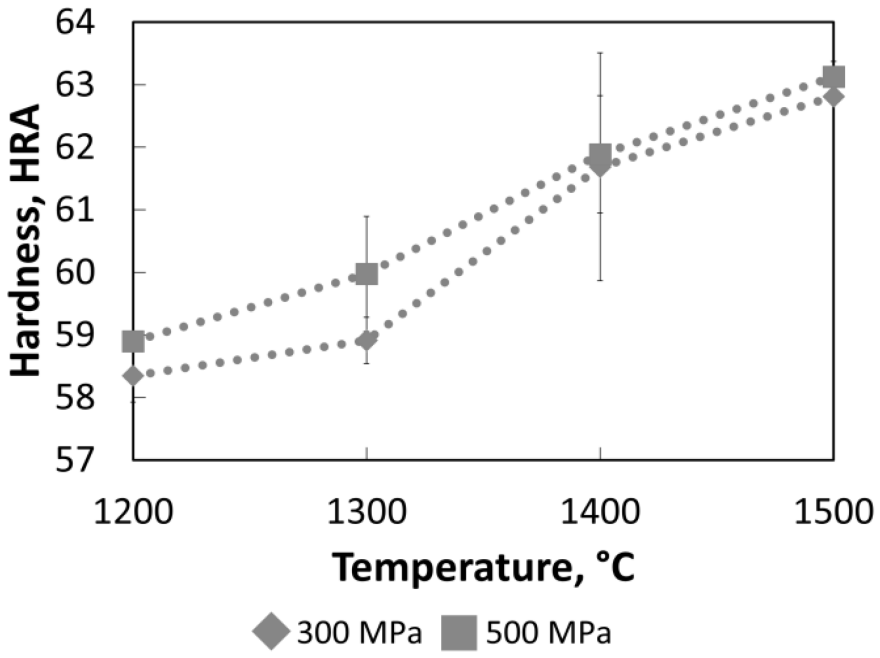

Fig. 53. The effects of sintering temperature on the Rockwell hardness (HRA scale) of HDH titanium, pressed at either 300 or 500 MPa, using 1.5% LC lubricant.

3.4.3.2 Tensile properties

Fig. 54 highlights a variety of tensile properties for titanium samples, prepared with the 1.5% LC lubricant, pressed at either 300 or 500 MPa, and sintered at

temperatures between 1200 and 1500°C. The elastic modulus shows a slight increase with the sintering temperature (Fig. 54(a)). Similar to the observed hardness increase (Fig. 53), this result is also the consequence of increasing sample densification. The current values are all slightly higher when compared to the ASTM Grade 1 to 4 (103 to 104 GPa). Regarding the yield strength (measured at 0.2 % offset), as shown in Fig. 54(b), the two series of samples revealed a generally similar trend. In this instance the yield strength values were within a narrow stress range for the lower sintering temperatures, until a clear reduction after sintering at 1500°C. These results indicate that, between 1200 and 1400°C, the sintering temperatures have negligible effect on the yield strength of the samples, which is only reduced when sintering at 1500°C. Therefore if the application demands lesser strength a lower sintering temperature could be considered (i.e. 1200-1400°C).

In terms of the UTS of the titanium P/M samples, a peak value was found for both low and high pressure compacted samples, where above this sintering temperature the strength then starts to decline (Fig. 54(c)). The maximum UTS of the two series was observed at 1300°C and 1400°C, for 300 and 500 MPa compaction pressures, respectively. The elongation to failure exhibited similar trends to the UTS (Fig. 54(d)). For samples compacted at 300MPa an initial reduction in the ultimate strain to failure occurs when sintering above 1300°C, while for those compacted at 500 MPa this apparent degradation occurs when sintering above 1400°C. As a result, although samples sintered at 1500°C had the highest sintered densities, they exhibited the poorest tensile failure response in terms of yield and failure stress, together with elongation to failure. In the present case it is clear that the optimum mechanical properties are not necessary obtained from the highest sintered density.

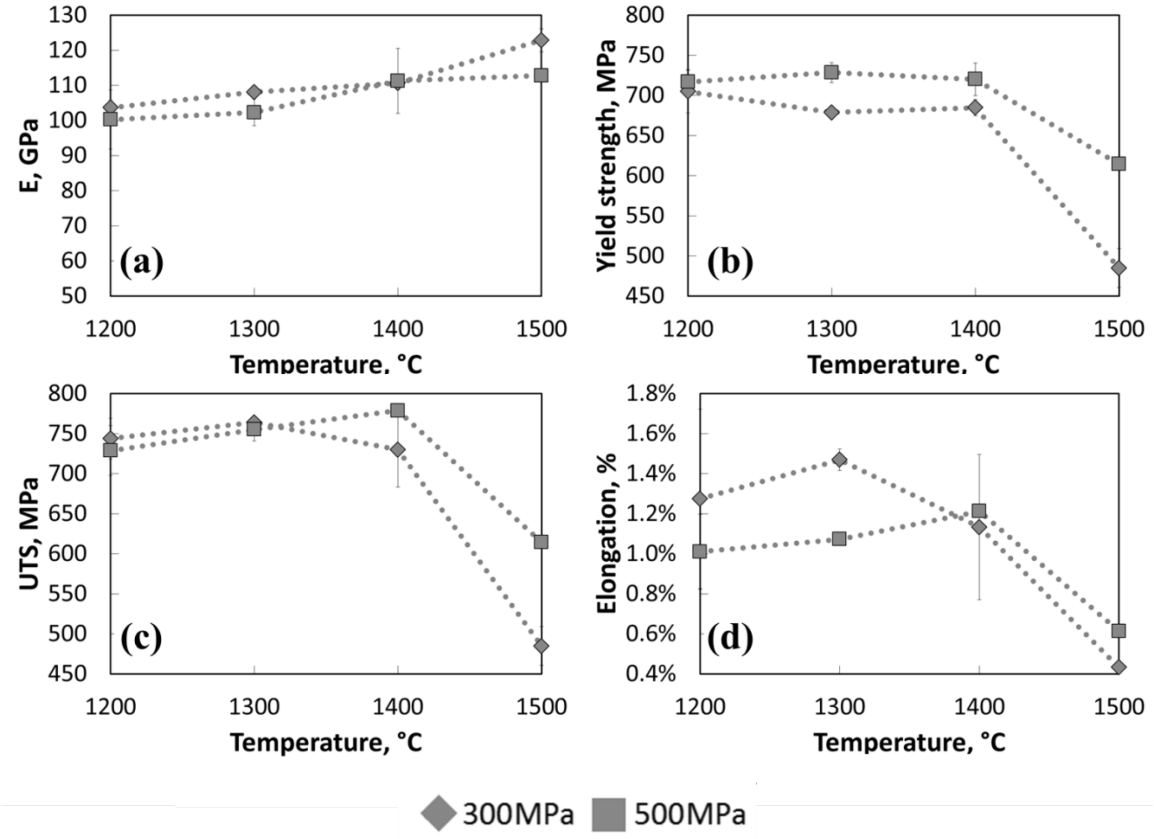

Fig. 54. Tensile properties of HDH titanium sintered at temperatures between 1200°C and 1500°C, and compacted at either 300 or 500 MPa, showing (a) elastic modulus, (b) yield strength, (c) ultimate tensile strength (UTS), and (d) elongation to failure.

Examining the tensile fracture surfaces of samples sintered at 1200°C and 1500°C it is apparent that a substantial topographical change is found in the fracture mode, as shown in Fig. 55. Sintering at 1200°C (Fig. 55(a,c)) results in an intergranular fracture morphology that is similar to the ductile failure behaviour which can be found in wrought titanium, although the elongation to failure is still low. Conversely, sintering at 1500°C leads to an apparent brittle fracture, with the clear presence of transgranular cleavage cracks (Fig. 55(b,d)) (Joshi, 2006). However, it is important to note that all of the elongation-to-failure values are less than 2%, and the samples are therefore considered to be brittle in nature. From the literature (Smart & Ellwood, 1959), products produced using similar press-and-sinter techniques and sintering temperatures can potentially achieve tensile elongation up to 10%.

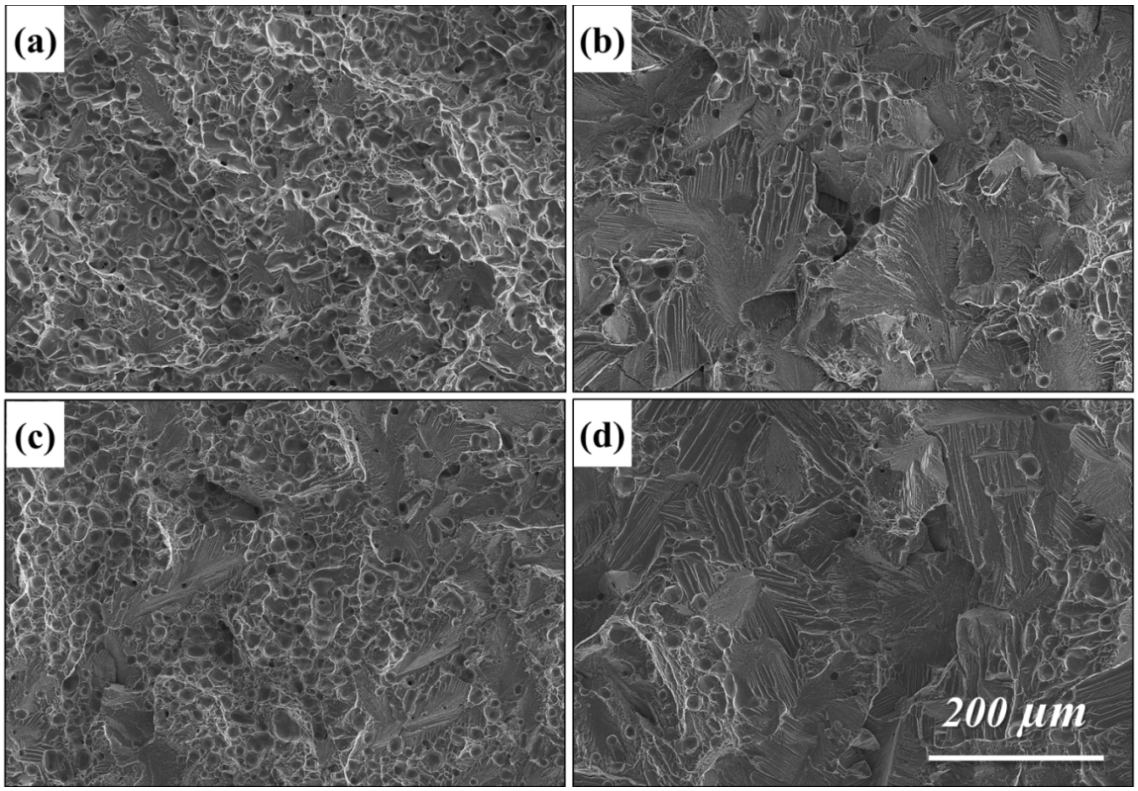

Fig. 55. SEM images of the fracture surfaces of HDH titanium samples fabricated with the following compaction and sintering conditions; (a) 300 MPa, 1200°C (b) 300 MPa, 1500°C (c) 500 MPa, 1200°C (d) 500 MPa, 1500°C.

From the above observations, the UTS and elongation to failure can be seen in two stages. Initially, both properties were improved as the sintering temperature was increased. At lower sintering temperatures, the dominant sintering contribution is the continuing elimination of porosity. Consequently the UTS was improved owing to improved densification. There is also some grain growth (Fig. 50), which potentially aids slightly in improving the ductility. At the highest sintering temperature, both the UTS and elongation to failure began to decline, although the density was continuing to increase along with the grain size. However, while the overall pore content decreases, this was observed to be largely through the elimination of the finer pores in the size distribution (Fig. 49 and Fig. 51), while the largest pores actually coarsened. Consequently, the *mean* pore size therefore increases with continued increase in sintering temperature (Fig. 51). It can also be seen from the SEM images in Fig. 52 that the pores develop a more facetted morphology at the higher sintering temperatures, potentially creating increased stress

concentration. It is proposed that those sites had a larger impact on the specimen ductility than the benefits that arose from the grain coarsening and caused the samples to fail in a premature manner.

In addition, it is clear from Table 10 that the initial oxygen content of the HDH titanium powder is relatively high (0.7 wt. %), and while reduced somewhat during sintering, it remains above the upper limit for CP titanium Grades 1-4 (ASTM B265). This relatively high retained oxygen content, which occupies interstitial sites within the α-titanium HCP lattice, is known to have a detrimental effect upon the failure strain (Donachie, 2000c). It has been reported that the presence of other impurities, such as carbon, hydrogen and nitrogen, can also have a potent effect on the mechanical properties on titanium (Donachie, 2000c). While the microstructure evolution arising through sintering has an influence on the samples to different levels (depending on the grain size and residual porosity), the retained impurities affect every sample. These interstitial impurities are observed to strengthen the titanium, while sacrificing ductility, and may arise from several sources, such as the initial raw material or processing steps. It is therefore important to utilise high purity sources of titanium wherever possible and to fully assess the processing steps to ensure that increased contamination does not arise. In particular, for the present case a lower oxygen content starting powder is favoured for future work, in combination with a refined delubrication step to avoid unnecessary carbon contamination.

It is proposed that the reduction in strength therefore arises from a combination of factors. Firstly, increasing grain size results in a clear transition to a brittle transgranular cleavage mode of fracture. Secondly, the *mean* pore size increases with temperature, and there was also a change in pore morphology with increasing sintering temperature from predominantly round pores to ones that exhibit a hexagonal faceting (Fig. 52). Finally the application of a higher sintering temperature (i.e. 1500°C) results in a small increase in the retained oxygen content, as shown in Table 12. This likely arises as a transition to nominally closed porosity will occur more rapidly at the higher sintering temperature such that the rate of oxygen diffusion out of the sample is reduced (i.e. path lengths to a free surface are effectively increased).

3.4.4 Effects of impurities

A further set of experiments were performed to assess the influence of specific contaminants, notably carbon from the lubricant and nitrogen from the delubrication atmosphere. Firstly, samples were subjected to a delubrication treatment in argon, rather than nitrogen. Secondly, samples were fabricated by CIP, thus eliminating the need for a lubricant and subsequent delubrication. Consequently, potential carbon and nitrogen contamination could be eliminated. CIP compaction pressure was limited to 220 MPa, so comparable uniaxially compacted samples were also pressed at 220 MPa for direct comparison.

The mechanical properties for these additional samples are presented in Table 13. Argon delubrication does not result in any significant property variation when compared to nitrogen, indicating that in this case the delubrication atmosphere did not play an important role in dictating the mechanical properties. In terms of lubricant effects, while the yield strengths of the uniaxially compacted and CIPed samples (both pressed at 220 MPa) are decreased, failure elongations are significantly higher, especially when no lubricant is used at all. Two factors should be considered in assessing this information. At the lower compaction pressure the retained porosity will be increased and the subsequent sintered density will be lower, thus resulting in a lower strength. However, for the uniaxially pressed samples the lower compaction pressure will result in less contact flattening between titanium particles, and therefore a reduced potential for entrapment of the lubricant between them; this will likely give rise to a lower final carbon contamination level and increased elongation to failure. Furthermore, when the lubricant is eliminated altogether, the elongation to failure is more than doubled; clearly in this instance the tensile response is dominated by the removal of potential interstitial contaminants in the form of carbon.

It is therefore clear from this study that *if* a lubricant is required for the powder metallurgical processing of titanium, which is likely the case for uniaxial compaction at high pressures, it must be selected in a careful manner such that retained carbon is minimised. Similarly, the delubrication treatment must be optimised to ensure the most efficient removal of the potential contaminant.

Table 13. The effects of compaction method (uniaxial vs. CIP) and delubrication atmosphere on the mechanical behaviour of HDH titanium (1300°C/2h).

Sample	E (GPa)	UTS (MPa)	Yield (MPa)	Elongation	Density
PS 300MPa*	108	764	679	1.47%	96.39%
PS 300MPa Ar delub.	105	760	683	1.47%	95.88%
PS 220MPa	101	753	660	1.98%	95.63%
CIP 220MPa	104	746	619	4.17%	95.03%

***from the previous results (Fig. 54)

3.5 CONCLUSIONS

In the present work a commercial HDH titanium powder has been used to assess powder metallurgical processing variables, including compaction pressure and method, lubricant type and concentration, delubrication atmosphere, and sintering temperature. It has been demonstrated that green density and strength increase with compaction pressure, while green density also increases with lubricant concentration (particularly LC wax). However, both of these aspects must be tempered by the practical need to minimise processing additive concentrations (as they must be later removed and can contribute to contamination), and also to prolong tooling life (i.e. minimising wear, which increases significantly at higher compaction pressures).

Nitrogen and argon have both been demonstrated to be suitable for delubrication, although some retained carbon is noted by chemical analysis, which is shown to have a detrimental effect on tensile elongation to failure. Increasing sintering temperature, between 1200 and 1500°C, increases the sintered density, which generally improves mechanical properties. However, both the resultant grain size and the mean pore size are also increased with sintering temperature (although the total pore volume decreases), which ultimately results in a transition from intergranular to transgranular fracture.

Chapter 4. PRELIMINARY INVESTIGATIONS OF TITANIUM BINARY SYSTEMS (Ti-Ni, Ti-Sn) PRODUCED BY POWDER METALLURGY APPROACH

4.1 INTRODUCTION

After studying the development of CP-titanium fabricated by the P/M press and sinter technology, further preliminary research was conducted relating to P/M processing of titanium binary systems. In the present instance two examples were assessed, namely Ti-Ni and Ti-Sn. This part of the work was principally aimed at the incorporation of liquid phase sintering (LPS) mechanisms into the base titanium powder. If LPS is able to be employed, it is anticipated that the densification can be facilitated and improved. As a result, lower sintering temperatures and/or shorter sintering times could be adopted, while still achieving the same level of densification. Potentially, this approach then has the subsequent benefit of reducing the production cost for titanium-based alloys.

In order to utilize the liquid phase sintering mechanism, the proper alloying element(s) must be selected. Two types of LPS have been examined in the present work. The first of these requires the retention of a persistent liquid phase volume at the sintering temperature, and is consequently referred to as “persistent” LPS; for the case of the current study, nickel has been selected as an appropriate additive. The other common type of LPS process involves a transient liquid phase that forms at relatively low temperatures (i.e. a low melting point component), and is ultimately able to be fully taken into a solid alloy phase at the elevated sintering temperature. Tin has been employed for this “transient” LPS process in the present study as it possesses a low melting point (232°C) and is an ideal candidate to develop a transient liquid phase during sintering. The Sn particles melt during the early stage of sintering, and then wet the titanium particles to potentially initiate low temperature particle rearrangement and hence densification.

For the purpose of further reducing the processing costs of titanium alloys, attempts to transform the time-consuming batch sintering (i.e. vacuum) to a continuous process were also conducted. However a protective atmosphere is required during the

process, with argon being an ideal candidate because of its inertness with respect to all metals. On the other hand, nitrogen should also be considered, owing to its lower cost and availability.

Based on these various processing factors, a preliminary investigation was carried out to develop binary Ti-Ni and Ti-Sn alloys. The two binary alloys were produced by the P/M press-and-sinter technique, as outlined in Chapter 3. The effects of solute concentration were studied as a function of sintering temperature, and related to the respective binary phase diagram using the thermodynamic predictive software program FactSage. In addition, the influence of sintering atmosphere was also assessed. Finally, the effects of these parameters upon the microstructure, composition and mechanical properties were investigated to better understand the sintering reactions in binary titanium P/M systems.

4.2 MATERIALS AND EXPERIMENTAL METHODS

The binary additive powders used in this segment of the study were Ni type 123 (100% grade), as shown in Fig. 56, obtained from Vale Inco (Sudbury, ON, Canada) and Sn (-325 mesh, 99.8% purity grade, stock#10379, lots#J23S050), as shown in Fig. 57, obtained from Alfa Aesar (Ward Hill, MA, USA). The titanium powder used was identical to that used for the research presented in Chapter 3. Table 14 highlights the basic particle size distribution obtained for each powder using the laser diffraction method with a Malvern Master Particle Sizer (Model# 20600, Worcestershire, UK). All samples were prepared using the same Licowax LC lubricant as mentioned in Chapter 3, at a concentration of 1.5 wt%, for compaction of the alloy blends described in the present chapter.

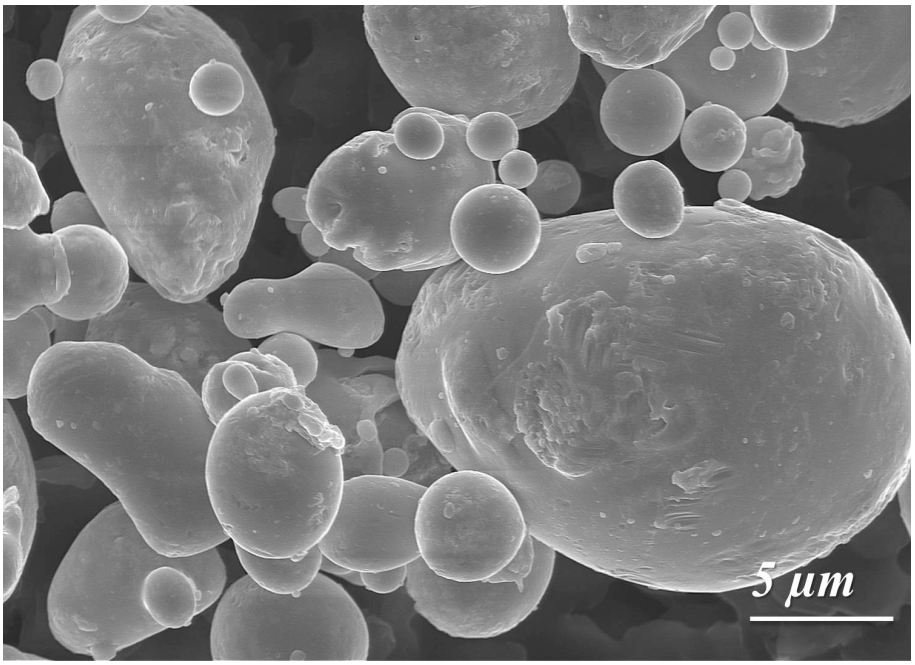

Fig. 56. SEM micrograph of the Sn powder.

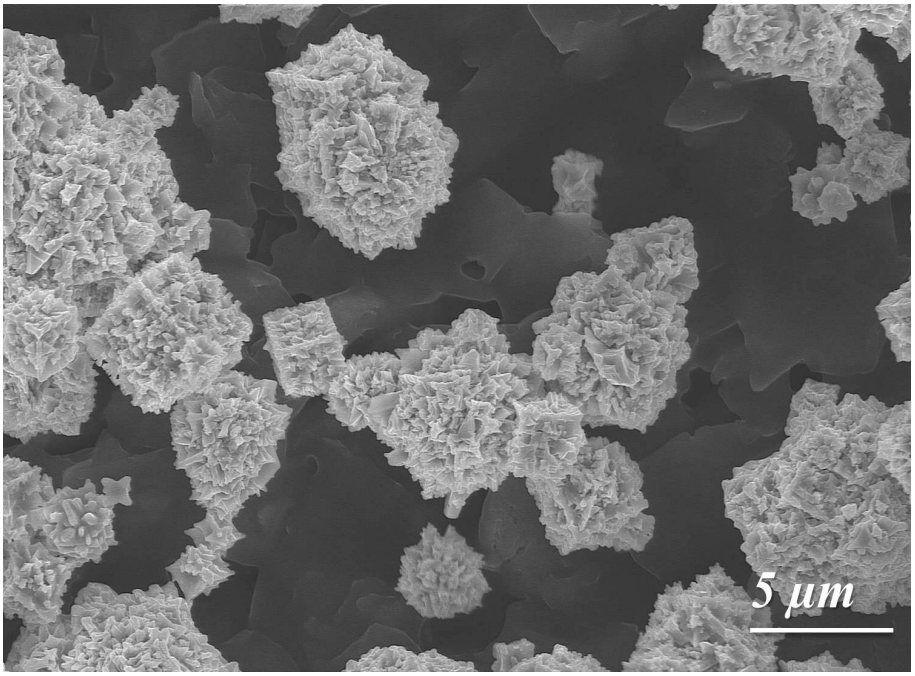

Fig. 57. SEM micrograph of the Ni 123 powder.

Table 14. Particle size analyses of both the nickel and tin powders, compared with the HDH titanium.

Particle size (μm)	Ni	Sn	HDH Ti
D_{90}	24.0	22.5	48.2
D_{50}	10.0	11.1	27.4
D_{10}	4.9	4.9	13.6

In this study, the experiments were mostly conducted according to the procedures outlined previously in Chapter 3, which includes compaction, delubrication and sintering, density measurement, hardness testing, tensile properties assessment, and the microstructure and morphology examination (i.e. optical microscopy, SEM, and XRD).

For the two binary systems (i.e. Ti-Ni and Ti-Sn), the solute element was blended with the CP titanium powder and 1.5 wt% LC wax (with solute concentrations ranging from 2.5% to 10 wt%). All blended samples were then compacted at 300MPa. While the general processing procedures were nominally identical to those described previously, the tensile samples were pressed directly to a dog-bone shape under a the compaction pressure of 300MPa, in accordance with the MPIF standard 10, rather than machined from Charpy bars, as outlined in Chapter 3. The delubrication stage was performed under nitrogen for all the binary samples. The theoretical densities of Ti-Ni and Ti-Sn alloys were calculated using a mixture rule, with the assumption that the volume was not changed after alloying. The property data was compiled using two samples/tests for each value in the figure; the standard deviations were also calculated and shown as error bars.

4.3 RESULTS AND DISCUSSION

4.3.1 Liquid fraction prediction

The amount of liquid that exists during the sintering stage can have an important determination on the effect of LPS, and it can be estimated directly from the relevant binary phase diagram. In the case of Ti-Ni alloys, the equilibrium phase diagram (Fig. 58)

indicates that a eutectic reaction occurs at 942°C, when the nickel content is approximately 12 wt%. At this eutectic temperature, the Ti-Ni alloy begins to form a liquid, while with lower Ni contents (i.e. the 2.5 to 10% designed in this study), the liquid phase forming temperature is increased. On the other hand, from the equilibrium Ti-Sn phase diagram (Fig. 59), it can be seen that Sn dissolves completely in the titanium to form a solid solution. Consequently, under equilibrium conditions, there is no liquid phase existing at any temperature until the liquidus line is reached.

In addition to an assessment of the Ti-Ni and Ti-Sn phase diagrams, predictive thermodynamic modelling software (FactSage, CRCT, École Polytechnique de Montréal, Montréal, Canada) was utilised to determine the relative liquid phase content during the sintering process. For the Ti-Ni alloy system, the results indicate that a liquid phase forms at temperatures as low as 1070°C when the Ni content is 10% (Fig. 60). Lower Ni content raises the minimum temperature for liquid formation. This trend agrees with the Ti-Ni phase diagram in that the liquidus temperature continues to drop with increasing Ni content. Regarding the FactSage result for the Ti-Sn alloys (Fig. 61), there is no persistent liquid phase present at any temperatures (i.e. under equilibrium conditions). In contrast, the transient liquid formation is expected to occur at lower temperature and wet the titanium particles to enhance densification. However, it is important to remember that sintering is usually not an equilibrium process, and the prediction based on the phase diagram may therefore not reflect the actual process occurring during sintering. Hence, the transient nature of liquid formation is not revealed when using such a method as FactSage.

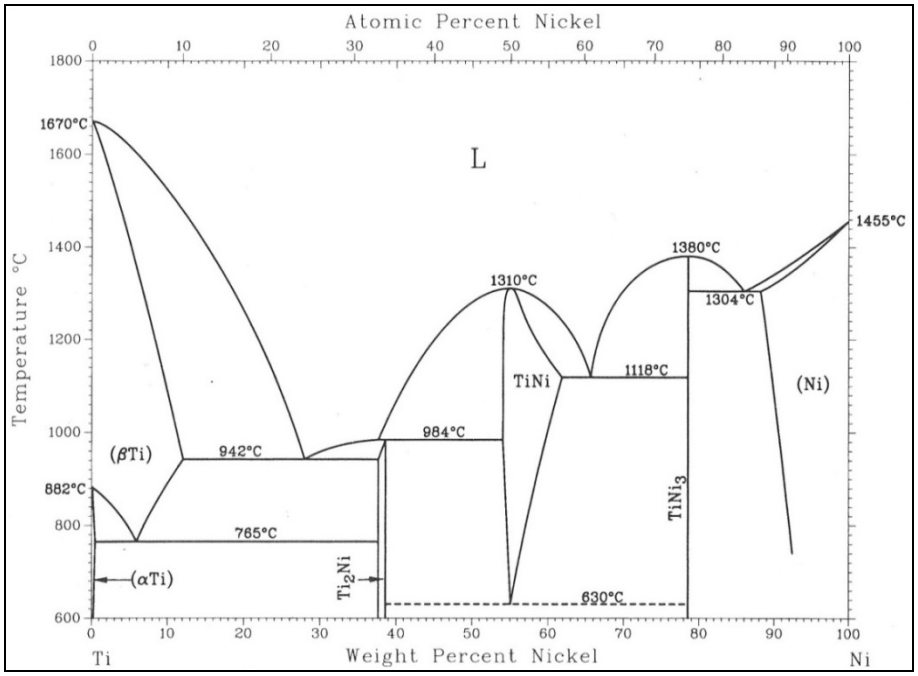

Fig. 58. The titanium-nickel phase diagram (ASM International. Handbook Committee, 1990).

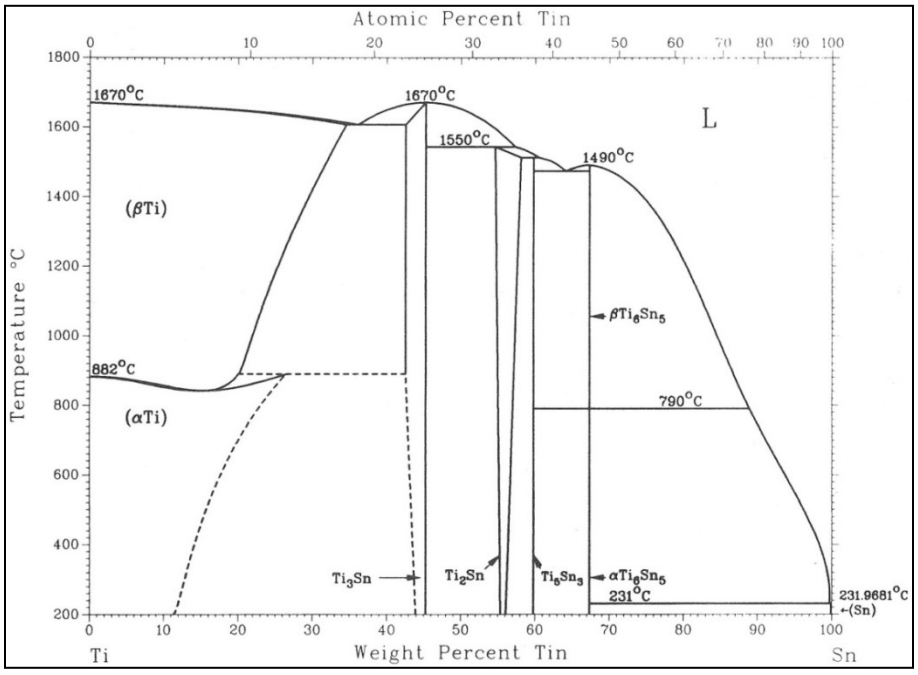

Fig. 59. The titanium-tin phase diagram (ASM International. Handbook Committee, 1990).

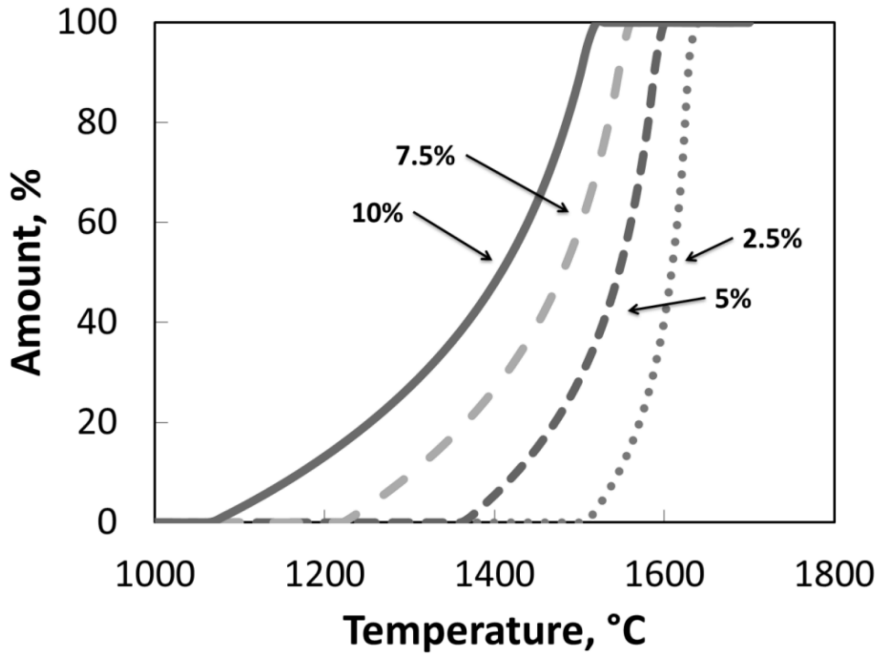

Fig. 60. Liquid phase fraction (wt%) prediction for the Ti-Ni (2.5 -10 wt%) binary alloys using FactSage.

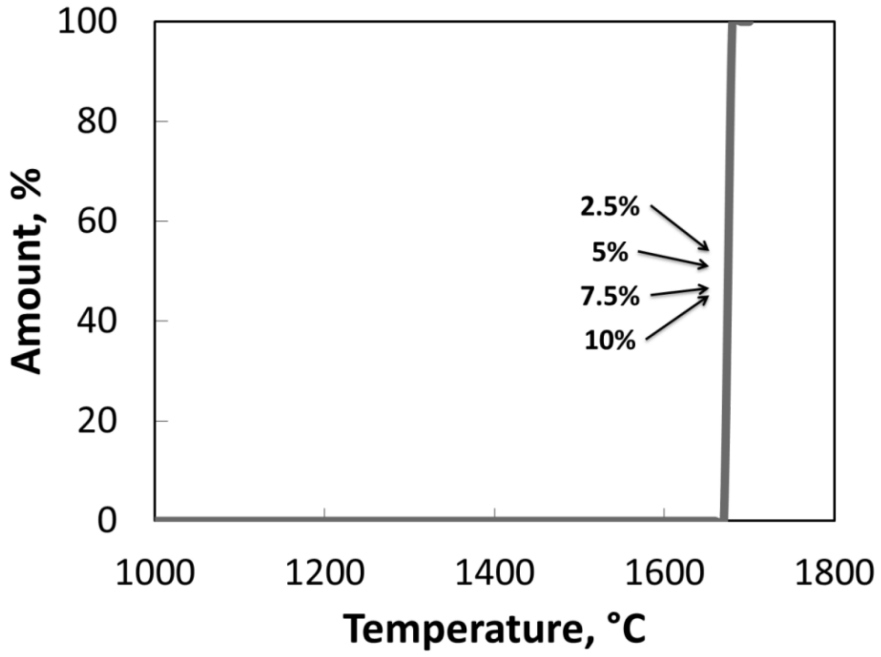

Fig. 61. Liquid phase fraction (wt%) prediction for the Ti-Sn (2.5 -10 wt%) binary alloys using FactSage.

4.3.2 Sintering response of binary titanium alloys

4.3.2.1 Effects of solute content and sintering temperature

From the above discussion, the solute content is potentially extremely important for the Ti-Ni system in terms of liquid phase assisted densification. The influence of solute content and sintering temperature upon sintered density are shown in Fig. 62. At 1100ºC, a clear density increase, which is an evident indication of LPS, is observed in the Ti-10%Ni samples. In other words, with the nickel content set at 10wt% the sintered density can be greatly enhanced and even exceed the value of pure CP titanium samples sintered at 1200°C. However, when the Ti-10%Ni composition was sintered at 1200°C there was excess liquid forming that adhered to the crucible (Fig. 63). The sintering temperature was consequently restricted to 1200°C or below, for the Ti-Ni alloys for the sake of preserving the crucibles. However, it is important to note that the alloys processed with nickel content less than 10% might not cause problem at slightly higher temperatures (e.g. 1250 or 1300ºC), especially when the lower Ni concentrations are employed (e.g. 2.5 or 5wt%).

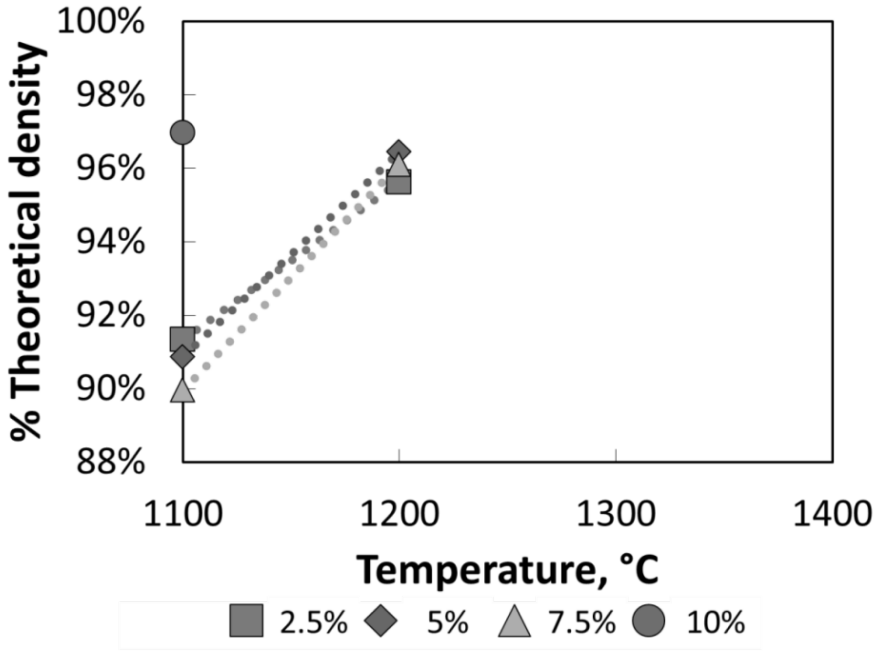

Fig. 62. Sintered densities of the Ti-Ni binary alloys prepared at 1100 and 1200°C.

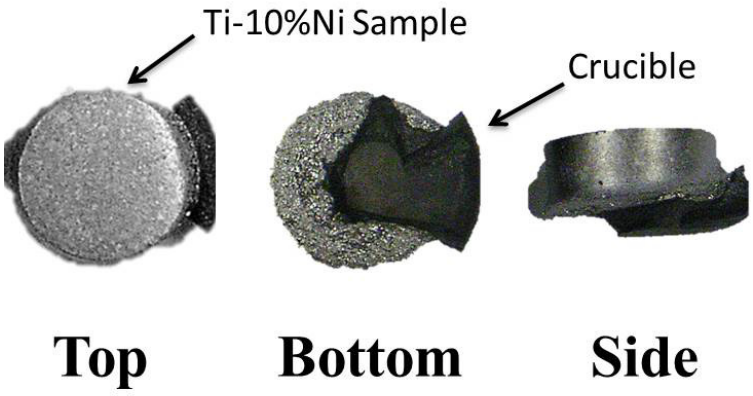

Fig. 63. Excess liquid phase formation for the Ti-10%Ni composition sintered at 1200°C.

As for the Ti-Sn alloys, the increase content of Sn element does not seem to have any significant benefit to densification, except for the lowest Sn containing alloy (i.e. Ti-2.5%Sn), which results in the highest sintered density at both 1300 and 1400°C.

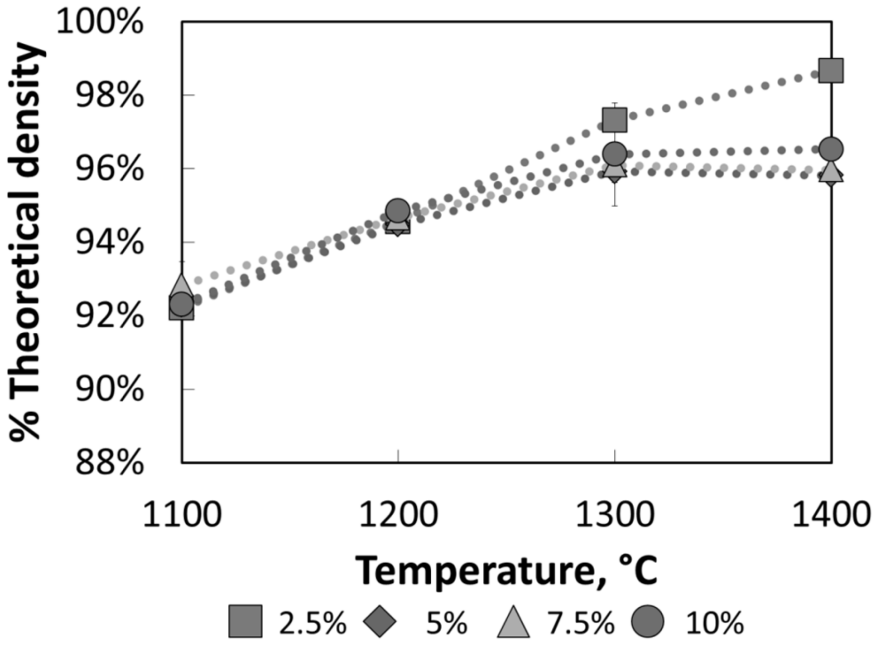

Fig. 64. Sintered densities of the Ti-Sn binary alloys prepared between 1100 and 1400°C.

When comparing the two binary alloys with the CP titanium described in the previous chapter, the potential benefits of LPS have emerged, as highlighted in Table 15. There are 3.4% and 1.7% density gains for the Ti-Ni and Ti-Sn alloys, respectively, when compared to the CP-Ti processed using the same sintering temperature, time and compaction pressure.

Table 15. Sintered density comparison of CP-Ti, Ti-Ni and Ti-Sn for samples prepared at 1200°C.

	CP-Ti*	Ti-Ni**	Ti-Sn***
Sintered density (% theoretical)	93.30%	96.45%	94.85%

*=from previous data Fig. 48
**=highest density of Ti-Ni achieved at 1200°C (Ti-5%Ni)
***=highest density of Ti-Sn achieved at 1200°C (Ti-10%Sn)

4.3.2.2 Effects of sintering atmosphere

The influence of the sintering atmosphere is evaluated in terms of the sintered density of samples, as shown in

Fig. 65 and Fig. 66. For both Ti-Ni and Ti-Sn alloys, sintering in argon generates slightly lower densities, but otherwise a generally similar response to the values obtained for vacuum sintered samples. The lower densities obtained in the argon atmosphere are likely due to the atmospheric environment (~800 torr) that may hinder entrapped gas from escaping out of the compact during sintering. Conversely, the lack of gas pressure in the vacuum environment helps minimise any gas remaining in the pores and therefore aids the densification. The surface morphology observed using SEM, shown in Fig. 67 and Fig. 68, also agrees with these observations. The morphology of the vacuum sintered samples is the densest, while the argon sintered samples appear more porous.

The use of a controlled nitrogen atmosphere generates a similar decrease in sintered density, when compared with the vacuum environment. The surface morphology shown in Fig. 67(c) and Fig. 68(c), which was confirmed as titanium nitride (TiN) by

EDS, may explain the observed decrease in density. The porous TiN ceramic surface layer, which can also be expected within surface connected porosity, may impair the level of volume shrinkage during sintering; the covalent nature of TiN results in relatively low self-diffusivity, thus retarding densification.

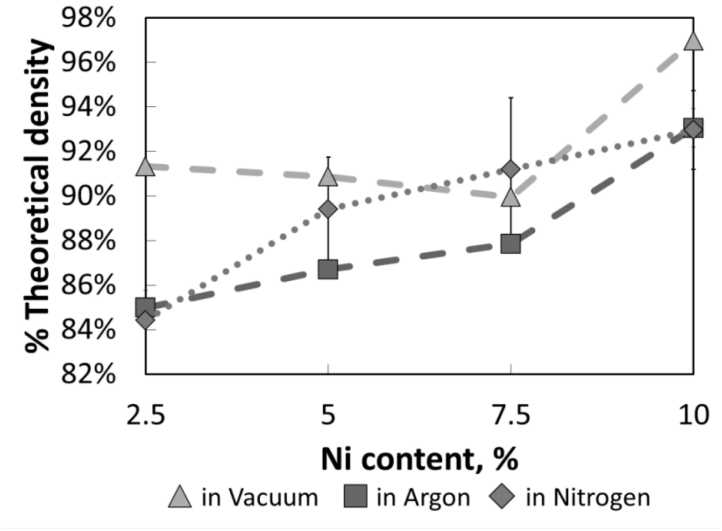

Fig. 65. The sintered density of Ti-Ni alloys prepared in various atmospheres (samples sintered at 1100°C for 120 minutes).

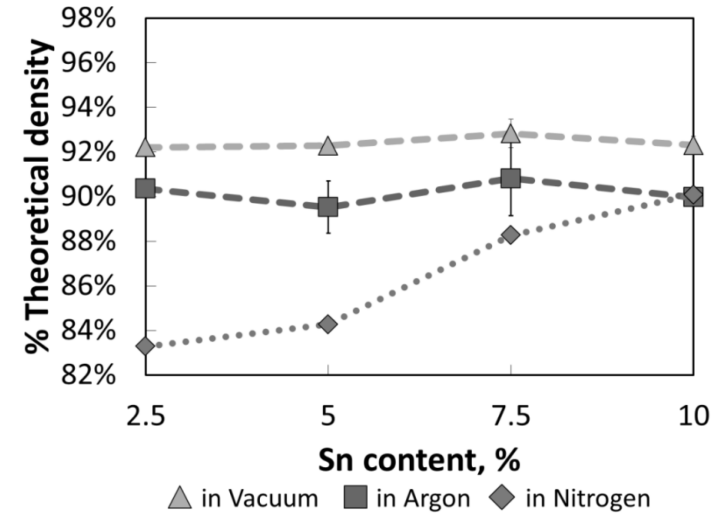

Fig. 66. The sintered density of Ti-Sn alloys prepared in various atmospheres (samples sintered at 1100°C for 120 minutes).

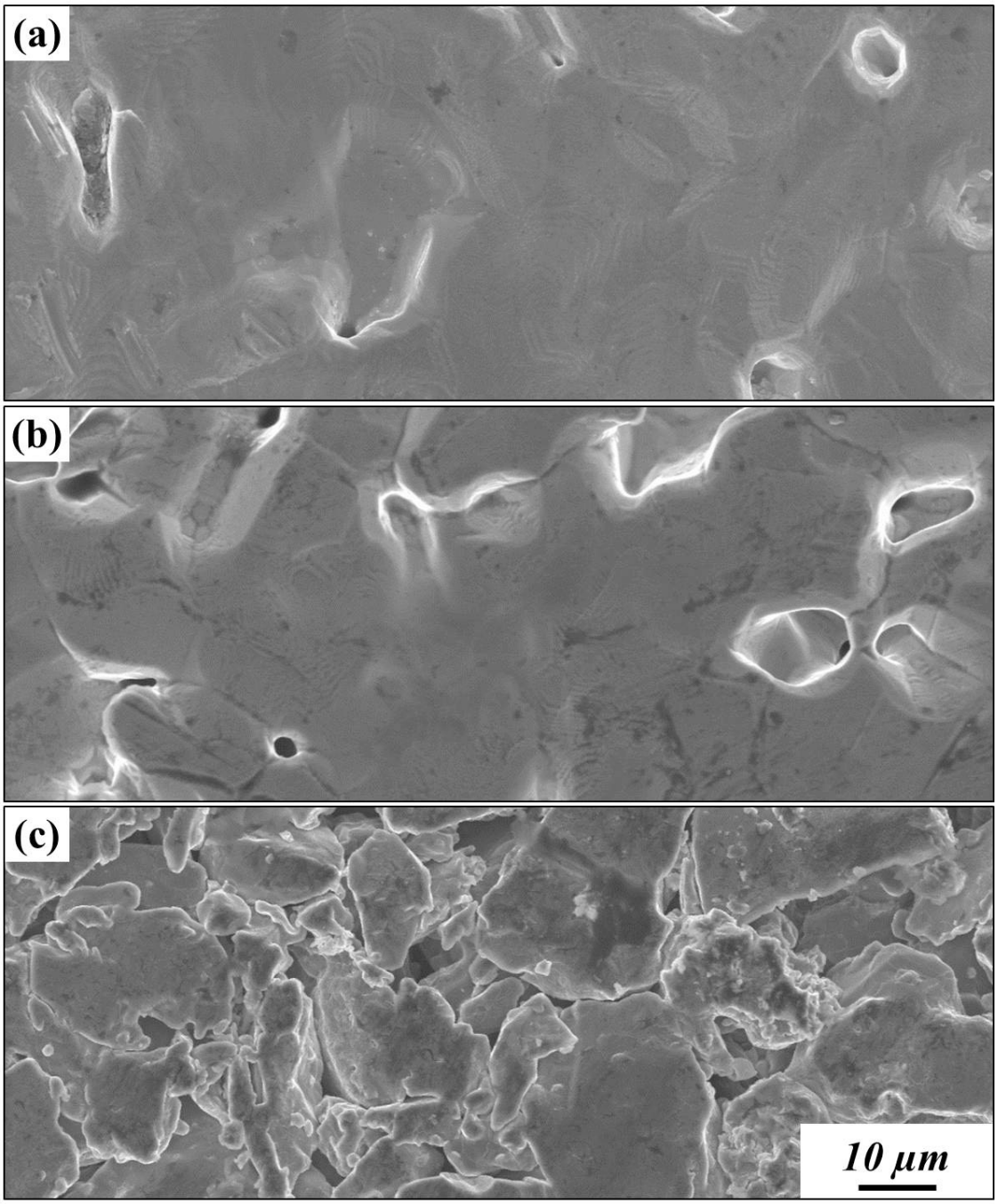

Fig. 67. SEM micrographs of the surfaces of the Ti-2.5Ni composition samples after sintering at 1100°C under (a) vacuum (b) argon (c) nitrogen atmosphere.

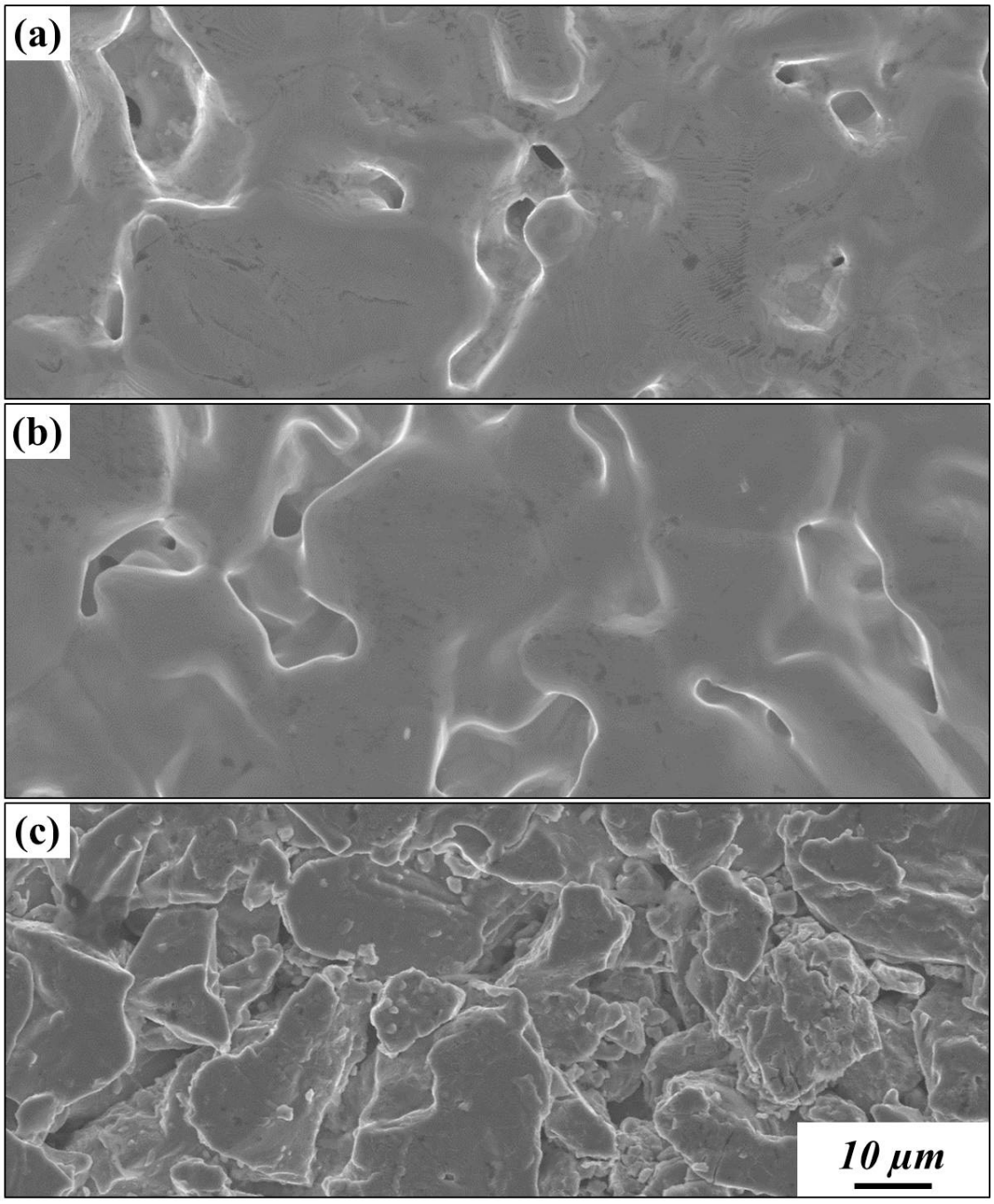

Fig. 68. SEM micrographs of the surfaces of the Ti-2.5Sn composition samples after sintering at 1100°C under (a) vacuum (b) argon (c) nitrogen atmosphere.

4.3.3 Mechanical properties

4.3.3.1 Hardness

The hardness values for the binary samples were obtained using the discs made for sintered density measurement. From the results presented in Fig. 69 and Fig. 70, the trend in hardness values generally corresponds to the sintered density obtained, in spite of some limited scatter of the measured values. Some small variation in hardness may be anticipated in materials containing residual porosity, for example when sampling localised regions containing higher or lower than average pore volumes

Similar to the sintered density observation reported in Section 4.3.2.1, the hardness is improved by 6.6% for Ti-Ni and 6.7% for Ti-Ni, when compared to the CP titanium samples described in Chapter 3, as shown in Table 16. The increase in hardness is believed to be the result of solid solution hardening from alloying in combination with the improved densification of the Ti-Ni and Ti-Sn alloys. It is also likely, based on the phase diagrams presented in Fig. 58 and Fig. 59, that secondary phase precipitation has occurred. This may be confirmed by more in-depth microstructural characterisation at a future stage.

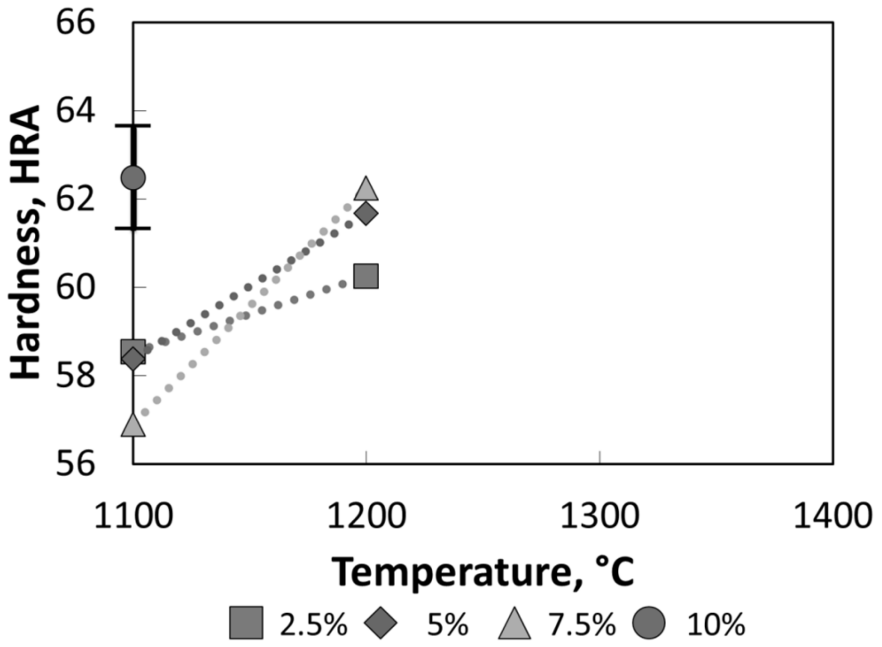

Fig. 69. The hardness of Ti-Ni alloys as a function of sintering temperature.

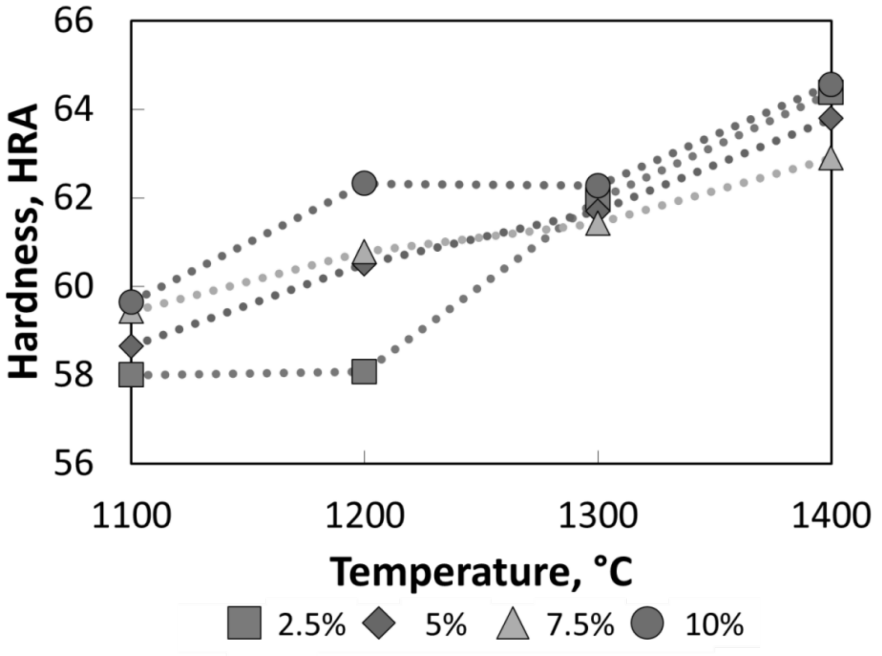

Fig. 70. The hardness of Ti-Sn alloys as a function of sintering temperature.

Table 16. A comparison of the hardness of CP-Ti, Ti-Ni and Ti-Sn samples, sintered at 1200°C.

	CP-Ti*	Ti-Ni**	Ti-Sn***
Hardness (HRA)	58.4	62.3	62.3

*=from previous data Fig. 53
**=highest hardness of Ti-Ni achieved at 1200°C (Ti-7.5%Ni)
***=highest hardness of Ti-Sn achieved at 1200°C (Ti-10%Sn)

4.3.3.2 Tensile properties

The tensile properties were examined using dog-bone shaped samples, formed directly to shape using the press-and-sinter method in an appropriate carbide die. Due to the concerns relating to melting of Ti-Ni samples at 1200°C, the tensile tests were initiated using test pieces prepared at a lower temperature of 1000°C. The effects of the solute content on selected tensile properties are shown in Fig. 71 to Fig. 76. These results reveal no definite trends. However there is a generally decreasing tendency in terms of the values recorded. The best tensile properties occurred for the 2.5% Ni and 2.5% Sn compositions, sintered under vacuum, whereas the poorest properties mostly occurred for samples with 7.5% solute content. It should be noted that the 10% Sn data is absent in the tensile results, owing to difficulties in making the samples. The Sn particles appeared to agglomerate and dewetting of Sn was apparent after delubrication (Fig. 80) or sintering (Fig. 81). This problem is likely caused by the uneven distribution of the Sn powder, or simply too high of a concentration (i.e. 10%), which forms an excessive amount of liquid that partially exudes out of the samples. It should be noted that for the two series of data obtained when sintering in either vacuum or argon, both begin at the same CP titanium (0%) value (Fig. 71-Fig. 76).

From the above results, the 2.5 %Ni and 2.5 %Sn titanium compositons were chosen for further evaluation of the effects of sintering temperature up to 1200ºC. The data obtained for these samples was then compared to CP titanium (N.B. the CP α-Ti data was obtained using cylindrical buttonhead samples machined from Charpy bars). The tensile properties obtained are presented in Fig. 77 to Fig. 79. It is apparent that the Ti-2.5%Ni samples present marginally better results for the temperature range of 1000°C

through to 1200°C. There are small gains in all the compositions from 1000°C to 1100°C. However all the results presented for 1200°C show a considerable decrease. This general observation is believed to be caused by sample distortion during sintering resulted from LPS (Robertson, 2009). Distortion was observed for all the sintered tensile test bars, to a greater or lesser extent. Besides, this distortion was also proposed causing from the desorption of hydrogen in the HDH powder during sintering (Low et al., 2007). The tensile values were likely affected due to stress concentration at different positions within the samples.

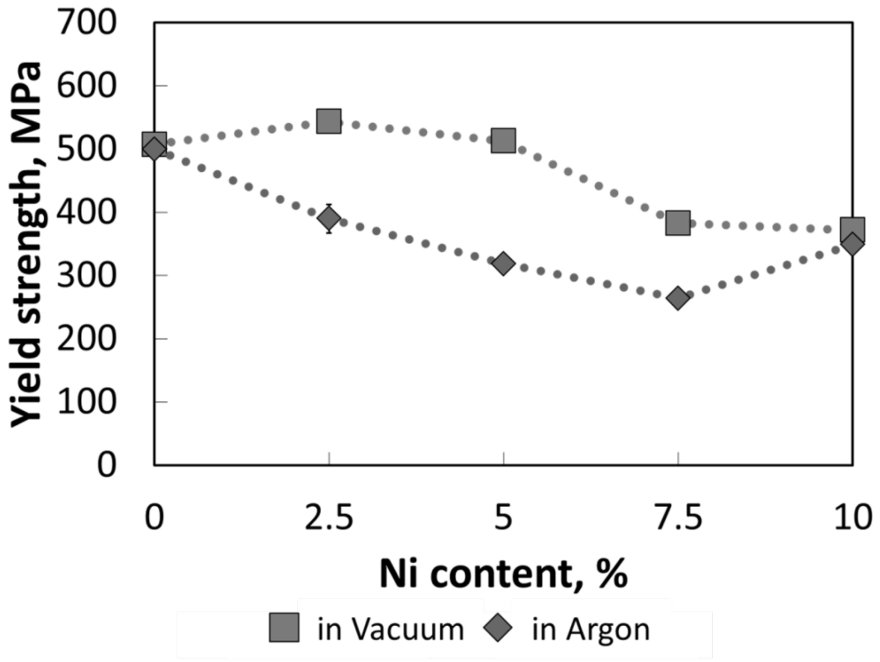

Fig. 71. Effects of solute content on the yield strength of Ti-Ni alloys sintered at 1000°C.

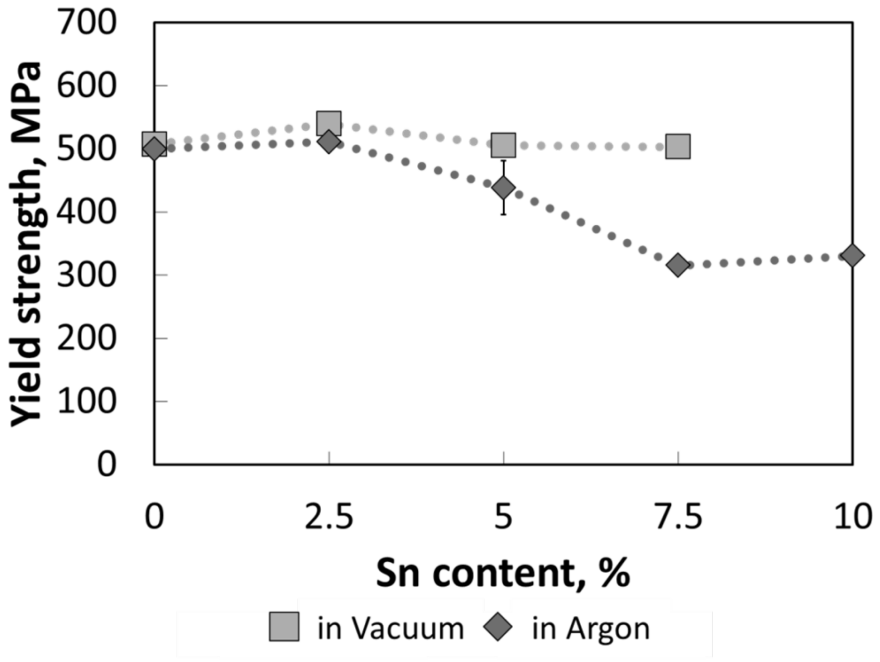

Fig. 72. Effects of solute content on the yield strength of Ti-Sn alloys sintered at 1000°C.

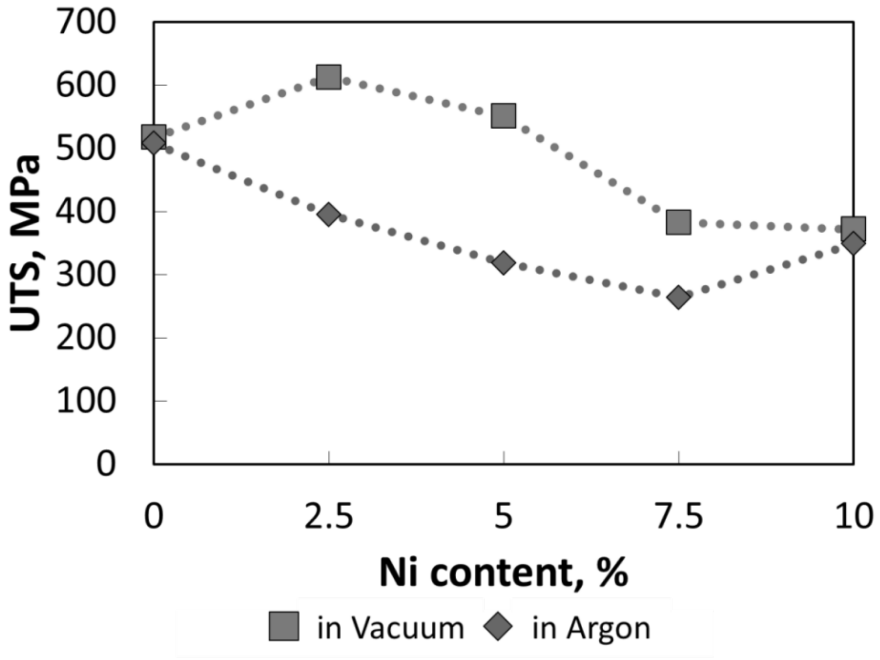

Fig. 73. Effects of solute content on the UTS of Ti-Ni alloys sintered at 1000°C.

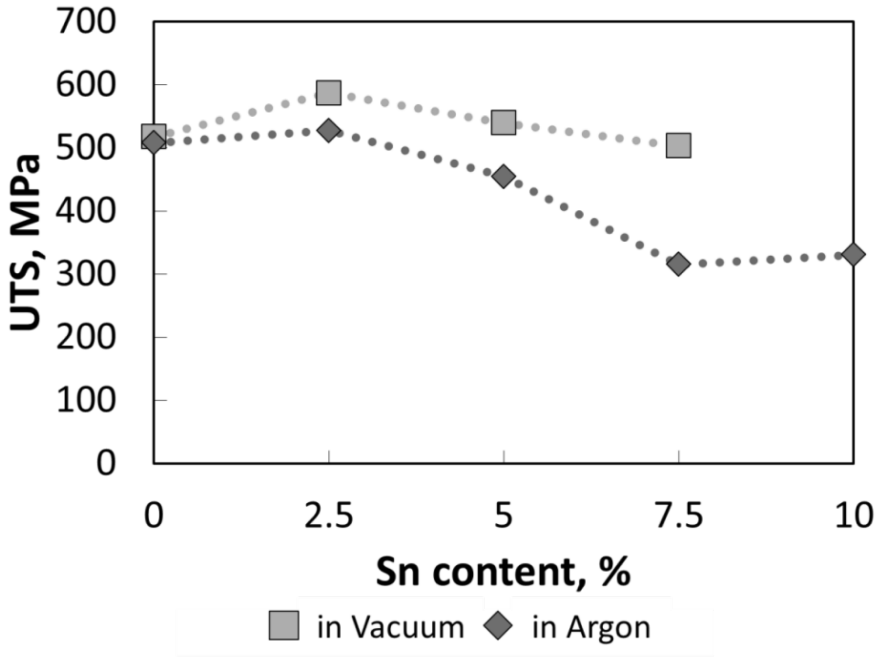

Fig. 74. Effects of solute content on the UTS of Ti-Sn alloys sintered at 1000°C.

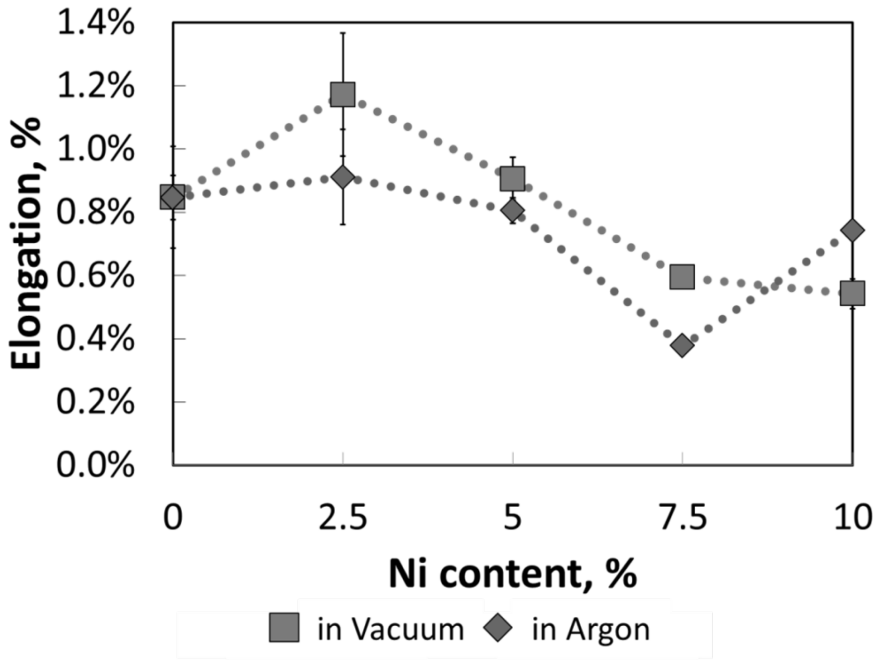

Fig. 75. Effects of solute content on the elongation to failure of Ti-Ni alloys sintered at 1000°C.

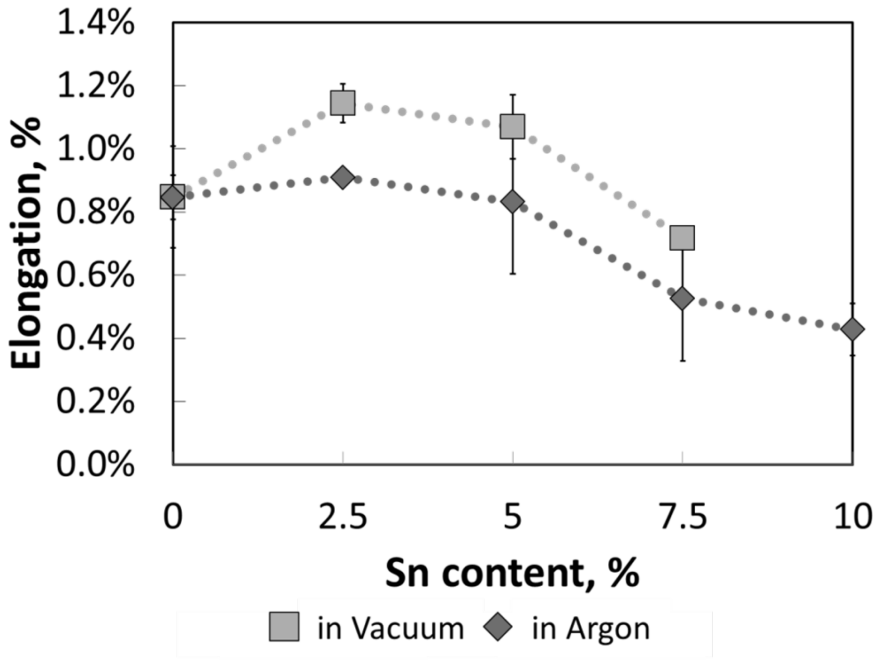

Fig. 76. Effects of solute content on the elongation to failure of Ti-Ni alloys sintered at 1000°C.

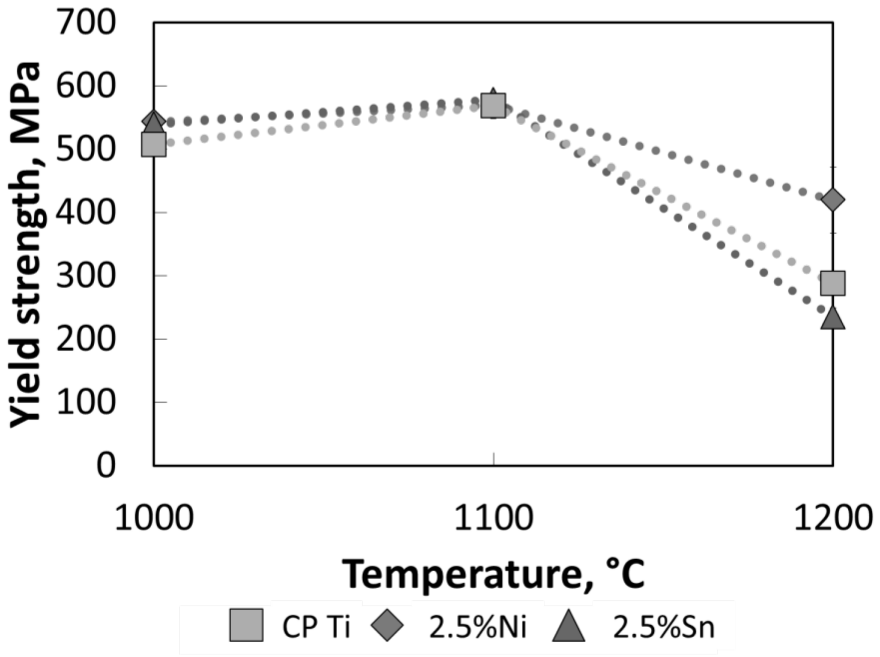

Fig. 77. Comparison of the effects of sintering temperature on the yield strength of CP titanium, Ti-2.5%Ni and Ti-2.5%Sn samples.

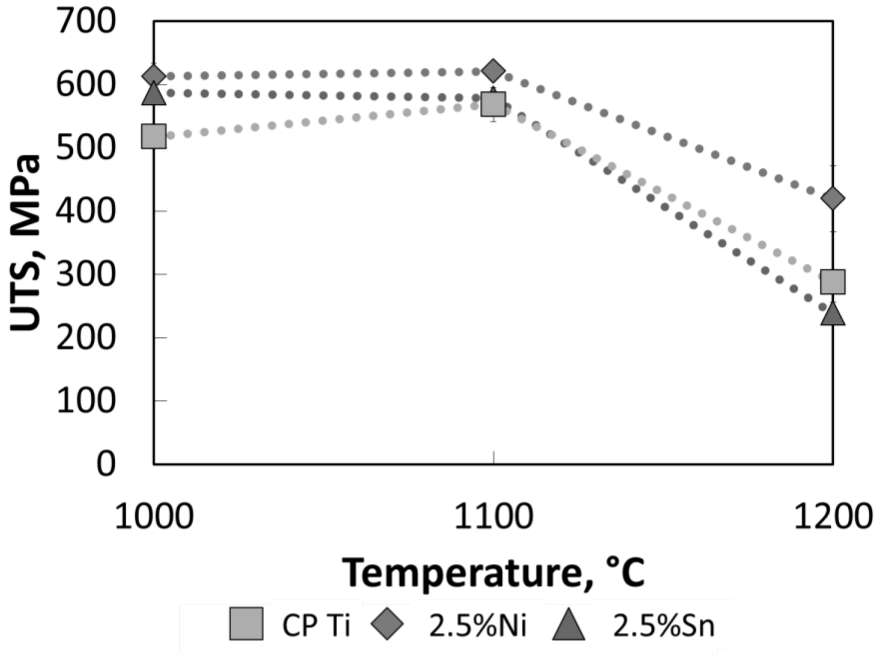

Fig. 78. Comparison of the effects of sintering temperature on the UTS of CP titanium, Ti-2.5%Ni and Ti-2.5%Sn samples.

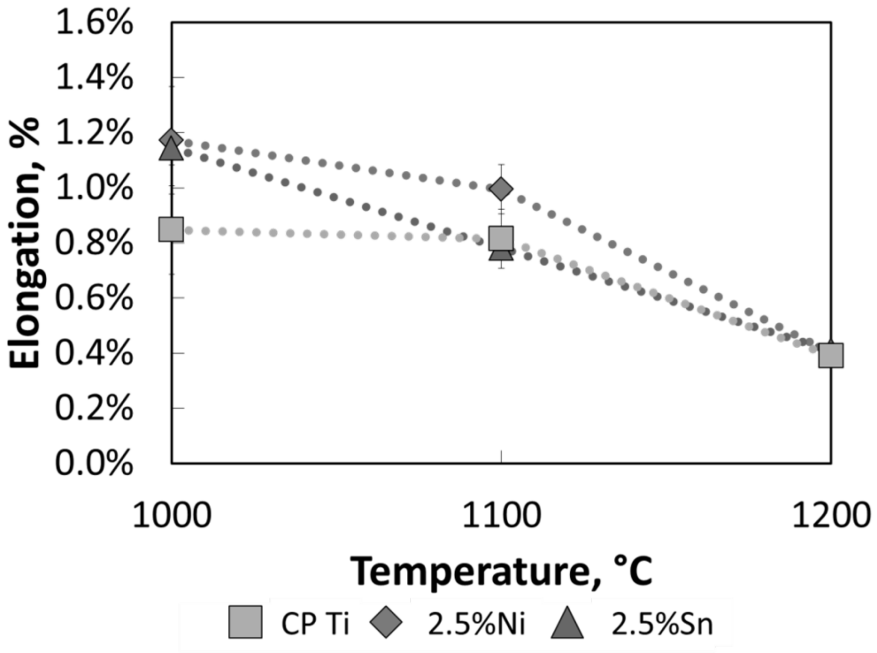

Fig. 79. Comparison of the effects of sintering temperature on the elongation to failure of CP titanium, Ti-2.5%Ni and Ti-2.5%Sn samples.

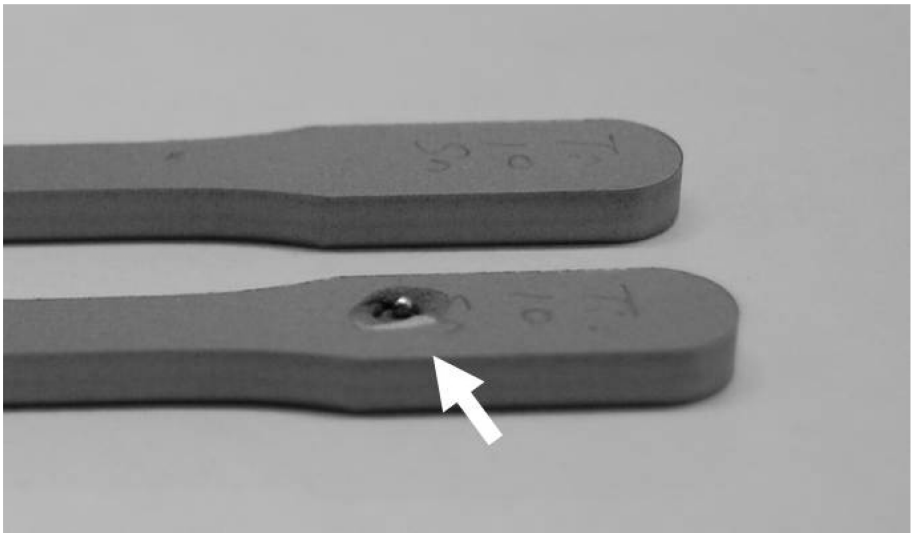

Fig. 80. Sn bead dewetting from the sample after delubrication.

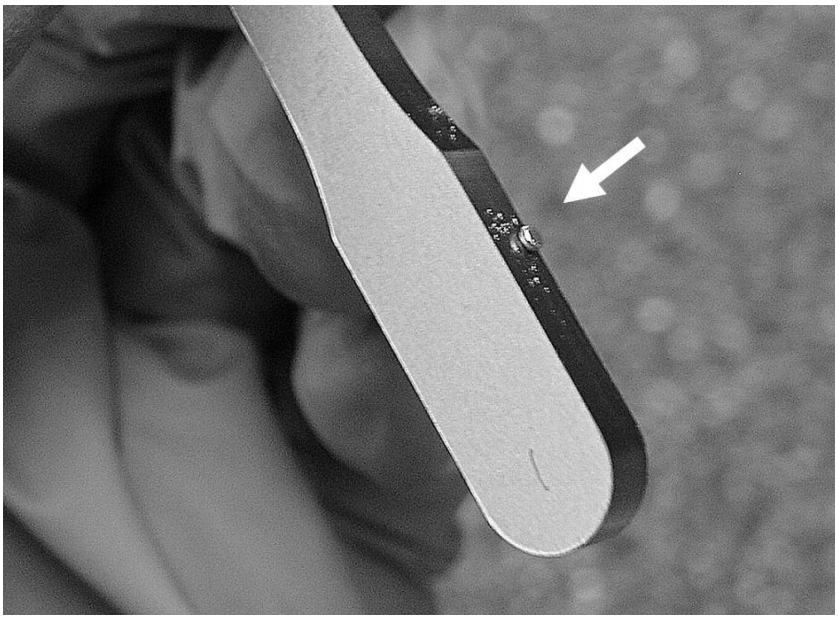

Fig. 81. Sn bead dewetting from the sample after sintering.

4.3.4 Composition and phase identification

When assessing the sintering reactions, composition as well as microstructure analyses were conducted. For the Ti-Ni alloys, optical micrographs revealed three phases (marked as A, B and C in Fig. 82(c)), in different ratios, as shown through Fig. 82. Further SEM imaging highlighting these phases is presented in Fig. 83, with both titanium and Ti_2Ni phase confirmed by EDS analysis. In addition, Ti_2Ni was also present in the XRD analysis, as shown in Fig. 84, which also confirmed the titanium matrix to be the lower temperature HCP α-Ti form. No evidence of the β-Ti phase was found in the XRD examination, although nickel is a β stabilizer.

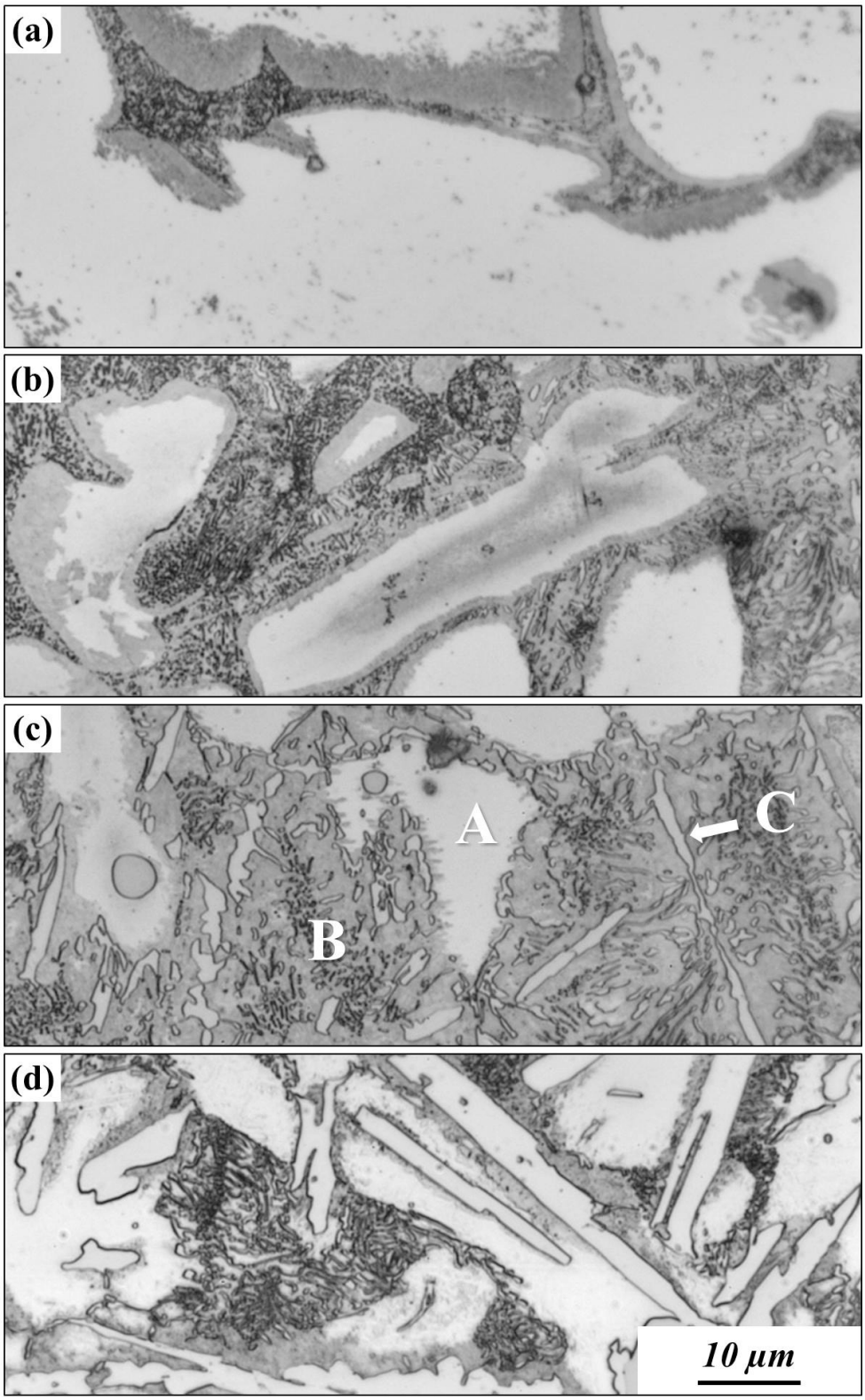

Fig. 82. Optical micrographs of vacuum sintered Ti-Ni alloys (1200°C) with (a) 2.5%, (b) 5%, (c) 7.5%, and (d) 10% Ni content.

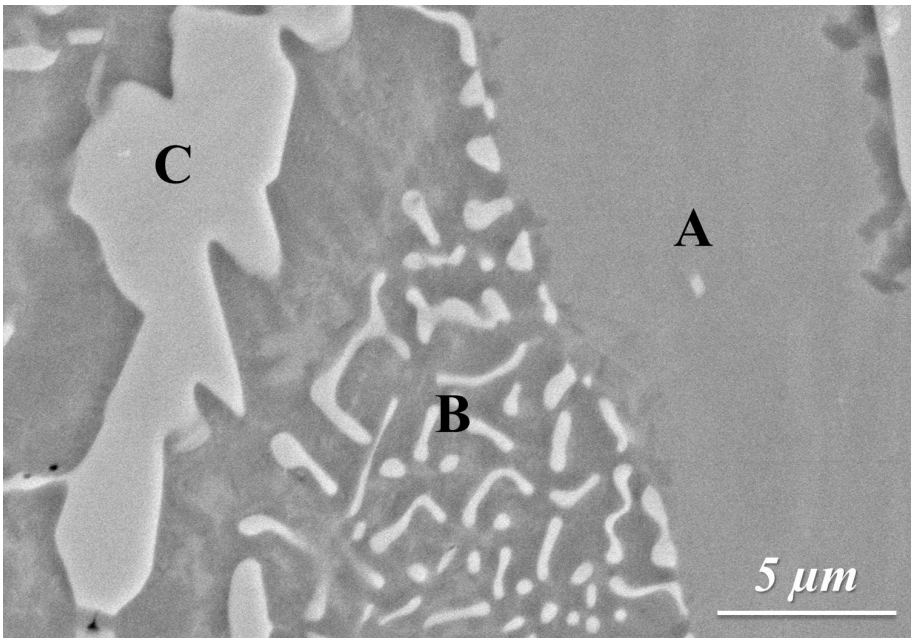

Fig. 83. SEM image of Ti-10%Ni sintered at 1200°C presenting distinct phases (A) HCP titanium, (B) eutectoid, and (C) the Ti_2Ni intermetallic phase.

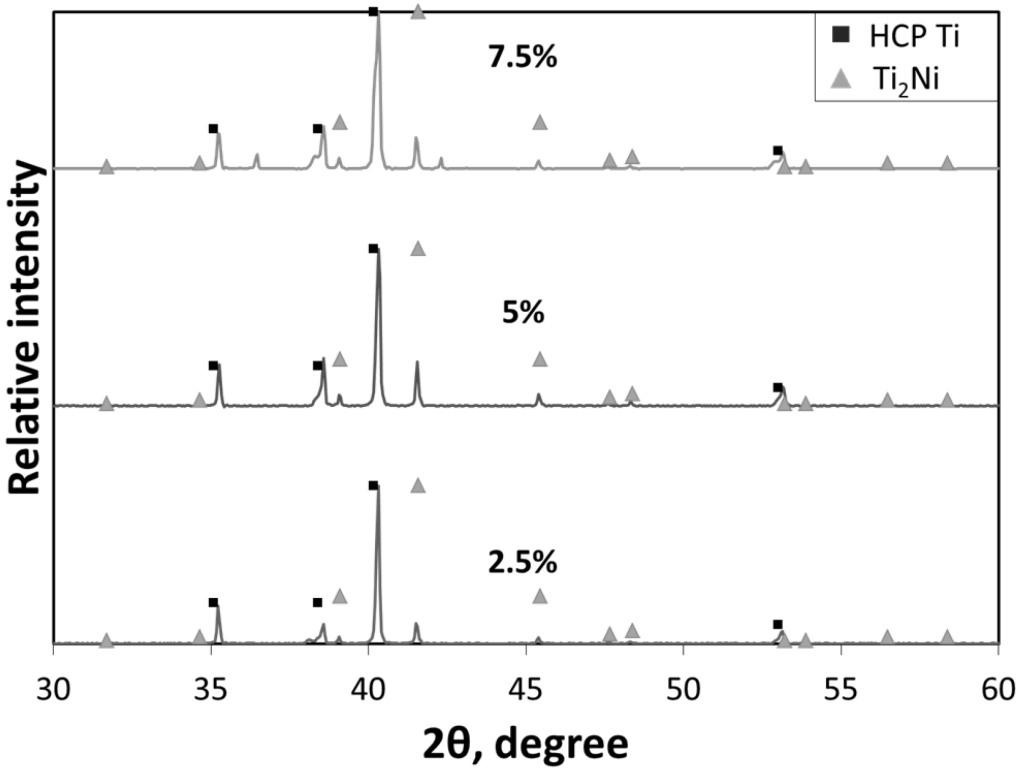

Fig. 84. XRD of Ti-Ni alloys sintered at 1200ºC.

In terms of the Ti-Sn binary alloys, the optical micrographs show similar microstructures, as presented in Fig. 85 (only 5% and 10% Sn content samples are shown), in all of the compositions. From the lower Sn content (Fig. 85(a)) to higher (Fig. 85(b)) there is no significant difference in terms of the observed microstructure, although the phases are difficult to reveal clearly. With the help of SEM, higher magnification images revealed the detailed features (Fig. 86). The EDS analyses identified the same chemistry, which means the distinct features may be different crystal structures (e.g. HCP and BCC titanium). However the XRD analysis did not reveal any other phase except the α-Ti. As a consequence, further analysis of these samples would be required to more fully understand the microstructural development.

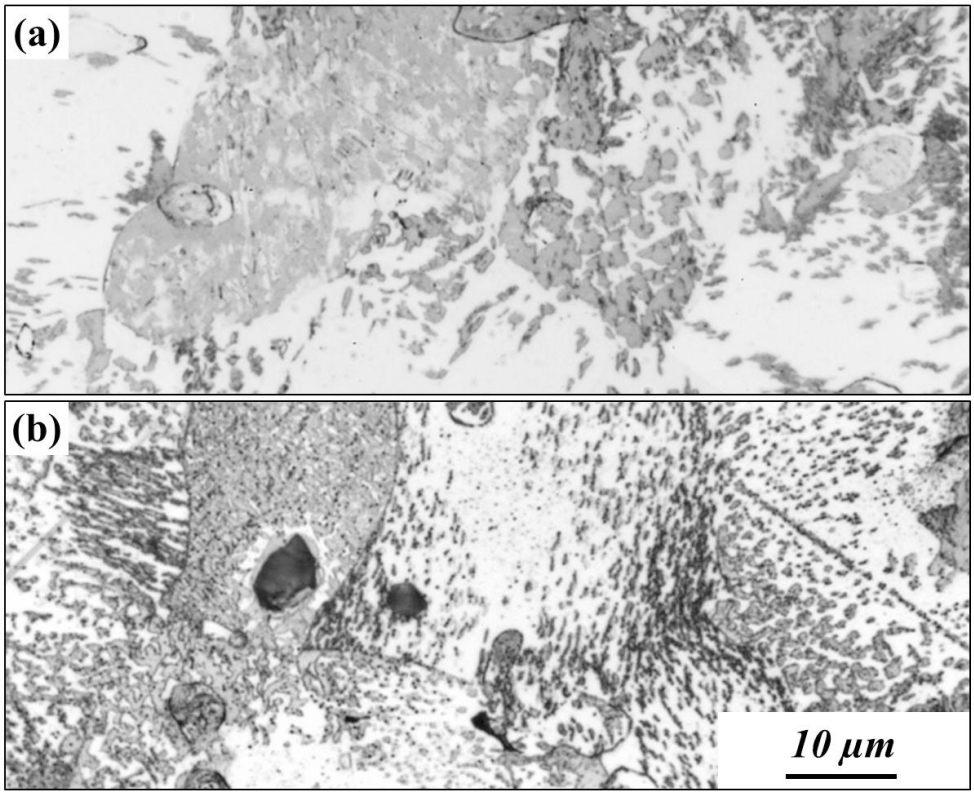

Fig. 85. Optical micrographs of vacuum sintered Ti-Sn alloys (1200°C) with (a) 5%, and (b) 10% Sn content.

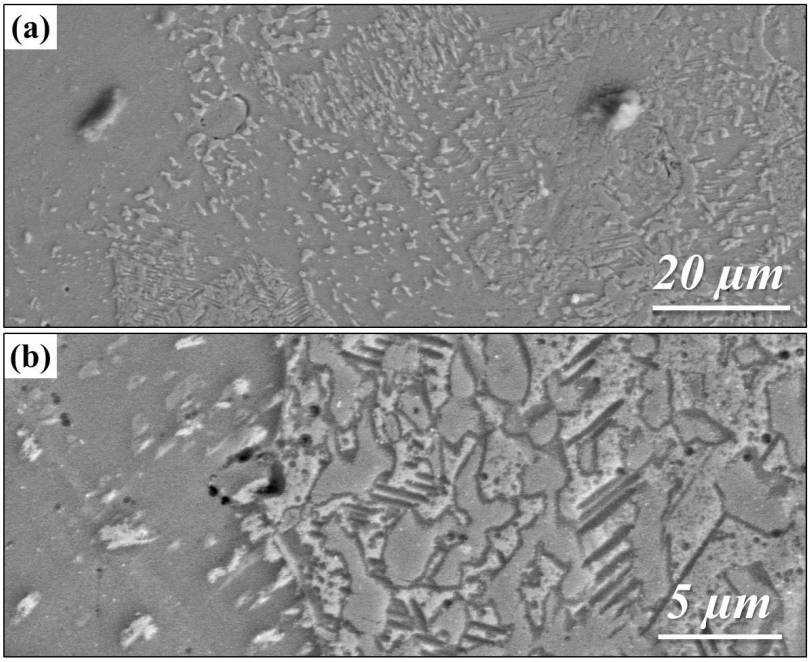

Fig. 86. SEM image of Ti-5%Sn surface morphology sintered at 1200°C (a) 1100X magnification, and (b) 4000X magnification.

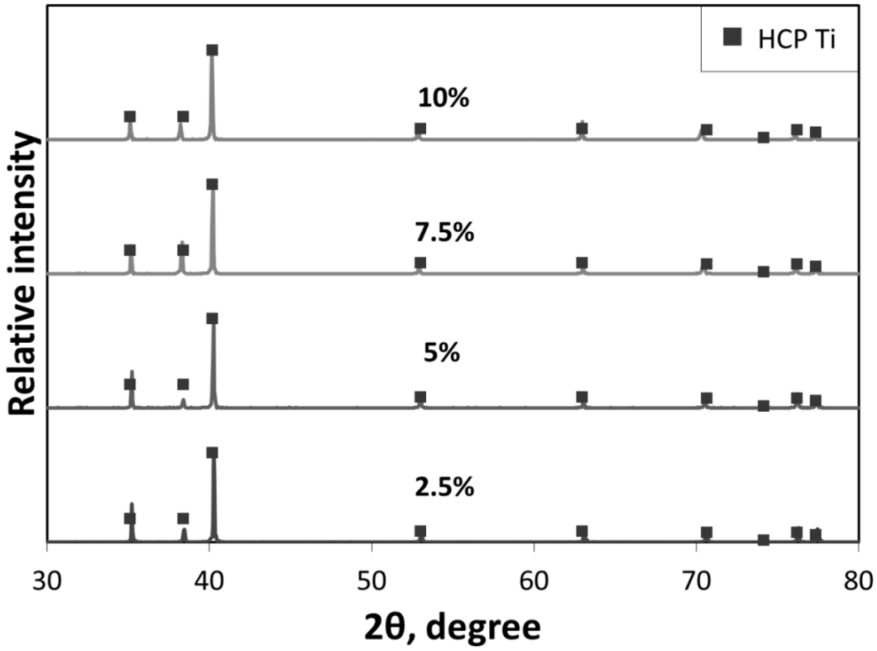

Fig. 87. XRD of Ti-Sn alloys sintered at 1200ºC.

4.4 CONCLUSIONS

Ti-Ni and Ti-Sn binary alloys were produced using the P/M press-and-sinter technique in this work. A preliminary investigation of the process parameter effects, densification behaviour and mechanical properties was carried out. From this study, it was shown that the densification was improved in both binary alloy systems compared to the CP titanium discussed in Chapter 3, and in particular for the Ti-Ni alloys. It was also demonstrated that argon has the potential of transforming the batch vacuum sintering process to a more cost effective continuous sintering approach.

Unfortunately several difficulties remain to be overcome. For the Ti-Sn system it is apparent that Sn beads can exude out of the samples after either the delubrication or sintering process. Furthermore, there was evidence of distortion of the dog-bone samples after sintering, which affected their resulting mechanical properties.

Chapter 5. CONCLUSIONS

Titanium and its alloys have gained considerable attention due to their superior properties over other metal competitors such as the steel and aluminum families (e.g. high strength-to-weight ratio, good high-temperature strength and excellent corrosion resistance). However, the high production cost is the main obstacle to broadening the applications of titanium-based alloys. Consequently, cost-effective raw material production and forming technologies are necessary. The present MASc study has focused on the powder metallurgy press-and-sinter technology for forming titanium. A fundamental study had been conducted on commercially pure (CP) titanium, as well as Ti-Ni and Ti-Sn binary alloys produced by the P/M approach.

This thesis has addressed the effects of a range of process parameters on the sintered product properties (i.e. densification behaviour, microstructure and mechanical properties) and has evaluated the optimal fabrication conditions. The alloying content and sintering atmosphere have been studied; and the microstructure and composition of the sintered products have also been analyzed. In addition, this study has highlighted the difficulties and limitations when producing titanium using the press-and-sinter approach.

Through the preceding discussions, some conclusions can be drawn and suggestions for the future works are recommended for the fabrication of CP titanium and titanium binary alloys:

5.1 CP TITANIUM

The higher compaction pressure (500MPa) helped the green compact formation by increasing the level of particle interlocking. However the risk of tooling damage also needs to be considered. The amount of lubricant used raises the concern of potential carbon contamination, and consequently the limit was set at 1.5 wt% to minimise this problem while also preventing potential tooling damage. In terms of densification, the use of higher sintering temperatures contributed to higher density products. Near fully-dense (~99% of theoretical) CP titanium can be fabricated when sintering at 1450°C for 4 hours.

Excellent tensile strengths (>750MPa) were obtained when sintering at 1300 or 1400°C, although mechanical properties were degraded above this upper temperature. However, the elongation to failure was relatively low for all sintered samples. Increasing temperature results in an increase in both the mean grain and pore size, although the overall pore volume decreased considerably. A further consequence of the increasing sintering temperature was a transformation from intergranular to transgranular fracture behaviour, which was partially responsible for the property degradation noted above.

It is suggested that the interstitial contaminants (i.e. oxygen, carbon and nitrogen), which are responsible for the poor CP-Ti ductility, should be minimized as much as possible to achieve better mechanical properties. Oxygen, which is the most potent impurity affecting the mechanical properties of titanium, was found in a high concentration not only in the sintered samples but also in the raw powder. Therefore a higher purity titanium powder is necessary to reduce the oxygen impurity from the beginning. Methods to avoid residual carbon, such as applying a different type of lubricant or a more thorough removal technique (i.e. extending delubrication time or changing temperature) should be also evaluated. On the other hand, nitrogen atmosphere should not be used in the delubrication step, in order to avoid any possible contamination. Moreover, from a processing economics perspective, it would be better if the delubrication stage can be integrated with the subsequent sintering step.

In the experimental work, cold isostatic pressing was employed to avoid any lubricant usage. The resultant elongation was significantly improved. However, the CIP machine used was limited in compaction pressure (~220MPa). A better instrument, with a higher pressure capability, should be applied for direct property comparison with the uniaxial pressed samples if possible.

5.2 TITANIUM BINARY ALLOYS

The increase in densification for Ti-10%Ni compositions is a clear indication of liquid phase sintering. The optical and SEM imaging confirmed the existence of a liquid phase (observed with a clear eutectic phase morphology) as well as the Ti_2Ni

intermetallic phase. The use of a higher sintering temperature led to a higher portion of the eutectic phase. On the other hand, Sn solute has less of an influence on densification. As the solute content was increased to 10%, several problems became apparent. For Ti-10%Ni, the issue of partial sample melting at 1200°C causes severe problems (e.g. massive distortion, crucible damage, etc.). In the case of Ti-10%Sn the exuding of Sn beads may occur after either delubrication or sintering, which damages the sample integrity. The tensile properties are consequently affected.

In this study, some experiments were not performed due to the processing or time limitations (e.g. melting). For a more complete study of these binary systems several further experiments are required, such as:

(i) examination of higher sintering temperatures (i.e. >1200°C) should be carried out for Ti-Ni alloys with less than 10%Ni (to avoid melting issues), and the corresponding hardness should be evaluated,

(ii) tensile tests should be performed on Ti-Ni and Ti-Sn compositions other than 2.5%, although the distortion problem should be solved beforehand (for example with the machined Charpy bars used for CP titanium),

(iii) the 10% Ni or Sn solute samples should be re-evaluated to determine whether the aforementioned problems can be overcome,

(iv) the effects of heating rate, which can also play an important role in sintering dynamics, should be assessed using differential scanning calorimetry (DSC) as control of the heating rate may provide the liquid phase adequate time to allow better wetting and atomic diffusion in the sample and prevent excess liquid formation.

In spite of some undesired limitations and difficulties in the presented experiments, this preliminary study of titanium binary alloys has provided essential knowledge and experience from the preceding work and has built a foundation for further titanium P/M development.

References

ASM International. Handbook Committee. (1990). *ASM handbook* (10th ed.). Materials Park: OH : ASM International.

Badini, C., Ubertalli, G., Puppo, D., & Fino, P. (2000). High temperature behaviour of a Ti-6Al-4V/Ti-Cp composite processed by BE-CIP-HIP method. *Journal of Materials Science, 35*(15), 3903-3912. Retrieved from http://dx.doi.org/10.1023/A:1004893700762

Barreiro, M. M. (2010). Titanium compacts produced by the pulvimetallurgical hydride-dehydride method for biomedical applications. *Biomedical Materials, 5*(2)

Cardarelli, F. (2008). Titanium and titanium alloys. In *Materials handbook: A concise desktop reference* (2nd ed., pp. 275-325) Springer.

Crowley, G. (2003). How to extract low-cost titanium. *Advanced Materials and Processes, 161*(11), 25-27.

De Oliveira, M. V. (2001). Titanium surgical implants processed by powder metallurgy. *Key Engineering Materials, 189*, 437-442.

Delo, D. P., & Piehler, H. R. (1999). Early stage consolidation mechanisms during hot isostatic pressing of Ti-6Al-4V powder compacts. *Acta Materialia, 47*(9), 2841-2852. Retrieved from http://dx.doi.org/10.1016/S1359-6454(99)00132-9

Deura, T., Matsunaga, T., Suzuki, R., Ono, K., & Wakino, M. (1998). Titanium powder production by $TiCl_4$ gas injection into magnesium through molten salts. *Metallurgical and Materials Transactions B, 29*(6), 1167-1174. doi:10.1007/s11663-998-0038-6

Donachie, M. J. (2000a). Heat treating. In *Titanium: A technical guide* (2nd ed., pp. 55-63) ASM.

Donachie, M. J. (2000b). Powder metallurgy. In *Titanium: A technical guide* (2nd ed., pp. 47-53) ASM.

Donachie, M. J. (2000c). Structure/Processing/Property relationships. In *Titanium: A technical guide* (2nd ed., pp. 95-121) ASM.

Even, C., Arvieu, C., & Quenisset, J. M. (2008). Powder route processing of carbon fibres reinforced titanium matrix composites. *Composites Science and Technology, 68*(6), 1273-1281. doi:DOI: 10.1016/j.compscitech.2007.12.014

Froes, F. H. (2005). *Developments in titanium P/M.* Retrieved October, 10, 2005, from www.webs1.uidaho.edu/imap/MPR%20Paper.pdf

Froes, F. H., Mashl, S. J., Moxson, V. S., Hebeisen, J. C., & Duz, V. A. (2004). The technologies of titanium powder metallurgy. *JOM, 56*(11), 46-48.

Furuta, T., & Saito, T. (1995). Fatigue properties of TiB particle reinforced P/M titanium matrix composite. Paper presented at the *Proceedings of the 1995 4th International Conference on Powder Metallurgy in Aerospace, Defense and Demanding Applications,* 173-180.

Gerdemann, S. J. (2001). Titanium process technologies. *Advanced Materials Processes, 159*(7), 41-43.

German, R. M. (2005). *Powder metallurgy and particulate materials processing : The processes, materials, products, properties and applications*. Princeton, NJ: Metal Powder Industries Federation.

Hanson, A. D., Runkle, J. C., Widmer, R., & Hebeissen, J. C. (1990). Titanium near net shapes from elemental powder blends. *International Journal of Powder Metallurgy (Princeton, New Jersey), 26*(2), 157-164.

He, G. (2006). Ti alloy design strategy for biomedical applications. *Materials Science Engineering.C, Biomimetic Materials, Sensors and Systems, 26*(1), 14-19.

Henriques, V. A. R. (2001). Production of titanium alloys for medical implants by powder metallurgy. *Key Engineering Materials, 189*, 443-448.

Hopkins, B. (2010). The powder process - using ultrafine titanium in manufacturing. *Materials World Magazine,* Retrieved from http://www.iom3.org/feature/powder-process-using-ultrafine-titanium-manufacturing?c=574

Hurless, B. E., & Froes, F. H. (2002). Lowering the cost of titanium. *AMPTIAC Quarterly, 6*

Ivasishin, O. M., Anokhin, V. M., Demidik, A. N., & Savvakin, D. G. (2000). Cost-effective blended elemental powder metallurgy of titanium alloys for transportation application. *Key Engineering Materials, 188*, 55-62.

Ivasishin, O. M., Bondareva, K. A., Bondarchuk, V. I., Gerasimchuk, O. N., Savvakin, D. G., & Gryaznov, B. A. (2004). Fatigue resistance of powder metallurgy Ti-6Al-4V alloy. *Problemy Prochnosti,* (3), 5-13.

Ivasishin, O. M., Savvakin, D. G., Froes, F. H., Mokson, V. S., & Bondareva, K. A. (2002). Synthesis of the Ti-6Al-4V alloy having low residual porosity by powder metallurgy method. *Poroshkovaya Metallurgiya,* (7-8), 54-64.

Joshi, V. A. (2006). *Titanium alloys an atlas of structures and fracture features*. Boca Raton: CRC/Taylor & Francis.

Kainer, K. U., & Metallische Verbundwerkstoffe. English (Eds.). (2006). *Metal matrix composites : Custom-made materials for automotive and aerospace engineering*. Weinheim, Germany: Wiley-VCH.

Kim, M., Chen, P. C., & Vedula, K. (1985). IMPROVEMENTS OF THE BLENDED ELEMENTAL PROCESSING OF Ti-6Al-4V ALLOY. Paper presented at the *Proceedings of the 1984 International Powder Metallurgy Conference. Volume 16: Ferrous and Nonferrous Materials. , 16* 547-562.

Low, R. J., Robertson, I. M., & Schaffer, G. B. (2007). Excessive porosity after liquid-phase sintering of elemental titanium powder blends. *Scripta Materialia, 56*(10), 895-898. Retrieved from http://dx.doi.org/10.1016/j.scriptamat.2007.01.040

Lutjering, G., & Williams, J. C. (2003). *Titanium* (second ed.) Springer Verlag.

Mendelson, M. I. (1969). Average grain size in polycrystalline ceramics. *Journal of the American Ceramic Society, 52*(8), 443-6.

Mohandas, K. S. (2004). FFC cambridge process and removal of oxygen from metal-oxygen systems by molten salt electrolysis: An overview. *Transactions of the Indian Institute of Metals, 57*(6), 579-92.

Moll, J. H. (2000). Utilization of gas-atomized titanium and titanium-aluminide powder. *JOM, 52*(5), 32-34.

MPIF. (2002a). Density of compacted or sintered powder metallurgy product. In *Standard test methods for metal powders and powder metallurgy products* (pp. 59-62). Princeton, New Jersey: Metal Powder Industries Federation.

MPIF. (2002b). Green strength for unsintered compacted powder metallurgy materials. In *Standard test methods for powders and powder metallurgy products* (pp. 37-40). Princeton, New Jersey: Metal Powder Industries Federation.

Neto, F. B., Azevedo, C. R. F., & Rodrigues, D. (2003). Ti-Al-V powder metallurgy (PM) via the hydrogenation-dehydrogenation (HDH) process. *Journal of Alloys and*

Compounds, 353(1-2), 217-227. Retrieved from http://dx.doi.org/10.1016/S0925-8388(02)01297-5

Norgate, T. E., & Wellwood, G. (2006). The potential applications for titanium metal powder and their life cycle impacts. *JOM, 58*(9), 58-63.

Pease, L. F., & West, W. G. (2002). *Fundamentals of powder metallurgy*. Princeton, N.J.: Metal Powder Industries Federation.

Peters, M., Hemptenmacher, J., Kumpfert, J., & Leyens, C. (2003). Structure and properties of titanium and titanium alloys. In C. Leyens, & M. Peters (Eds.), *Titanium ans titanium alloys fundamentals and applications* (pp. 1). Weinheim: Wiley-VCH.

Petit, J., Berata, W., & Bouchet, B. (1992). Fatigue crack growth behaviour of Ti-6Al-4V at elevated temperature in high vacuum. *Scripta Metallurgica Et Materialia, 26*(12), 1889-1894. Retrieved from http://dx.doi.org/10.1016/0956-716X(92)90054-I

Pickens, J. (2004). Low-cost titanium for ships and tanks. *Advanced Materials Processes, 162*(5), 37-39.

Polmear, I. (2005). *Light alloys* (4th ed.) Butterworth-Heinemann.

Robertson, I. M. (2009). Swelling during liquid phase sintering of Ti-Ni alloys. *Powder Metallurgy, 52*(3), 213-24.

Saito, T., Furuta, T., & Yamaguchi, T. (1995). Development of low cost titanium matrix composite. Paper presented at the *Proceedings of the Symposium on Recent Advances in Titanium Metal Matrix Composites,* 33-44.

Saito, T. (2004). The automotive application of discontinuously reinforced TiB-Ti composites. *JOM, 56*(5), 33-36.

Schaeffer, A. (2008). The study of prototypes of dental implants obtained by the titanium powder injection molding process: In vivo study. *Materials Science Forum, 591*, 179-186.

Sibum, H. (2003). Titanium and titanium alloys- from raw material to semi-finished products. In *Titanium and titanium alloys: Fundamentals and applications* (pp. 231-244) Wiley-VCH.

Smart, R. F., & Ellwood, E. C. (1959). The powder metallurgy of titanium-tin containing up to 15% tin. *Powder Metallurgy, 4*, 108-119.

Smith, W. F. (1992). *Structure and properties of engineering alloys* (2nd ed.) McGraw-Hill College.

Taddei, E. B., Henriques, V. A. R., Silva, C. R. M., & Cairo, C. A. A. (2004). Production of new titanium alloy for orthopedic implants. *Materials Science and Engineering: C, 24*(5), 683-687. doi:DOI: 10.1016/j.msec.2004.08.011

Ward-Close, C., Godfrey, A. B., & Thompson, S. R. (2005). Titanium made the EDO way should see prices drop. *Metal Powder Report, 60*(7-8), 20-25. Retrieved from http://dx.doi.org/10.1016/S0026-0657(05)70451-3

Yamamoto, Y. (2010). Consolidation process in near net shape manufacturing of armstrong CP-Ti/Ti-6AI-4V powders. *Key Engineering Materials, 436*, 103-11.